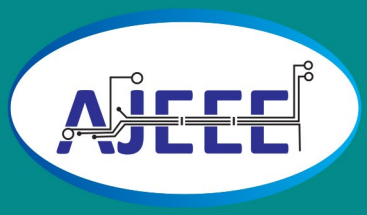

ISSN: 2582-0257

ADBU Journal of
Electrical and Electronics Engineering

An International Peer Reviewed Open Access Journal exploring innovative research findings in Electrical and Electronics Engineering & Technology and its Allied sciences

Volume 2 Issue 2

ASSAM
DON BOSCO
UNIVERSITY

ISSN: 2582-0257

ADBU Journal of
Electrical and Electronics Engineering

An International Peer Reviewed Open Access Journal exploring innovative research findings in Electrical and Electronics Engineering & Technology and its Allied sciences

Volume 2 Issue 2

ASSAM
DON BOSCO
UNIVERSITY

ADBU Journal of Electrical and Electronics Engineering (AJEEE)

ISSN: 2582-0257

Website: www.tinyurl.com/ajeee-adbu , http://journals.dbuniversity.ac.in/ojs/index.php/AJEEE

Volume 2, Issue 2

Published in September, 2018

Contents

FACTS controllers' impact on Power Quality: A comparative analysis

Pulakesh Kumar Kalita[1], Satyajit Bhuyan[2], Jesif Ahmed[3]

[1]Department of Electrical and Instrumentation Engineering, Assam Engineering College, Gauhati University,
Jalukbari, Guwahati -781013, Assam, INDIA.
*pulakesh07@rocketmail.com**

[2]Department of Electrical and Instrumentation Engineering, Assam Engineering College, Gauhati University
Jalukbari, Guwahati- 781013, Assam, INDIA
satyajitbhuyan1962@gmail.com

[3]Department of Electrical and Electronics Engineering, Assam Don Bosco University
jesif.ahmed@dbuniversity.ac.in

Abstract: ***For last couple of decades, the demand for electrical power has increased manifold. As we have limited resources of power generation, it results into heavy loading of the transmission line, which leads to stability, voltage sag/swell and reactive power issues. Application of FACTS controllers in a power system is a promising and more efficient way for transfer and control of a bulk amount of power. This paper focuses on voltage dependency on reactive power and control of the same for improvement in the power quality. A comparative analysis of steady-state power flow control of a power system transmission network using FACTS controllers namely SVC, STATCOM and TCSC are performed. The performance of these FACTS controllers in the control of power flow on a given test bus system is analyzed. Voltage magnitude is compared for shunt-connected controllers to analyze the efficiency. Reactance modeling and power injection modeling techniques are used to incorporate the FACTS controllers into Newton-Raphson load flow algorithm. Numerical results on a benchmark 5 bus test system with incorporation of each of the FACTS controllers are presented.***

Keywords: Power Quality, Voltage control, Reactive Power, FACTS, SVC, STATCOM, TCSC.

1. Introduction

With the introduction of deregulatory electricity market the utilities must ensure a reasonable quality of power supply with high reliability. In addition to effects of the deregulation and creation of today's electricity market, utilities have to supply increased loads; also composed of power electronic based equipment, to the customer. To meet these increased loads, utilities would like to strengthen the transmission system by building more interconnectors. However, this is restricted by economic and social issues. Again, with widespread use of power electronic and sophisticated equipment Power quality has assumed increasing importance. A power quality problem is any occurrence manifested in voltage, current, or frequency deviation that results in failure or mis-operation of customer equipment [1]. This results in economic impacts on utilities, their customer, and suppliers of load equipment. The increase in the loading of the transmission lines sometimes can lead to voltage collapse due to the shortage of reactive power delivered at the load centers. This is due to the increased consumption of the reactive power in the transmission network and the characteristics of the load. To maintain economic & secure operation of large interconnected systems the safe operating margin can be substantially reduced by introduction of fast dynamic control on reactive and active power through power electronic controllers, making the AC transmission network more flexible and reliable [2]. For maximization of power transfer capabilities, compensation of FACTS Controllers (series and shunt types) is required. The voltage magnitudes in the buses are held close to their nominal values by compensation through FACTS Controllers and in addition, line currents and total systems losses are also reduced. In this context, sophisticated and versatile devices called FACTS Controllers are effectively used in adjusting the bus voltage magnitude thereby contributing for the improvement in voltage stability of the power system [3]. By making change in the bus voltage amplitude, bus voltage angle and transmission line reactance with the help of FACTS Controllers, the flow of power can be controlled. STATCOM, SVC, TCSC, etc., are some of the FACTS Controllers, which are used for mitigating power system network problems and improving the power quality. As the power supply can only control the quality of the voltage and has no control over the

load-dependent current, hence the quality of voltage is considered to be equivalent to power quality [4].

2. Power Quality: causes and issues

2.1 Causes of deterioration in Power Quality

Main natural causes are
- Faults or lightning strikes on transmission lines
- Falling of trees on distribution feeders
- Equipment failure

Some of man-made causes are
- Load or feeder/transmission line operation viz. transformer energization, capacitor or feeder switching
- PE loads such as ups, ASD, converters, arc furnaces and induction heating systems
- Switching of large loads [5]

2.2 Common Power Quality issues

Harmonics: Excessive losses and heating in motors, capacitors, and transformers connected to the system.

Flicker: Visual irritation, the introduction of many harmonic components in the supply power and their associated equipment.

Transients: Tripping, components failures, flashover of instrument insulation hardware booting, software glitches, poor product quality etc.

Voltage sags: Devices /process down time, effect on product quality, failure / malfunction of customer equipment and associated scrap cost, clean-up costs, maintenance and repair costs etc.

3. Reactive Power

Reactive power is the latent soul of power transmission system. It is very precious in keeping the system voltage stable. It is generated when current waveform is not in phase with voltage waveform because of energy conserving elements like inductor or capacitors [6]. Components of current in phase with voltage generate active power that does the real work. Reactive power is required for producing magnetic and electric fields in inductors and capacitor respectively.

The voltage in the transmission line can be varied with a variation of reactive power. This can be illustrated as follows-

Q_1 = Reactive power demand by the load
Q_2 = Reactive power supplied by source

$Q_R = Q_1 - Q_2$ (in receiving end)

$$Q_R = \frac{V_R V_S \cos\delta - V_R^2}{X_L} \quad (1)$$

Assuming $\delta \to 0$ or $\cos\delta \to 1$

$$Q_R = \frac{V_R V_S - V_R^2}{X_L} \quad (2)$$

On solving we get

$$V_R = \frac{V_S}{2} \pm \frac{\sqrt{{V_S}^2 - 4X_L Q_R}}{2} \quad (3)$$

Hence, the change in reactive power causes required change in the receiving end voltage. With the help of various devices, the reactive power generation has been controlled. For maintaining economic and secure operation of a large interconnection system, fast dynamic control over reactive and active power by high power electronic controllers is introduced. This makes the system more reliable and flexible to adapt to changing conditions caused by contingencies and load variations. Reactive power compensation is considered as a powerful tool for optimizing the power flow on transmission networks. Inadequate supply or demand of reactive power leads to voltage collapses and has been a major cause of several recent major power outages worldwide [7].

For a typical transmission line,

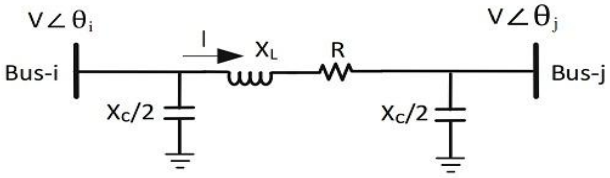

Fig. 1: π-model single line diagram

The line capacitance supplies $Q_{produced}$ reactive power and the line inductance consumes $Q_{consumed}$ for an ideal line (R = 0).

$$Q_{produced} = \frac{V^2}{X_c} \quad (4)$$

$$Q_{consumed} = I^2 X_L \quad (5)$$

Where V =bus voltage
X_C=line capacitance reactance
X_L= line inductive reactance
I =line current

At surge impedance loading,
$Q_{produced} = Q_{consumed}$

Surge impedance

$$Z_0 = \frac{V}{I} = \sqrt{\frac{X_L}{X_C}} \quad (6)$$

And $$SIL = \frac{V^2}{Z_0} \quad (7)$$

From above expression, we can say that an ideal line loaded at its surge impedance loading does not produce or consume reactive power, so it will have same voltage at both ends. Hence, the balance of both consumption and production of reactive power at a particular loading level result in a flat voltage profile along the line. Consumption of reactive power increases with the square of the current, thus we face difficulty to transport reactive power along long lines.

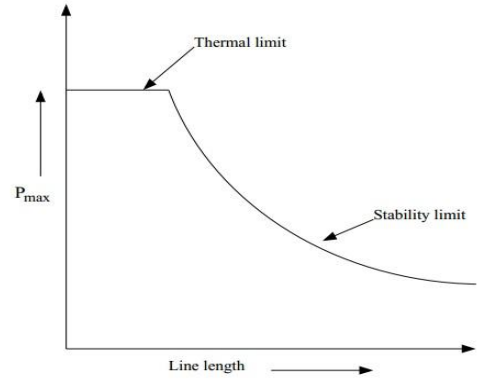

Fig. 2: Power transfer capacity as a function of line length [2]

Reactive power flow can be controlled by Series and Shunt compensation devices. Conventionally switched shunt/series compensators and phase shifting transformers have been utilized. Modern power electronic based devices are now used for reactive power compensation. These are categorized as FACTS controllers. Compensator's application improves the power transfer capability. The power-δ curve below (fig. 3) shows the variation of power transfer with respect to power angle for various compensation methodologies, keeping compensation fixed at 50%.

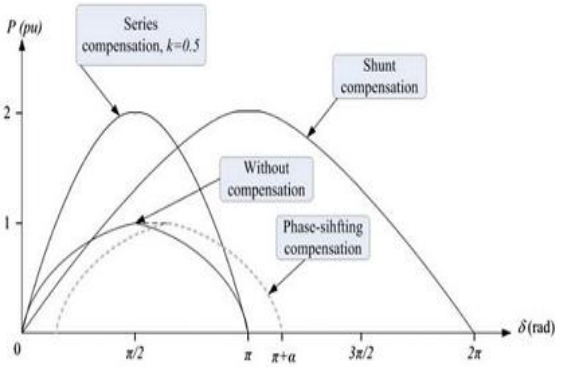

Fig. 3: P-δ curve

4. FACTS

FACTS is defined as, "Alternating current transmission system incorporating power electronic based and other static controllers to enhance controllability and increase power transfer capability" [8, 9]. The facts controllers are defined as "a power electronic based system and other static equipment that provides control of one or more AC transmission system parameters"[2].

Depending on PE devices used in control, the FACTS controllers can be classified as:

A) Variable Impedance
B) VSC based

Variable impedance type controllers include:

i) SVC (Static Var Compensators) (shunt connected)
ii) Thyristor Controlled Series Capacitor or Compensator (TCSC) (series connected)
iii) Thyristor Controlled Phase Shift Transformer (TCPST)

VSC based FACTS controllers:

i) Static Synchronous Compensator (STATCOM) (Shunt)
ii) Static Synchronous Series Compensator (SSSC) (Series)
iii) Interline Power Flow Controller (IPFC) (combined)
iv) Unified Power Flow Controller (UPFC) (combined)

FACTS controllers are power electronic based devices that can change parameters like impedance, voltage and phase angle, very rapidly and continuously. Therefore, they have the ability to control reactive power flow pattern and enhance the usable capacity of the existing lines. FACTS devices are good to improve the power system efficiency, improve power factor and reduced in harmonics. A comparison of few common FACTS controllers is provided in Table 1 [12].

Table 1: Common FACTS controllers

Sl. No	FACS Devices	Load Flow	Voltage Control	Transient Stability	Dynamic stability
1	SVC	Low	High	Low	Medium
2	STATCOM	Low	High	Medium	-do-
3	UPFC	High	High	Medium	-do-
4	TCSC	Medium	Low	High	-do-
5	SSSC	Low	High	Medium	-do-

4.1 SVC (Static Var Compensator)

Static Var Compensator systems are applied by utilities in transmission lines for several purposes. The primary purpose is usually for rapid control of voltage at weak points in the network. Installation may be at the midpoint of transmission interconnections or at the line ends. The location can be determined by the sensitivity of voltage at the critical buses with respect to the reactive power

injection (ΔVi/ΔQj). Static VAR compensator is shunting connected static generators/absorber whose outputs are varied so as to control voltage of electric power system. In its simple form, SVC is connected as a fixed capacitor-thyristor controlled reactor (FCTCR) configuration.

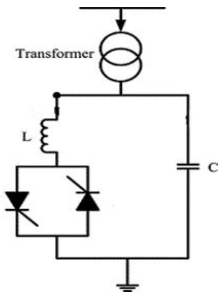

Fig. 4: SVC building block

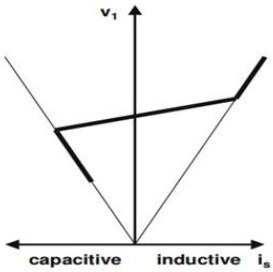

Fig. 5: SVC voltage/current chracteristics

The SVC is connected to a coupling transformer, which is a connected transformer that is connected directly to the a.c. bus whose voltage is to be regulated. The effective reactance of the FC-TCR is varied by firing angle control, of the anti-parallel thyristor. The firing angle can be controlled through a PI controller in such a way that the voltage of the bus, where the svc is connected is maintained at the reference value. The dynamic reactive control at the load bus increases power transfer and can solve the problem of voltage instability (collapse) caused by contingency conditions.

4.2 STATCOM (Static Synchronous Compensator)

STATCOM is a shunt connected Static Var Compensator whose capacitive or inductive output current can be controlled independently of the ac system voltage. Fig. 6 shows a simple one-line diagram of STATCOM based on VSC.

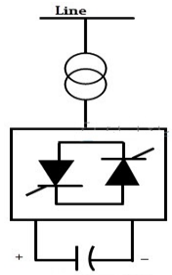

Fig. 6: STATCOM structure

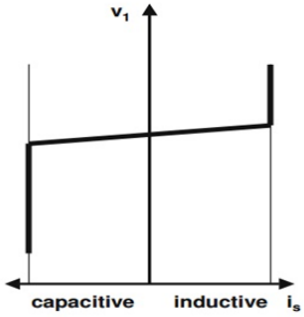

Fig. 7: STATCOM voltage/current characteristics

The voltage source converters convert dc voltage to a voltage by using GTO and the ac voltage is inserted into the line through the transformer. If the output of the VSC is more than the line voltage, converter output voltage then converter absorbs lagging vars from the source. STATCOM requires less space, has faster response and It can be interfaced with real power sources such as a battery, fuel cell or SMES (superconducting magnetic energy storage). Also, the reactive current can be maintained constant by STATCOM during low voltage condition.

4.3 TCSC (Thyristor Controlled Series Capacitor)

TCSC is series compensated FACTS device which consists of a series capacitor bank shunted by a thyristor-controlled reactor in order to provide a smoothly variable series capacitive reactance. Fig.8 shows a single line diagram of a TCSC controller.

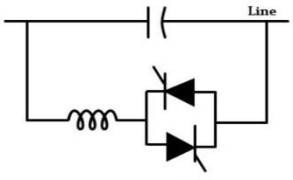

Fig. 8: TCSC structure

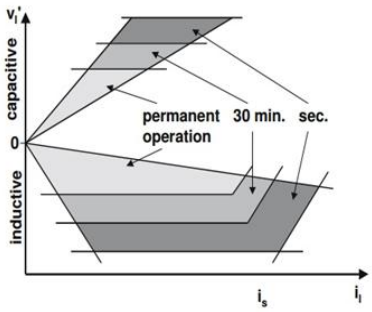

Fig. 9: TCSC operational diagram

The TCSC is based on thyristor without gate turnoff capability. In TCSC, a variable thyristor controlled reactor is connected across a series capacitor when the firing angle of the TCR is 180°, the reactor becomes non-conducting and the series capacitor has the normal impedance. As the firing angle is decreased below 180°, the capacitive reactance increases. When the firing angle is 90°, the reactor becomes fully conducting and total impedance becomes inductive. With the 90° firing angle, the TCSC helps in limiting fault current. It can be used to mitigate SSR. The TCSC was also labeled as RANI (Rapid Adjustment of Network Impedance) in the work done by Vithayathil *et al*. [10]. In work done by Sujatha Subhash, B. N. Sarkar and K. R. Padiyar [11], a technique for finding optimal location of TCSC has been proposed.

5. Modeling

The IEEE 5-bus network is used to assess FACTS equipment capacities. It contains two generators each one has voltage and speed regulators. The buses are connected via seven tie lines of varying lengths. The lengths are calculated on the basis of the theory of traveling waves. This is explained later. The distributed parameters of transmission lines are in accordance with the frequency of generated AC by the generators. Three-phase RLC series loads are connected to the load buses. The first bus is considered as the swing or slack bus. Each bus is equipped with load flow measuring blocks, which provides information about bus voltage magnitudes and respective angles. Transformers are connected wherever it is required in accordance with the theory of FACTS controllers. So as the Powergui block is necessary for simulation of any Simulink model containing Simpower-systems blocks. It is used to store the equivalent Simulink circuit that represents the state-space equations of the model. We used the method of discretization of the electrical system for a solution at fixed time steps.

From the standard IEEE 5-bus system, the p.u. values for various line parameters are taken. The concept of traveling waves is utilized for determination of line's electrical length.

$$\beta l = \left(\frac{\pi}{180}\right)\theta \quad (8)$$

$$\left(\frac{2\pi f}{v_p}\right) l = \frac{\pi\theta}{180} \quad (9)$$

$$l = 13888.9\theta m \quad (10)$$

With the help of above equation calculation of physical length is possible and implemented. The datasheet for standard 5-bus system is utilized for calculation of various parameters of the system.

Table 2: Line data of IEEE 5-bus system

From bus	To bus	Resistance	Reactance	Capacitance	Susceptance
1	2	0.02	0.06	0	0.06
1	3	0.08	0.24	0	0.05
2	3	0.06	0.18	0	0.04
2	4	0.06	0.18	0	0.04
2	5	0.04	0.12	0	0.04
3	4	0.01	0.03	0	0.02
4	5	0.08	0.24	0	0.05

The base voltage chosen is 230KV and base power is 100MVA. The transmission line is in the range of short transmission line category; hence capacitance of line is neglected. The various facts devices are implemented in the bus system with requisite changes and modulation, and analysis is done by using a programmable voltage source. The comparison of power flow analysis on the 5bus test system is done without using FACTS controllers' viz. SVC, STATCOM, TCSC. However, for this 5-bus test system, only voltage magnitude was taken into consideration during the comparison. In all four cases, it is observed that the incorporation of FACTS controllers have improved the bus voltage profile and power flow of the whole network.

SVC implementation :

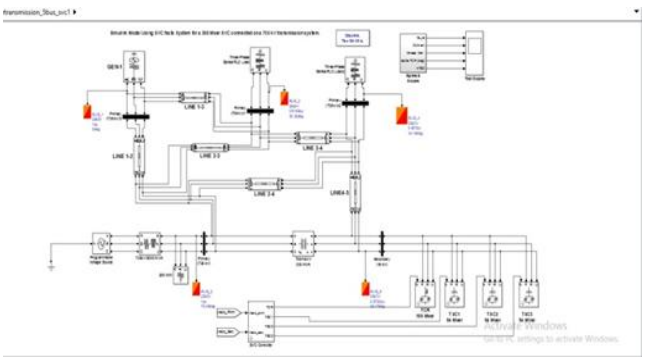

Fig. 10: SVC implementation

STATCOM implementation :

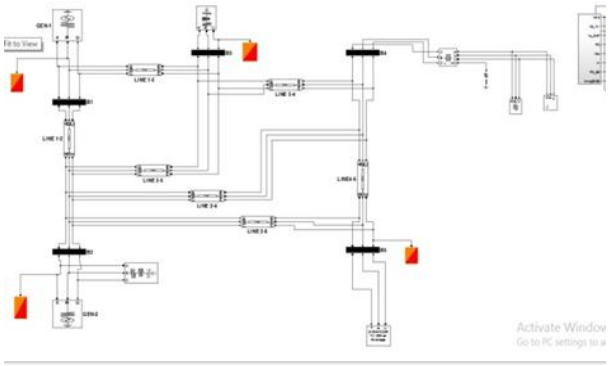

Fig. 11: STATCOM implementation

TCSC implementation :

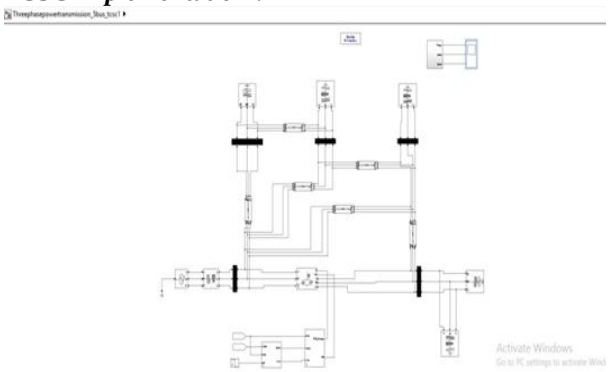

Fig. 12: TCSC implementation

6. Output

SVC is shunt connected controller and it controls the voltage magnitude in the system. As the voltage magnitude falls the reactive power supply is provided by SVC to compensate the voltage magnitude. The reactive power flow is controlled by the thyristor valves present in the SVC module (Fig. 13).

The output of STATCOM implemented bus system is much better than that of obtained by SVC. The controllability of STATCOM is better to SVC because of usage of modern power semiconductor switches (Fig. 14).

The series connected FACTS controller TCSC helps in improving the power flow. Almost 250% increase in power flow can be seen by the output of scope (Fig. 15).

As shunt compensators are primarily dealing with the voltage profile control, hence, a comparison of voltage magnitude is made in the 5-bus test system. In all the cases, it is observed that the incorporation of FACTS devices has improved the bus voltage profile and the power flow of the whole network. The Fig. 16 below shows the bus voltage profile before and after incorporating FACTS devices into the test bus system. The voltage limit was set to be at 0.9 pu and 1.1 pu. This is to ensure that voltage stability is achieved. From the figure, it can be seen that the voltage magnitude of the system without FACTS devices is lower than with the existence of FACTS device. Thus installation of FACTS device into low voltage profile system has improved the overall voltage profile of the system. The voltage magnitude of bus-1 and bus-2 were not affected due to the presence of generator at the bus which makes it a PV bus. From the figure, STATCOM is shown to possess the better ability to improve the voltage profile as it was able to raise the overall voltage profile closer to 1.0pu as compared with test system with SVC model.

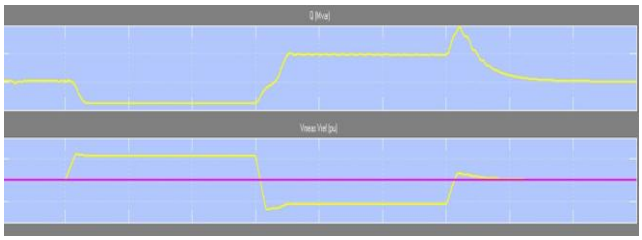

Fig. 13: Control by SVC

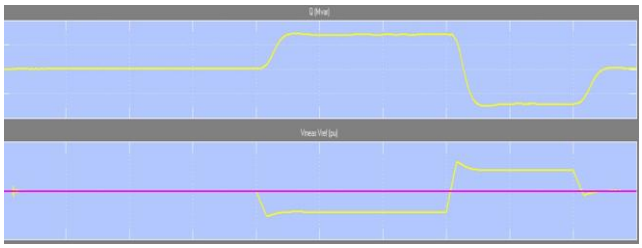

Fig. 14: Control by STATCOM

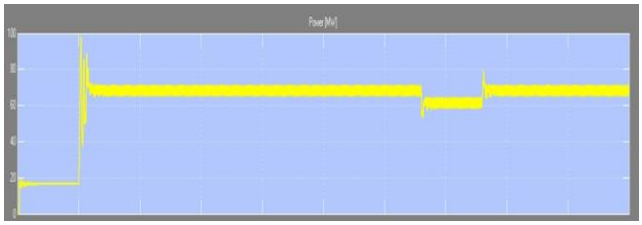

Fig. 15: Power Flow control by TCSC

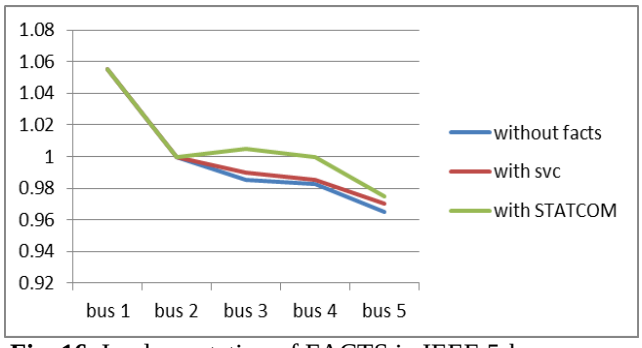

Fig. 16: Implementation of FACTS in IEEE 5-bus system

7. Conclusions

In this paper, the performance of SVC, STATCOM, and TCSC in terms of voltage magnitude and power flow are compared. It is cleared that FACTS devices improve the power flow and voltage profile in the system in which they are connected. Shunt connected devices such as SVC and STATCOM improves the voltage of the bus in which it is connected and series devices TCSC improve the power flow. Also, STATCOM gives superior performance than SVC for power measurement, bus voltage, rotor angle and terminal voltages of the multi-machine system. The FACTS controllers based on VSC have several advantages over the variable impedance type. A STATCOM is much more compatible and compact than an SVC for similar rating and is technically superior. It can supply required reactive current even at low values of the bus voltage and can be designed to have inbuilt short-term overload capability. Also, a STATCOM can supply active power if it has an energy source or large energy storage at its DC terminals.

The only drawback with VSC based controllers is the requirement of using self-commutating power semiconductor devices such as GTO, IGBT etc. Thyristors do not have this capability and cannot be used although they are available in higher voltage rating and tend to be cheaper with reduced losses. With advancement in power, electronic technologies new and more versatile controllers have been developed. Devices with a higher degree of freedoms such as UPFC; proposed by Gyugyi [13], will get more focus as they are capable of controlling both voltage regulation and power flow in the system.

References

[1] R. S. Vedam and M. S. Sarma, *Power Quality: VAR Compensation in Power Systems*, CRC Press, FL, 2009, ISBN: 13: 978-1-4200-6480-3.

[2] K. R. Padiyar, *FACTS Controllers in Power Transmission and Distribution*, 2nd Edition, New Age International (P) Limited Publisher, New Delhi, 2016, ISBN (13): 978-81-224-2541-3.

[3] B. Viswanath, K. Revathi and T. R. Jyothsna, "FACTS Controllers for Enhancement of Power System Performance: State-of-the-art", *International Journal of Pure and Applied Mathematics*, Vol. 114, Issue No. 8, 2017, pp. 265-273.

[4] R. C. Dugan, M. F. McGranagham, S. Santoso and H. W. Beaty, *Electrical Power Systems Quality*, 3rd Edition, McGraw Hill Professional, NY, 2012.

[5] A. Ghosh and G. Ledwich, *Power Quality Enhancement Using Custom Power Devices*, Springer Science & Business Media, NY, 2012, ISBN 978-1-4613-5418-5

[6] N. M. Tabatabali, A. J. Aghbolaghi, N. Bizon and F. Blaabjerg (Eds.), *Reactive Power Control in AC Power Systems*, 1st Edition, Springer International Publishing, 2017. Doi: https://doi.org/10.1007/978-3-319-51118-4

[7] R. M. Mathur and R. K. Varma, *Thyristor-Based FACTS Controllers for Electrical Transmission Systems*, Wiley-IEEE Press, NY, 2002.

[8] N. G. Hingorani, "Flexible AC Transmission", *IEEE Spectrum*, Vol. 30, Issue No. 4, pp.40-45, April 1993. Doi: 10.1109/6.206621

[9] N. G. Hingorani and L. Gyugyi, *Understanding FACTS: Concepts and Technology of Flexible AC Transmission Systems*, Wiley-IEEE Press, 1999.

[10] J. Vithayathil, C. Taylor, M. Klinger and W. Mittelstadt, "Case Studies of Conventional and Novel Methods of Reactive Power Control on AC Transmission Systems", *CIGRE*, SC 38-02, Paris, 1988.

[11] S. Subhash, B. N. Sarkar and K. R. Padiyar, "Sensitivity Based Determination Of Suitable Locations for Controlled Series Compensation for Enhancement Of Steady-State Stability in a Large Power System", *In the Proceedings of IFAC Symposium on Control of Power Systems and Power Plants*, Beijing, August 1997.

[12] A. Narain and S. K. Srivastava, "An Overview Of FACTS Devices used for Reactive Power Compensation Techniques", *International Journal of Engineering Research & Technology (IJERT)*, Vol. 4, Issue No. 12, December 2015.

[13] L. Gyugyi, "Unified Power Flow Controller Concept for Flexible AC Transmission Systems", *IEE Proceedings C - Generation, Transmission and Distribution*, Vol. 139, Issue No. 4, July 1992, pp. 323-331. Doi: https://doi.org/10.1049/ip-c.1992.0048

Authors' Profiles

Pulakesh Kumar Kalita holds first class B.E. degree in Electrical Engineering from Assam Engineering College in 2015. He is

currently studying in 4th Semester M.E. (Power System) in Assam Engineering College. His areas of interest are Power Quality, Power Electronics, etc.

Dr. Satyajit Bhuyan, Ph.D., is working as an Associate Professor in Assam Engineering College, India. He received his Ph.D. in Power System from Jadavpur University (India) in 2006. His field of interest includes power electronics, power quality, FACTS, etc.

Jesif Ahmed, M.Tech., is working as an Assistant Professor in the Department of Electrical and Electronics Engineering, School Of Technology, Assam Don Bosco University, Guwahati, Assam, India. He is pursuing his Ph.D. from Gauhati University, Assam, India. His research interest includes study of electricity market, Power system optimization and transmission congestion management.

Stability Improvement of Power System due to Wind Farm and Fault using FACTS Devices

Julene Seka H. Thabah[1], Darihun Sawkmie[2], Maitshaphrang Lyngdoh[3], Smriti Dey[4]

[1,2,3,4] School of Technology, Assam Don Bosco University
Airport Road, Azara, Guwahati - 781017, Assam, INDIA.
[1]*julenethabah@gmail.com**, [2]*dary4km@gmail.com*, [3]*lyngdoh24@gmail.com*, [4]*smriti.dey@dbuniversity.ac.in*

Abstract: ***Wind energy is gaining the most interest among a variety of renewable energy resources, but the disadvantage is that wind power generation is intermittent, depending on weather conditions. FACTS devices are used to increase the transient stability on the presence of faults and the integration of renewable sources, like wind energy. Due to continuously varying wind speed components and also due to fault the active and reactive power along with terminal voltage fluctuates continuously. STATCOM and UPFC are two important FACTS devices; provide the desired reactive-power generation and absorption, entirely using electronic processing of the voltage and current waveforms in a voltage source converter (VSC). By connecting STATCOM and UPFC into the lines, the active power, reactive power, and terminal voltage is maintained constant and it also helps to improve the transient stability of the system. STATCOM can control voltage magnitude and, to a small extent, the phase angle in a very short time and UPFC can control voltage magnitude as well as phase angle and therefore, can improve the system performance. In this paper, improvement of transient stability in wind farm under fault have been studied using STATCOM and UPFC in MATLAB SIMULINK software.***

Keywords: Transient Stability, Wind farm, FACTS, STATCOM, UPFC.

1. Introduction

Wind power industry is developing rapidly, more and more wind farms are being connected into the power systems to utilize the available wind energy for reducing electricity price and generating clean energy. There will be more significant growth in wind energy. Although the great development in the technology of electricity generation from wind energy, there is only one way of generating electricity from wind energy is to use wind turbines that convert the energy contained in flowing air into electricity [2]. Electric power generation using wind turbines has attracted the attentions of utilities due to high generation capacity and low maintenance cost of such turbines.

The most common type of wind turbine is the fixed speed turbine with squirrel cage induction generator directly connected to the grid. These wind turbines based induction generators require reactive power for compensation. If power is not sufficiently supplied, then the electromagnetic torque of the wind generator decreases significantly. Then the difference between mechanical and electromagnetic torques becomes large, and the wind generator and turbine speeds increase rapidly. As a result, the induction generator becomes unstable, and it requires to be disconnected from the power system. However, the recent trend is to decrease the shutdown operation because a shutdown of a large wind farm can have a serious effect on the power system operation such as loss of generation and load demand, voltage and frequency variations, power imbalance [3].

2. Theoretical Background

2.1 Introduction

Increasing of power demands and economic growth as well as the rapid increase of CO2 emission which creates the global warming problem has stimulated the desire for renewable energy sources like wind energy, solar energy etc. Electric power generation using wind turbines has attracted the attentions of utilities due to high generation capacity and low maintenance and cost of such turbines.

The most common type of wind turbine is the fixed speed turbine with squirrel cage induction generator directly connected to the lines. These wind turbines based induction generators require reactive power for compensation. If sufficient reactive power is not supplied, then the electromagnetic torque of the wind generator decreases significantly. Then the difference between mechanical and electromagnetic torques becomes large, and the wind generator and turbine speeds increase rapidly. As a result, the induction generator becomes unstable, and it requires to be disconnected from the power system. In order to improve the transient stability of wind farm,

FACTS devices are used, and simulation is done using MATLAB SIMULINK software.

2.2 Transient stability

Transients are caused by a sudden change of state. The causes can be both external and internal, affecting the other parts too. Whenever there are lightning strikes and itching transients on power lines, the high voltage will be clamped by the lightning arresters to handle the equipment without damage.

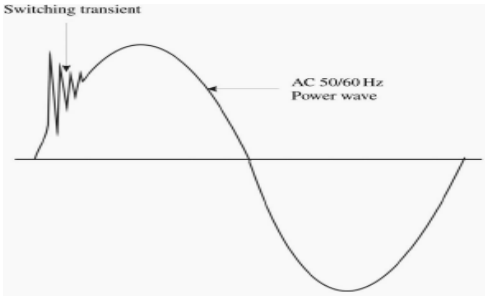

Fig 2.1: Diagram of switching transient

Transient are frequently caused by switching of inductive or capacitive loads,and also another cause include facility load switches, on/off disconnects (on energized lines), capacitor banks switch, tap changing transformers, integration of renewable energy sources with the grid etc. Transient stability is the ability of a power system to maintain synchronism when subjected to a large disturbance. The time frame of interest in transient stability studies is usually 3–5 s following the disturbance. The duration may extend up to 10–20 s for a very large system with dominant inter-area swings. The main aspects of the wind farm that affect the transient stability are:

a) **Location of wind generator**: Especially when high wind resources are located in one particular area leading to highly modified power flows including increased tie-line flows, critical fault clearing times can be considerably reduced, and additional lines might be required.
b) **Generator technology**: Variable speed wind generators can improve transient stability margins, when being equipped with low voltage ride-through capability, reactive current boosting and ideally with fast voltage control.
c) **Connection of large wind farms to lower voltage levels**: The integration of wind generation into sub-transmission and distribution systems has a negative impact on transient stability because the reactive contribution is highly limited due to reactive losses in sub-transmission and distribution systems.

2.3 Wind turbine generator power system

The system used a higher efficiency low-speed permanent magnet wind generator (PMWG) where gear box has been eliminated. In low-speed permanent magnet alternator, the rotor rotates at the same speed as the rotor of the turbine. The Permanent Magnet Alternators (PMA) is directly connected to the wind turbine; this results in a simple mechanical system. The system is comprisedof a permanent magnet alternator, rectifier, dc-dc converter, and an inverter as shown in the block diagram below Fig. 2.2. The voltage generated by the PMA machine is rectified using a three-phase passive rectifier, which converts the AC voltage generated by the Permanent Magnet Alternators into a DC voltage. The DC output voltage is boosted to a higher dc voltage. This DC voltage is then converted back into AC voltage using a pulse width modulated (PWM) inverter which is connected to the grid.

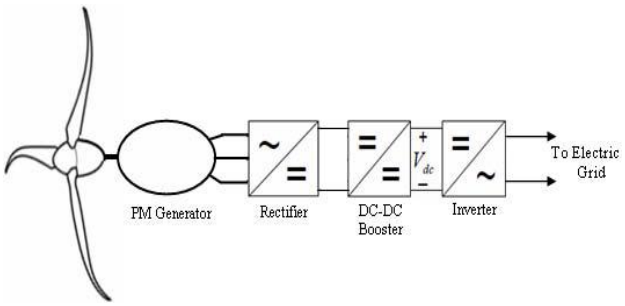

Figure 2.2: Wind Power System Block Diagram

A large number of wind generators connected to form a wind farm. When wind farm generation is given to the grid, it unbalances the current as well as voltage. These can be overcome by using FACTS devices such as STATCOM which is the best method for shunt connected and UPFC which is the best method for combination of both shunt and series-connected devices.

2.4 STATCOM

Static Synchronous Compensator (STATCOM) is a power electronic device that uses force commutated devices like IGBT, GTO etc. to control the reactive power flow through a power network and thereby increasing the stability of power network. It is a shunt device, i.e. it is connected in shunt with the line. It is also known as a Static Synchronous Condenser (STATCON). It is a member of FACTS devices.

2.4.1 Working principle of STATCOM

STATCOM generates or absorbs reactive power to the lines as well as from the lines to compensate for

small voltage variations at the connection point of the wind farm with the grid [7].

To understand the working principle of STATCOM, Let us consider two sources V_1 and V_2 are connected through an impedance $Z = R_a + X$ as shown in figure 2.3.

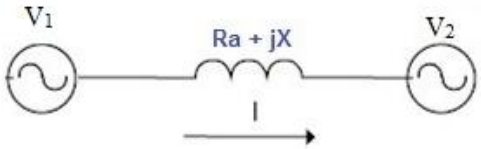

Figure 2.3: Working Principle of STATCOM

By assuming $R_a = 0$, The Reactive Power Flow Q is given as

$$Q = \frac{V_2}{X}[V_1 COS\delta - V_2]$$

In the above reactive power flow equation, angle δ is the angle between V_1 and V_2. So by maintaining angle $\delta = 0$ reactive power flow will become

$$Q = \frac{V_2}{X}[V_1 - V_2]$$

Similarly, Active power flow will become

$$P = \frac{V_1 V_2}{X} Sin\delta = 0$$

From the above equations, it is observed that the flow of active power becomes zero and the flow of reactive power depends on $(V_1 - V_2)$. So, for the flow of reactive power there are two possibilities made as shown below:

1) If the magnitude of V_1 is more than V_2, then reactive power will flow from source V_1 to V_2.
2) If the magnitude of V_2 is more than themagnitude of V_1, reactive power will flow from source V_2 to source V_1.

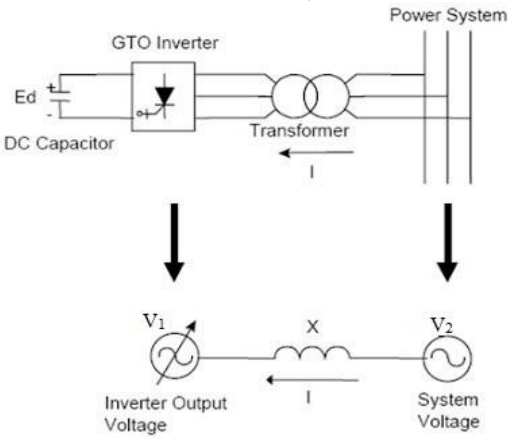

Figure 2.4: A simplified diagram along with an equivalent electrical circuit of STATCOM

As can be seen from the figure above, source V_1 represents the output voltage of the STATCOM. In there is reactive power demand in the power system, STATCOM will increase its output voltage V_1 while maintaining the phase difference between V_1 and V_2 to zero (it shall be noted here that there will always exist small phase angle between V_1 and V_2 to cater for the leakage impedance drop in the interconnecting Transformer). As $V_1 > V_2$, reactive power will flow from STATCOM to the power system. Thus STATCOM supplies reactive power and acts as the reactive power generator.

Again, if the voltage of power system increases due to load throw off, STATCOM will reduce its output voltage V_1 and therefore will absorb reactive power to stabilize the voltage to a normal value.

2.5 Unified Power Flow Controller

2.5.1 Configuration of UPFC

The UPFC consists of two voltage-source converters; one converter is connected to the power system through a shunt transformer, whereas the other converter is inserted into the transmission line through a series transformer. The converters are connected by a common DC-link where the capacitor is coupled and it allows a bi-directional real power flow between the output terminal of shunt converter and the input terminals of series converter. The basic system configuration of UPFC structure is shown in figure 2.5.

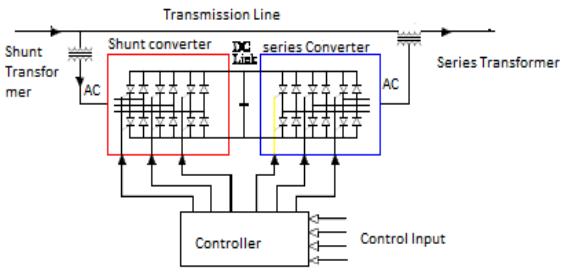

Figure 2.5: UPFC Configuration

A combination of STATCOM and SSSC which are coupled via a common dc link to allow by directional flow of real power between the series output terminals of SSSC and the shunt output terminals of STATCOM, and are controlled to provide concurrent real and reactive series line compensation without an external electrical energy source. It is generalized by synchronous voltage source. UPFC can inject controllable magnitude (V) and angularly unconstrained ($0° \leq \rho \leq 360°$) voltage. From the phasor diagram it is clear that the increasing value of 'V' will increase the magnitude as well as SPA between sending end and receiving end voltage or vice versa. So UPFC can be used as SPA reduction for power system restoration.

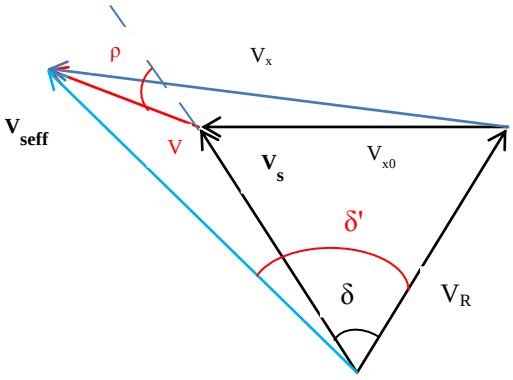

Figure 2.6: Phasor representation of UPFC

a) Shunt converter

The shunt branch of UPFC consists of a DC Capacitor, Shunt converter. It can absorb or generate only reactive power because the output current is in quadrature with the terminal voltage. The shunt-connected branch is used primarily to provide the real power demanded by series converter through the common DC link terminal. Also, it can generate or absorb reactive power independently of the real power, it can be used to regulate the terminal voltage at the sending end; thus shunt converter regulates the voltage at the input terminals of the UPFC. Another role of shunt branch of UPFC is a direct control of the DC capacitor voltage, and consequently an indirect regulation of the real power required by the series UPFC branch. The circuit losses plus the amount of real power required by the series converter have to be supplied by the shunt converter. In some cases desired real power flow from the series converter to shunt converter is possible, in this case, the series converter would supply the required real power plus the losses to the shunt converter. The shunt converter controls the dc voltage and the bus voltage at the shunt converter transformer. This paper, the shunt converter is used to control the sending-end bus voltage magnitude by locally generating and absorbing reactive power.

b) Series converter

The series branch of UPFC is comprised of a DC Capacitor, series converter and a series connected transformer. It can act as a voltage source injected in series to the transmission line through series connected transformer. The real power from series converter to shunt converter and vice versa, and hence it is possible to introduce positive or negative phase shifts between voltage at the source and at the load respectively. The series injected voltage (Vse) can have any phase shift with respect to the terminal voltage at the source. Therefore, the area of UPFC becomes the circle limited with a radius defined by the maximum magnitude of Vse, The series converter controls the active and reactive powers flow through transmission line by adjusting the magnitude and phase angle of the series injected voltage. The series converter directly controls real power of the line by controlling the magnitude of the series injected voltage. The series converter is used to generate the voltage and phase shift at the fundamental frequency. This voltage is added directly to terminal voltage by the series connected coupling transformer and in series to the transmission line. The transmission line current passes through the series transformer, and in the process exchanges real and reactive power with the series converter.

2.5.2 Principle of operation of unified power flow controller UPFC

UPFC comprised of two converters VSC1 and VSC2, operated from a DC link provided by a dc storage capacitor. These arrangements operate as an ideal ac to ac converter in which the real power can freely flow either in direction between the ac terminals of the two converters. Each converter can generate or absorb reactive power as its own ac output terminal.

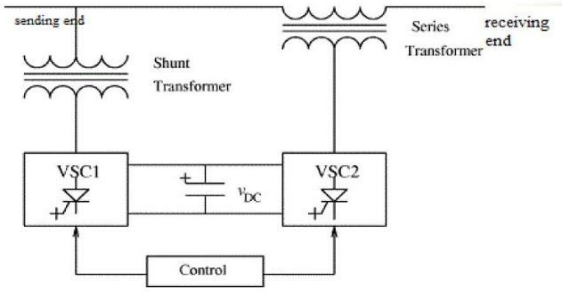

Figure 2.7: Basic UPFC scheme

As shown in the figure above VSC1 is connected to in shunt to the transmission line via a shunt transformer and VSC2 is connected in series through a series transformer. The DC terminal of two VSCs is coupled and this creates a path for active power exchange between the converters. The injected voltage with controllable magnitude and phase angle in series with the line via an injection transformer the main function of UPFC is provided by VSC. This injected voltage act as a synchronous ac voltage source. The current flows through voltage source resulted in reactive and active power exchange between it and the ac system. At the dc terminal the reactive power exchanged is generated internally by the converter. At the ac terminal the real power exchanged is converted into dc power which appears at the dc link as a real power demand and VSC1 is to supply or absorb the real power demanded by converter2 at the common dc link to support real power exchange resulting from

the series voltage injection. The dc link power demand of VSC2 is converted back to ac by VSC1 and coupled to the transmission line bus via shunt connected transformer. In addition, VSC1 can also generate or absorb controllable reactive power if it is required and thereby provide independent shunt reactive compensation for the line. Thus, VSC1 can be operated at a unity power factor or to be controlled to have a reactive power exchange with the line independent of the reactive power exchanged by VSC1. Therefore, there can be no reactive power flow through the UPFC dc link.

2.5.3 *STATCOM versus UPFC*

a) STATCOM has the advantage of smaller in dimension as compared to UPFC which is sophisticated.

b) STATCOM is much simpler unlike UPFC which is more complex.

c) UPFC has a faster response as compared to STATCOM.

d) UPFC is more expensive and complicated as compared to others FACTS devices.

2.5.4 Application of STATCOM and UPFC

a) The networks that have a poor power factor and often poor voltage regulation STATCOM is installed. The most common use of this device is for voltage stability.

b) Voltage stability is one of the biggest problems in power systems.

c) UPFC are proposed to improve the overall performance of a DFIG-based WECS during voltage sag and voltage swell events at the grid side.

3. Proposed Method

To improve stability and quality of power due to the instability created by wind generation integration as well as fault in the power systems and the improvement is done by using STATCOM and UPFC.

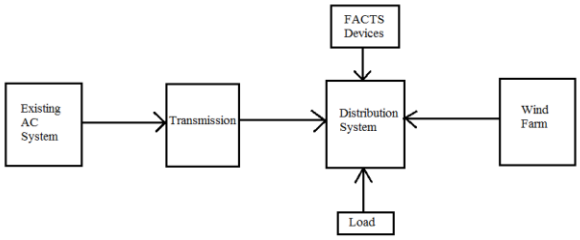

Figure 3.1: Block diagram of the proposed system

A power system with wind generation is designed here. When wind generation is connected with the existing AC system, instability in the system takes place. Thus FACTS device is connected with the system to reduce the voltage and power fluctuations caused due to wind generation and during fault.

Firstly, the STATCOM which is a shunt compensator is connected with the system to improve the stability.

Secondly, UPFC which is a combined compensator is connected with the system to improve the stability of the system.

Here, performance of the STATCOM and UPFC is analyzed with the help of load voltage and power waveforms.

3.1 Simulink model and implementation

The proposed model is designed in SIMULINK tool of MATLAB software. Voltage profile is checked here in normal condition (no fault condition) and in faulted condition with and without STATCOM and UPFC

3.1.1 Transmission line model under normal condition

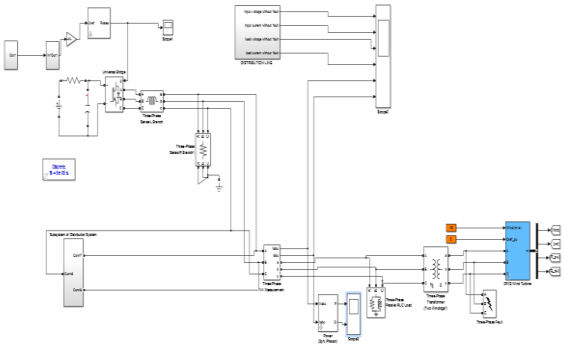

Figure 3.5: Simulation of the system with STATCOM with L-L-L-G fault

In this simulation, a STATCOM is simulated for checking the output and input waveform of the system. In this system, a subsystem is connected into the line which consists of the system simulated without the presence of fault, Wind Turbine and STATCOM. A STATCOM is connected in parallel to the line. Fault of 0.02 to 0.1 sec is applied to this system and is connected in parallel to the system.

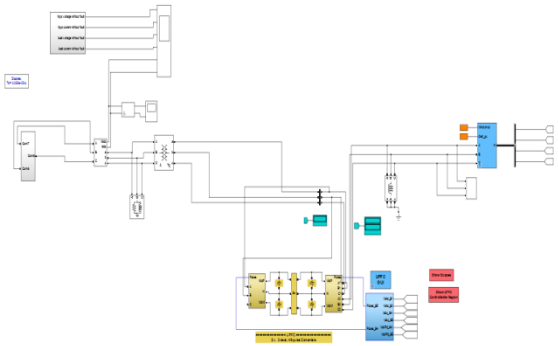

Figure 3.6: Simulation of the system with UPFC

In this simulation, the system with fault is extended by connecting a UPFC and is simulated for checking the output and input waveform of the system. The UPFC consist of two 100MVA, three-level, 48-pulse GTO-based converters, one connected in shunt and one connected in series. The simulation models of the transmission line with UPFC with the application of fault are given in figure 3.6.

4. Results and Analysis

4.1 Voltage waveforms with wind Turbine and STATCOM

During normal condition the voltage level in each phase of both input and load are almost same because of small voltage drop in the system. The magnitude of the load voltage is almost 11kV.

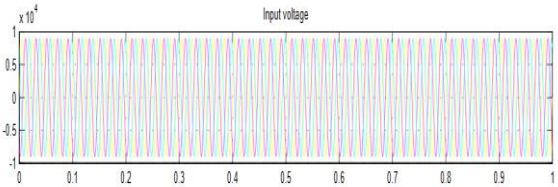

Figure 4.1: Input voltage under normal condition

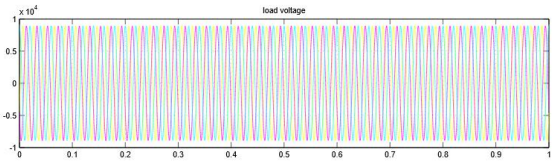

Figure 4.2: Load voltage under normal condition

4.2 Load voltage with fault

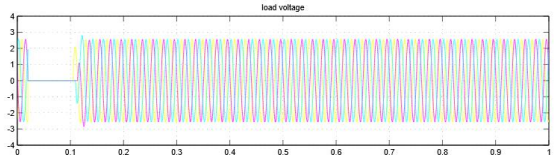

Figure 4.3: Load voltage on the presence of fault

During the application of fault for time duration of 80ms i.e. from 0.02s to 0.1s the load voltage of all the three phase drops to almost zero.

4.3 Load voltage with wind farm and fault

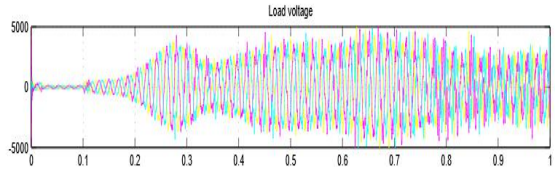

Figure 4.4: Waveform of Load voltage

From the fig 5.4 when a three phase to ground fault is applied with fault resistance of 0.001Ω for time duration of 80ms i.e. from 0.02s to 0.1s the voltage becomes approximately zero.

4.4 Load voltage with STATCOM

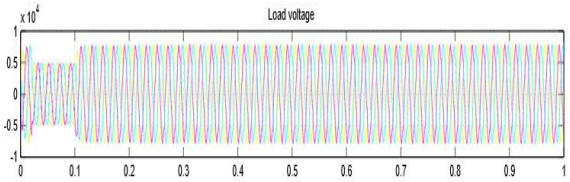

Figure 4.5: Load voltage waveform with STATCOM

Figure 4.5 shows the simulation of the system is carried out by introducing the STATCOM to compensate the voltage sag occurred. From the test model, it is found that after connecting the STATCOM, the load voltage is similar to the supply voltage which indicates that the STATCOM installed in the line is working properly.

4.5 Active and reactive power with STATCOM

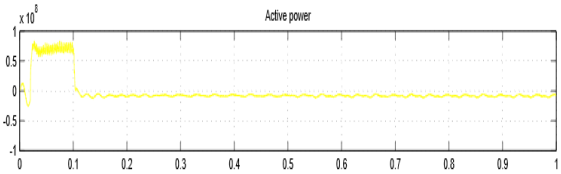

Figure 4.6: Waveform of active power through the line with STATCOM

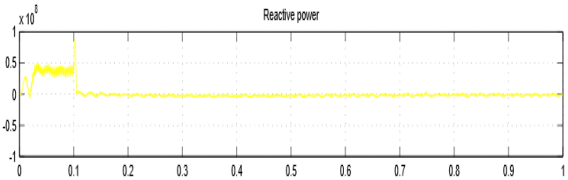

Figure 4.7: Waveform of reactive power through the line with STATCOM

Figure 4.6 and figure 4.7 shows Active and Reactive power in the line, a fault is applied from 0.02s to 0.1s. It is observed from the figures that during fault the active and reactive powers increases from its normal values. Even with the present of STATCOM during fault condition the power increases.

4.6 Load voltage with UPFC

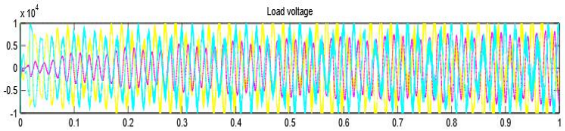

Figure 4.8: Waveform of load voltage through the line with UPFC

Figure 4.8 showsthe simulation of the system is carried out by introducing the UPFC to compensate the voltage sag occurred. From the test model, it is found that after connecting the UPFC, the load voltage is similar to the supply voltage even when fault is applied; but a lot of harmonics is present.

4.7 Active and reactive power with UPFC

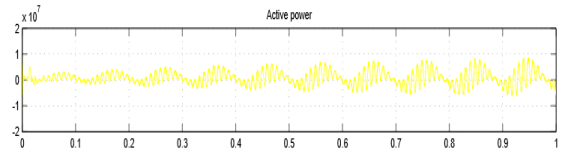

Figure 4.9: Waveform of active power through the line with UPFC

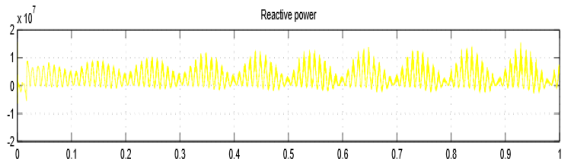

Figure 4.10: Waveform of reactive power through the line with UPFC

Figure 4.9 and figure 4.10 shows Active and Reactive power flows through the line during fault condition i.e. on the application of fault from 0.02s to 0.1s. It is observed from the figures that during fault the active and reactive powers decreases slightly than the active and reactive power when STATCOM is connected with the system, which indicates that incase of power compensation UPFC is better than STATCOM.

5. Conclusion

Wind power which is one of the important renewable sources is considered in order to analyze the effect of this generation on voltage operation and at the voltage stability limits. It can also be concluded that STATCOM and UPFC can withstand the successive disturbances of the system more efficiently than other FACTS devices. In this system many problems occur, and these problems are compensated by using STATCOM and UPFC. They full fill the reactive power requirement when fault occur in the system, because when fault occurred voltage low and system get unstable. The impacts of the STATCOM on the stability of the system during different fault locations and different fault duration times are studied. The control and performance of UPFC using shunt and series controller is studied. It is observed that during abnormal condition the voltage experience a large amount of fluctuation in comparison to the normal condition. The STATCOM and UPFC are connected to the three-phase transmission system and the results are compared.

It is observed during fault condition the active and reactive powers in case of UPFC reduces slightly more as compared to active and reactive power when STATCOM is connected to the system, which indicates that incase of power compensation, UPFC is better than STATCOM.

6. Limitations

The performance of the STATCOM shows that the power during fault is much high compared to the UPFC, i.e., the designed STATCOM was unable to maintain power through the line constant. The limitation is that harmonics caused due to operation of converters in UPFC is still present in the system. Proper filter circuit can be used to improve the performance of both UPFC.

7. Future Research

In this work, we have designed STATCOM with PI Controller. The performance shows that the load voltage during fault is not exactly same as the voltage before fault so the performance of the STATCOM can be increased by using other controllers like Fuzzy controller. Here performance of UPFC is shown with the use of available blocks in the Simulink library, so the design of UPFC as well as wind farm can also be done using MATLAB Simulink software. Fuzzy controller can also be used for UPFC control to improve the performance of UPFC.

References

[1] B. Bouhadouza, G. Ahmed and M. Hacene, “Application of STATCOM to Increase Transient Stability of Wind Farm”, *American Journal of Electrical Power and Energy*

Systems, Vol. 2, Issue No. 2, 2013, pp. 50-56. Doi: 10.11648/j.epes.20130202.14

[2] O. Noureldeen, M. Rihan, B. Hasanin, "Stability improvement of fixed speed induction generator wind farm using STATCOM during different fault locations and durations", *Ain Shams Engineering Journal*, Vol. 2, Issue No. 1, 2011, pp.1-10. Doi: 10.1016/j.asej.2011.04.002

[3] Q. Salem and I. Altawil, "Transient Stability Enhancement of Wind Farm Connected to Grid Supported with FACTS Devices". *International Journal of Electrical Energy*, Vol. 2, Issue No. 2, June 2014. Doi: 10.12720/ijoee.2.2.154-160

[4] M. T. Hagh, A. R. Milani and A. Lafzi, "Dynamic Stability Improvement of a Wind Farm Connected to Grid Using STATCOM", *Proceedings of 2008 5th International Conference on Electrical Engineering/Electronics, Computer, Telecommunications and Information Technology*, Krabi, 2008, pp. 1057-1060. doi: 10.1109/ECTICON.2008.4600614

[5] V. Chavhan and A. A. Ghute, "Stability Improvement of Wind Generation Using FACTS Device", *Proceedings of Technical Research Paper Competition for Students (TRPCS-2K17)*, 23 March 2017, G. H. Raisoni College of Engineering and Management, Amravati, Maharashtra, India. Retrieved from https://www.ijsr.net/conf/TRPCS2017/TRPCS2K17-15.pdf

[6] V. Patel and R. K. Paliwal, "A Study on Improvement of the Transient Stability Using STATCOM in DFIG Based Wind Farm", *International Journal of Modern Trends in Engineering and Research*, Vol. 2, Issue No. 3, March 2015. Retrieved from https://www.ijmter.com/papers/volume-2/issue-3/a-study-on-improvement-of-the-transient-stability-using-statcom-in-df.pdf

[7] M. Amiri and M. Sheikholeslami, "Transient Stability Improvement of Grid Connected Wind Generator Using SVC and STATCOM", *Proc. of International conference on Innovative Engineering Technologies (ICIET'2014)*, Dec. 28-29, 2014, Bangkok (Thailand). Doi: org/10.15242/IIE.E1214025

[8] V. S. Kumar, A. F. Zobaa, R. D. Kannan and K. Kalaiselvi, "Power Quality and Stability Improvement in Wind Park System Using STATCOM", *Jordan Journal of Mechanical and Industrial Engineering*, Vol. 4, Issue No. 1, pp. 169-176. Retrieved from http://jjmie.hu.edu.jo/files/v4n1/24.pdf

[9] S. Gupta, R. K. Tripathi and R. D. Shukla, "Voltage Stability Improvement in Power Systems using Facts Controllers", *2010 International Conference on Power, Control and Embedded Systems*, Allahabad, 2010, pp. 1-8. Doi: 10.1109/ICPCES.2010.5698665

[10] M. K. Deshmukh and C. B. Moorthy, "Review on Stability Analysis of grid connected Wind Power Generating System", *International Journal of Electrical and Electronics Engineering Research and Development (IJEEERD)*, Vol. 3, Issue No.1, pp.01-33, Jan-March 2013. Retrieved from https://pdfs.semanticscholar.org/df55/0094415823206090dfacdac11a276d312449.pdf

[11] A. K. Mishra, R. Lekshmana, S. P. Chowdhury and S. Chowdhury, "Review of Wind Turbine System and its Impact for Grid Stability" *Journal of Electrical Engineering*, Vol. 11, Issue No. 1, 2011, pp. 153-165.

A Review on Application of Biosensors for Cancer Detection

Nilakshi Devi[1], Shakuntala Laskar[2]

[1,2]Department of Electrical and Electronics Engineering, School of Technology, Assam Don Bosco University, *Airport Road, Azara, Guwahati -781017, Assam, INDIA.*
[1]*nilakshidevi4@gmail.com**, [2]*shakuntala.lashkar@dbuniversity.ac.in*

Abstract: ***Cancer is a deadly disease that has devastated many lives over the years. Cancer, when detected in the early stage, can be cured through proper treatment, increasing the life expectancy of the patient. Thus, it is very important to detect cancer at the early stage. The current method of cancer detection is biopsy which is a total invasive medical procedure. Owing to the several limitations of the time-consuming procedure of biopsy researchers and scientist all over the globe have turned their attention towards the development of instruments for rapid and non-invasive detection of cancer through detection of clinically recognized cancer biomarkers present in blood and other body fluid of cancer patients. This paper discusses some of the novel biomarkers used for cancer diagnosis along with the potential use of biosensors in early detection of cancer.***

Keywords: Biomarkers, Biopsy, Biosensors, Cancer

1. Introduction

Cancer is a deadly disease responsible for many deaths over the years. More than 575,000 people die of cancer, and 1.5 million people are diagnosed with cancer per year only in the U.S. [1]. Cancer is caused due to uncontrolled cell growth. There are over 100 types of different cancers arising in different parts of the body [2]. Some of the common cancers are Kidney, Liver, Ovarian, Colon, Stomach etc. The exact cause of cancer is yet to be known to medical science. It is believed that cancer risk can be reduced by avoiding tobacco, limiting alcohol intake, limiting exposure to UV rays from the sun and maintaining a regular healthy diet. According to the World Health Organization, (WHO), the number of new cases is expected to rise by 70% over the next 20 years [3]. Tumor is mainly are of two types: Benign and Malignant. A benign tumor is less harmful and can be removed through surgery whereas malignant tumors are aggressive and decrease the life expectancy of the patient. A tumor when metastasized becomes cancer and spread from one organ to another throughout the body through blood. Such cancers are responsible for the majority of deaths around the world. Thus, early detection of cancer is of utmost importance. The current method of detection of cancer is biopsy which is an invasive process. A Biopsy is a medical procedure which requires the insertion of medical instruments in the patient's body for removal of certain tissues to be examined to find the presence of cancer cells. Such a process is time-consuming and further has many limitations. Patients undergoing biopsy complains of weak health, nausea, insomnia etc. with further post-biopsy effects. Thus, the need for non-invasive detection has come into importance in the modern time. In addition, the need of rapid detection is of utmost importance to give immediate results to the patients so that their treatment can be started without wasting any time. Thus, this need for rapid non-invasive detection of cancer has led the researchers to develop instruments which would detect cancer early without the need of an invasive procedure. This has led to the development of biosensors for non-invasive rapid early detection of cancer.

2. Cancer Biomarkers

Due to several disadvantages of invasive procedure of cancer detection researchers and scientist from all over the globe have turned their attention towards non-invasive diagnosis of cancer using Cancer Biomarkers. According to the National Cancer Institute, a biomarker is a biological molecule found in blood, other body fluids, or tissues that is a sign of normal or abnormal process of a condition or disease such as cancer [4]. Biomarkers may be proteins, nucleic acids or peptides. In medicine however, cancer biomarkers are limited to proteins only. The presence of biomarkers in blood or any other body fluids confirms the presence of cancer cells in the body. There are different biomarkers for different types of cancers. For example, the biomarkers CYFRA (Cytokeratin19fragments), CEA (Carcinoembryonic antigen), EGFR (epidermal growth factor response), SCC (squamous cell carcinoma antigen are used for detection of lung cancer [5]. Biomarkers MUC-1(CA27.29 and CA

15-3) and carcinoembryonic antigen are the two biomarkers that are approved by the Food and Drug Administration (FDA) for monitoring and treatment of the advanced or recurrence breast cancer [6]. Biomarkers such as CA-125, CA 72-4 have been clinically used for ovarian cancer [7]. Biomarker CA 19-9 has been clinically used to detect Pancreatic Cancer [8]. Alpha-fetoprotein biomarker is widely used for detection of hepatocellular carcinoma (HCC) [9]. Prostate Specific Antigen (PSA) is the most widely used biomarker for prostate cancer [10]. High levels of CEA, mutated KRAS, TP53, APC are recognized biomarkers for colorectal cancer [11]. Carbonic anhydrase IX (CA-IX) biomarker is used to Renal Cell Carcinoma [12]. The recognized biomarkers for oral cancer are IL-8, IL-1-β and S100P [13]. High levels of epidermal growth factor receptor (EGFR) alongwith expression of 0-6 methylguanine-DNA methyltransferase (MGMT) have been clinically used as a biomarker for malignant brain cancer (gliblastomas) [14]. Mutation of oncogenes such as FLT3, KIT are considered as biomarkers for acute leukemia [15]. Human papillomavirus (HPV) is the single most important etiological agent in cervical cancer, contributing to neoplastic progression through the action of viral oncoproteins, mainly E6 and E7 [16]. Classic biomarkers for gastric cancer diagnosis include carcinoembryonic antigen and cancer antigen 19-9, while microRNA and DNA hypomethylation are proposed as novel biomarkers [17]. RASSF1A methylation has been considered as a biomarker in melanoma (skin cancer) patients [18]. In the modern era the two disciplines of proteomics and genomics have helped the researchers to identify novel biomarkers for cancer detection [19]. Today different biomarkers have been used clinically for screening, diagnosis and monitoring for different cancers. Biomarkers are found in different quantities in blood, saliva and other body fluids [20]. Biomarkers have been recognized as a novel approach for early cancer detection.

3. Biosensors

Owing to the non-invasive early detection of cancer researchers over the globe have started to design and develop biosensors that could detect cancer efficiently. Biosensors are devices that are designed to detect a specific biological analyte by essentially converting a biological entity (protein, DNA, RNA) into an electrical signal that can be detected and analyzed [21]. Since the sensor senses biological materials the word “Bio” comes into play. The biological material can be enzymes, antibodies, micro-organisms, nucleic acids etc. Prof. Leland C. Clark Jr. is known as the “father of biosensors” and the modern day glucose sensor is based on his research [22]. The three most important elements of a biosensor are a biological recognition element, a transducer and a signal processing system [23]. The biological element must be highly specific, stable and immobilized. Based on the biological recognition element biosensors are classified into the following categories: enzymatic, protein, receptor based, DNA and whole cell biosensors [24]. The transducer converts recognition signal events into electrical signals. Based on the signal transduction mechanism biosensors are further classified into the following categories: Electrochemical, Thermal, Optical and Mass Sensitive Sensors [25]. Electrochemical transducers are the most widely used in sensor technology but however, optical transducers are gaining importance in the modern era due to their several advantages. Signals from the transducer are passed to an electronic system for amplification and display.

4. Biosensors for Cancer Marker Detection

Researchers and scientist are trying to design and develop biosensors for detecting cancer markers to detect early cancer. The use of biosensors for protein biomarker analysis has been developed as an attractive and cost effective technique for the development of point of care devices [26]. Electrochemical biosensors have played a significant role in cancer marker detection [27]. Sensors based on spectroscopy of surface plasmons, sometimes referred to as surface plasmons resonance sensors (SPR) are being used for label free detection of cancer markers [28]. Piezoelectric biosensors have also been exploited for cancer marker detection due to their light weight, high sensitivity and low power requirement [29]. W. Tan *et al.* [30] have developed a surfaced immobilized optical protein sensor to detect an IL-8 marker for oral cancer detection. J. Yuan *et al.* [31] have developed an SPR based biosensor for the detection of cancer markers in ovarian cancer. T. Kumeria *et al.* [32] have developed a microchip biosensor based on nanoporous aluminia for detection of circulating tumor cells. A. Malima *et al.* [33] have developed a highly sensitive microscale in-vivo sensor enabled by the electrophoretic assembly of nano particles for multiple biomarker detections. Optical Biosensors are gaining importance in the modern era for detection of biomarkers due to its high sensitivity, specificity, small size, rapid and cost effectiveness [34]. High multi disciplinary approaches like nanotechnology, MEMS (micro electro mechnaical systems), NEMS, biotechnology etc have been used in the implementation of new optical biosensors.

5. Conclusion

Due to the several limitations in conventional detection techniques of cancer researchers and scientist are turning their attention towards the development of biosensors for efficient rapid non-invasive detection of cancer markers. Cancer markers confirm the presence of cancer cells in the body. These markers are present in blood, saliva or any other body fluids. Novel biomarkers for different cancers are still in the process of research, although a few of them have been clinically used for screening and monitoring of cancer patients. The development of biosensors paves a new novel approach for rapid early detection of cancer. Different biosensors have been designed by researchers for efficient of the cancer markers. Optical biosensors are gaining importance over other biosensors due to its several advantages. However, the development of biosensors for multiple cancer marker detection is still a big challenge to the scientist and researchers. Integration of high multi disciplinary approaches along with the use of nanomaterials in development of biosensors will enhance the sensitivity of these devices and make it more efficient for early detection of cancer which is the need of the hour.

References

[1] "Cancer: What you need to know", *Medical News Today*. [Online]. Available: https://www.medicalnewstoday.com/info/cancer-oncology (Accessed: Sept. 12, 2018).

[2] "Cancer: What you need to know", *Medical News Today*. [Online]. Available: https://www.medicalnewstoday.com/info/cancer-oncology (Accessed: Sept. 12, 2018).

[3] "Cancer: What you need to know", *Medical News Today*. [Online]. Available: https://www.medicalnewstoday.com/info/cancer-oncology (Accessed: Sept. 12, 2018).

[4] N. L. Henry and D. F. Hayes, "Cancer Biomarkers", *Molecular Oncology*, Vol. 6, 2012, pp. 140-146. Doi: https://doi.org/10.1016/j.molonc.2012.01.010

[5] Hoseok, I. and J. Y. Cho, "Lung Cancer Biomarkers" in *Advances in Clinical Chemistry*, Gregory S. Makowski (ed.),Vol. 72, pp. 107-170, Elsevier, US, 2015. Doi: https://doi.org/10.1016/bs.acc.2015.07.003

[6] L. H. Gam, "Breast Cancer and Protein Biomarkers", *World Journal of Experimental Medicine*, Vol. 2, Issue No. 5, 2012, pp. 86-91. Doi: http://dx.doi.org/10.5493/wjem.v2.i5.86

[7] G. Mor *et al.*, "Serum Protein Markers for Early Detection of Ovarian Cancer", *Proceedings of the National Academy of Sciences*, May 2005, Vol. 102, Issue No. 21, pp. 7677-7682. Doi: https://doi.org/10.1073/pnas.0502178102

[8] M. Herreros-Villanueva and L. Bujanda, "Non-invasive Biomarkers in Pancreatic Cancer Diagnosis: what we versus what we have", *Annals of Translation Medicine*, Vol. 4, Issue No. 7, 2016. Retrieved from http://atm.amegroups.com/article/view/9796

[9] J. Lou, L. Zhang, S. Lv, C. Zhang and S. Jiang, "Biomarkers for Hepatocellular Carcinoma", *Biomarkers in Cancer*, Vol. 9, 2017, pp. 1-9. Doi: http://doi.org/10.1177/1179299X16684640

[10] P. O. Gaudreau, J. Stagg, D. Soulières and F. Saad, "The Present and Future of Biomarkers in Prostate Cancer: Proteomics, Genomics, and Immunology Advancements", *Biomarkers in Cancer*, Vol. 8 (Suppl. 2), 2016, pp. 15-33. Doi: https://doi.org/10.4137/BIC.S31802

[11] G. Lech, R. Słotwiński, M. Słodkowski and I. W. Krasnodębski, "Colorectal Cancer Tumor Markers and Biomarkers: Recent Therapeutic Advances", *World Journal of Gastroenterology*, Vol. 22, Issue No. 5, 2016, pp. 1745-1755. Doi: http://dx.doi.org/10.3748/wjg.v22.i5.1745

[12] N. J. Farber, C. J. Kim, P. K. Modi, J. D. Hon, E. T. Sadimin and E. A. Singer, "Renal cell carcinoma: the search for a reliable biomarker", *Translational Cancer Research*, Vol. 6, Issue 3, 2017, pp. 620–632. Doi: http://doi.org/10.21037/tcr.2017.05.19

[13] S. Saxena, B. Sankhla, K. S. Sundaragiri and A. Bhargava, "A Review of Salivary Biomarker: A Tool for Early Oral Cancer Diagnosis", *Advanced Biomedical Research*, Vol. 6, 2017, pp. 90. http://doi.org/10.4103/2277-9175.211801

[14] A. El-Jawahri, D. Patel, M. Zhang, N. Mladkova and A. Chakravarti, "Biomarkers of Clinical Responsiveness in Brain Tumor Patients: Progress and Potential", *Molecular Diagnosis & Therapy*, Vol. 12, Issue No. 4, July 2008, pp. 199–208. Doi: https://doi.org/10.1007/BF03256285

[15] J. Prada-Arismendy, J. C. Arroyave and S. Röthlisberger, "Molecular Biomarkers in Acute Myeloid Leukemia", *Blood Revie*ws, Vol. 31, Issue 1, 2017, pp. 63-76. Doi: https://doi.org/10.1016/j.blre.2016.08.005

[16] E. K. Yim and J. S. Park, "Biomarkers in Cervical Cancer", *Biomarker Insights*, Vol. 1, 2006, pp. 215-225. Doi: https://doi.org/10.1177%2F117727190600100015

[17] Z. Jin, W. Jiang and L. Wang, "Biomarkers for Gastric Cancer: Progression in Early Diagnosis and prognosis", *Oncology Letters*, Vol. 9, Issue No. 4, 2015, pp. 1502-1508. Doi: https://doi.org/10.3892/ol.2015.2959

[18] E. S. Greenberg, K. K. Chong, K. T. Huynh, R. Tanaka and D. S. B. Hoon, "Epigenetic Biomarkers in Skin Cancer", *Cancer Letters*, Vol. 342, Issue No. 2, 2014, pp. 170-177. Doi: https://doi.org/10.1016/j.canlet.2012.01.020

[19] S. Kumar, A. Mohan and R. Guleria, "Biomarkers in Cancer Screening, Research and Detection: present, past and future: A Review", *Biomarkers*, Vol. 11, Issue No. 5, 2006, pp. 385-405. Doi: https://doi.org/10.1080/13547500600775011

[20] R. Mayeux, "Biomarkers: Potential Uses and Limitations", *NeuroRx*, Vol. 1, Issue No. 2, 2004, pp. 182-188. Doi: https://doi.org/10.1602/neurorx.1.2.182

[21] B. Bohunicky and S. A. Mousa "Biosensors: the new wave in cancer diagnosis", *Nanotechnology, Science and Applications*, Vol. 4, 2011, pp. 1-10. Doi: https://doi.org/10.2147/NSA.S13465

[22] "Leland Clark", *Wikipedia*. [Online]. Available: https://en.wikipedia.org/wiki/Leland_Clark (Accessed: 12 Sept. 2018).

[23] V. Perumal and U. Hashim, "Advances in Biosensors: Principle, architecture and applications", *Journal of Applied Biomedicine*, Vol. 12, Issue No. 1, 2014, pp. 1-15. Doi: https://doi.org/10.1016/j.jab.2013.02.001

[24] I. E. Tothill, "Biosensors for cancer marker diagnosis", *Seminars in Cell and Developmental Biology*, Vol. 20, Issue 1, Feb. 2009, pp. 55-62. Doi: https://doi.org/10.1016/j.semcdb.2009.01.015

[25] I. E. Tothill, "Biosensors for cancer marker diagnosis", *Seminars in Cell and Developmental Biology*, Vol. 20, Issue 1, Feb. 2009, pp. 55-62. Doi: https://doi.org/10.1016/j.semcdb.2009.01.015

[26] S. A. Soper *et al.*, "Point-of-care biosensor systems for cancer diagnostics/prognostics", *Biosensors and Bioelectronics*, Vol. 21, Issue No. 10, 2006, pp. 1932-1942. Doi: https://doi.org/10.1016/j.bios.2006.01.006

[27] J. Wang, "Electrochemical Biosensors: towards point-of-care cancer diagnostics", *Biosensors and Bioelectronics*, Vol. 21, Issue 10, 2006, pp. 1887-1892. Doi: https://doi.org/10.1016/j.bios.2005.10.027

[28] S. Chaitra, C. Veena, K. S. Rao and P. Sharan, "SPR based biosensors for detection of abnormal growth of tissues", *2017 International Conference on Nextgen Electronic Technologies: Silicon to Software (ICNETS2)*, Chennai, 2017, pp. 149-153. Doi: 10.1109/ICNETS2.2017.8067918

[29] M. T. Islam and M. Ashab-Uddin, "Biosensors, the Emerging Tools in the Identification and Detection of Cancer Markers", *Journal of Gynecology and Women's Health*, Vol. 5, Issue No. 4, 2017. Doi: http://dx.doi.org/10.19080/JGWH.2017.05.555667

[30] W. Tan *et al.*, "Optical Protein sensors for detecting cancer markers in saliva", *Biosensors and Bioelectronics*, Vol. 24, Issue No. 2, 2008, pp. 266-271. Doi: https://doi.org/10.1016/j.bios.2008.03.037

[31] J. Yuan, R. Duan, H. Yang, X. Luo and M. Xi. "Detection of serum human epididymis secretory protein 4 in patients with ovarian cancer using a label-free biosensor based on localized surface plasmon resonance", *International Journal of Nanomedicine*, Vol. 7, 2012, pp. 2921-2928. Doi: https://doi.org/10.2147/IJN.S32641

[32] T. Kumeria, M. D. Kurkuri, K. R. Diener, L. Parkinson and D. Losic, "Label-free reflectometric interference microchip biosensor based on nanoporous alumina for detection of circulating tumour cell", *Biosensors and Bioelectronics*, Vol. 35, Issue No. 1, May 2012, pp. 167-173. doi: https://doi.org/10.1016/j.bios.2012.02.038

[33] A. Malima *et al.*, "Highly sensitive microscale in vivo sensor enabled by electrophoretic assembly of nanoparticles for multiple biomarker detection" *Lab on A Chip*, Vol. 12, Issue No. 22, 2012, pp. 4748-4754. Doi: http://dx.doi.org/10.1039/C2LC40580F

[34] P. Damborský, J. Švitel and J. Katrlík, "Optical Biosensors", *Essays in Biochemistry*, Vol. 60, Issue No. 1, 2016, pp. 91-100. Doi: https://doi.org/10.1042/EBC20150010

Authors' Profile

Nilakshi Devi is a Ph.D. research scholar in the Department of Electrical and Electronics Engineering, Assam Don Bosco University. She is currently working on development of biosensor for cancer detection. She has completed her M.Tech. in Electronics and Communication Engineering in 2016 from ADBU. Her research area includes Sensors, Fiber Optic Sensors, Biosensors, Image Processing and Artificial Intelligence.

Dr. Shakuntala Laskar is working as Professor and HOD of EEE Department, Don Bosco College of Engineering and Technology (School of Technology), Assam Don Bosco University. She received her bachelor degree in Electrical Engineering from Assam Engineering College, Gauhati University and M.Tech. and Ph.D. from IIT Khagrapur.

Analysis of Self Excited Induction Generator for Standalone Micro-Hydro Scheme

Dinesh Kumar Mallik[1], Jesif Ahmed[2]

[1]Council for Technical Education and Vocational Training, Nepal
*dineshmallik45@gmail.com**

[2]School of Technology, Assam Don Bosco University
jesif.ahmed@dbuniversity.ac.in

Abstract: ***Most of population which they do not have electricity are living in remote rural areas or off grid, to provide electricity for remote areas is a challenging task which require a huge investment and infrastructure, it is therefore convenient to provide them with decentralized energy system like distributed generation or hybrid system etc. utilizing the available renewable energy. This paper presents study results about the dynamic analysis of self-excited induction generator for micro-hydro power plant in which generation is carried out by the use of self-excited induction generator (SEIG). It can be a very effective solution to the power shortage in the hilly regions of developing countries, like Nepal, Bhutan etc. It is more economical than other possible electric power sources, because it requires simple design and semi-skilled persons; local manufacturers can manufacture the components. SEIG is becoming more and more popular, mainly due to its low cost, simple construction, robustness of its rotor design and low maintenance requirements. When Induction motor is used as a generator, the major problem is its terminal voltage fluctuation at varying load and varying speeds. To predict the dynamic behavior of SEIG driven by a constant torque from micro-hydro turbine is carried out by using MATLAB/SIMULINK under different loading conditions. The model has been developed using "SimPowerSystem" library from MATLAB to perform the simulation.***

Keywords: Induction Generator, Induction Motor, SFIG, Electronic load controller, dump load, SVC, Hydro-turbine, MATLAB SIMULINK

1. Introduction

The increasing concern toward environmental problems (global warming which is caused by emission of green house gases), the depletion of fossil fuel, the oil prices uncertainty, growing energy demand and the need for low generation cost has led to look for an alternatives and sustainable source of energy by harnessing abundance renewable energy which is available in the nature such as wind, solar, biogas, micro, mini, and small hydro, at this time the generation of electricity has been mainly dominated by conventional sources such as Thermal, Nuclear etc.to meet the growing demand for energy and also to electrify the remote areas where the extension of grid is not economical and unfeasible [1,2].

Wind and hydro systems requires electro-mechanical energy conversion system to convert the kinetic energy available in water as for hydro system or kinetic energy available in wind as for wind system to rotational mechanical energy through prime mover to drive the generator which is couple with the prime mover directly or indirectly through coupling arrangement to produce electricity [3].

Previously synchronous generator dominate the generation of electricity but induction generator emerge and become more applicable in the field of renewable energy because of their relative advantages over the synchronous generator, the induction generator is rugged can with stand rough condition, brushless, low cost, and low maintenance and operation cost, self-protected against short-circuit, and it is capable of generating power at various range of speed, it require external source for excitation to generate a rotating magnetic field, the required reactive power for excitation can be supplied from the grid in this mode known as grid connected induction generator, or it can be supplied by a capacitor connected to the stator terminal in this mode it is known as self-excited induction generator [2].

When an induction machine is driven by prime-mover (water turbine or wind turbine) to speed higher than synchronous speed in negative sleep the induction machine can operate as generator mode. When capacitors are connected across stator terminal it can operate in self-excited mode [4-8].

Minimum excitation capacitors required for excitation can be calculated by analytical method [9,10], Fuzzy Logic approach [11], nodal

admittance method, loop analysis method and L-C resonance method [12-14,15].

The major drawback of using self-excited induction generator (SEIG) in micro-hydro power plant is its terminal voltage and frequency fluctuation at varying loads and speed. Frequency can be controlled by using converter and inverter whereas terminal voltage can be controlled by adjusting the value of excitation capacitors connected in stator terminals of SEIG and its speed [16-19].

2. Working of Induction Generator

An induction generator or asynchronous generator is a type of alternating current (AC) electrical generator that uses the principles of induction motors to produce power. Mostly Induction generators are used to generate the power in small scale. Generally to reduce the installation cost of micro-hydro power plant or wind power plant Induction generator is used. The working principle of Induction Generator (IG) is same as that of induction Motor (IM). When three phase supply is fed to the IM, a RMF (Rotating Magnetic Field) is produced which rotates at the speed of synchronous speed $(N_s = \frac{120f}{P}$, Where ' N_s' is synchronous speed in rpm, 'f' is frequency in Hz and 'P' is no. of poles). When RMF is passed over the static rotor, current is induced which cause rotor flux, the polarity of rotor flux is opposite to the RMF and hence rotor drags behind the RMF and rotates in the same direction as RMF rotates. The Induction motor normally turns slightly lesser than synchronous speed, hence sleep (s) is developed.

The difference between synchronous speed (N_s) and rotor speed (N_r) is so called slip and it is expressed in percentage (%).

$$\%\, Slip(S) = \frac{N_s - N_r}{N_s} \times 100 \qquad \text{---------- (1)}$$

If rotor is rotated at more than synchronous speed (N_s) by using prime- mover (water turbine) the slip will become –ve and the rotor current is generated in the opposite direction. This generated rotor current produces the RMF in the rotor which push back on to the stator field. This causes a stator voltage which pushes current flowing out of the stator windings against the applied voltage. Thus it will work as an induction generator. As the rotor speed is increased above the synchronous speed, the induced voltage and the current in the rotor bars and the stator coils will increase as the relative speed between the rotor and the stator's rotating field and hence the slip increases. This in turn will require a higher torque to maintain the rotation. The output voltage of the generator is controlled by the magnitude of the excitation current [20].

3. Developed Scheme

In this model, 3-phase induction motor is rotated by water turbine which rotates at constant speed. A fixed capacitor bank is connected across IG terminals in star or delta (for 3-Φ output) or C-2C (for 1- Φ output) manner. A capacitor bank is used to supply the VAR demanded by the IG for excitation.

Generally for micro-hydro power plant impulse turbine is used. Pelton turbine and cross-flow turbines are categorized under impulse turbine which is used for high head and low discharge and water inlet and outlet is radially. To minimize the cost of MHPP, generally cross-flow turbine is used because it can be made locally.

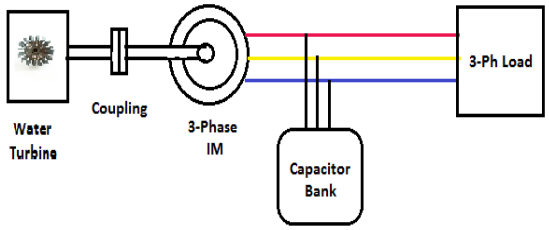

Fig. 1: Block diagram of proposed mole

The output power of hydro turbine can be estimated by using the potential equation. For 4 KW of generation assumed data's are shown in table 1 below.

Table 1: Turbine input parameters

Net head (H) (in m)	Flow rate (Q) (m^3/sec.)	Turbine efficiency (η)	Power (P) = $\boldsymbol{H * Q * \rho * g * \eta}$, watt $\boldsymbol{\rho}$ = 1000 Kg/m^3 $\boldsymbol{g}$ = 9.81 m/sec^2
5	0.1	0.85	4169

4. Modeling of self-excited Induction Generator (SEIG)

The *d-q* axes equivalent circuit diagram of self excite induction generator (SEIG) is shown in figures 2(a) and 2(b) below.

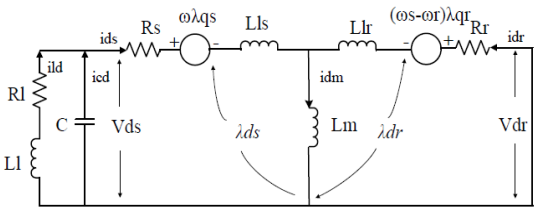

Fig. 2(a): *d*-axis circuit of SEIG

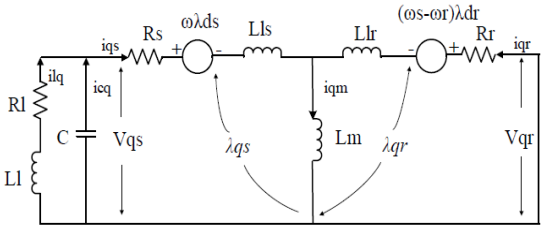

Fig. 2(b): q-axis equivalent circuit of SEIG

To analysis the d-q equivalent circuit of three phase induction generator, it is more convenient to convert the inductances into reactances to simplify the circuits. Let ω_b the base angular speed in rad/sec,

$$\omega_b = 2\pi f_s; \qquad X_{ls} = \omega_b L_{ls}$$
$$X_{lr} = \omega_b L_{lr}; \qquad X_m = \omega_b L_m \quad \text{-------- (2)}$$
$$\frac{1}{X_{lm}} = \left(\frac{1}{X_{ls}} + \frac{1}{X_{lr}} + \frac{1}{X_m}\right)$$

And the flux linkage can also be changed as follows:

$$\emptyset_{ds} = \omega_b \lambda_{ds}; \quad \emptyset_{qs} = \omega_b \lambda_{qs};$$
$$\emptyset_{dr} = \omega_b \lambda_{dr}; \quad \emptyset_{qr} = \omega_b \lambda_{qr} \quad \text{----------} \quad (3)$$

Where,

ω_b, ω_s, ω_r = base, stator and rotor angular speed (rad/sec.)

X_{ls}, X_{lr}. X_m = stator, rotor and magnetising leakage reactances.

$\emptyset_{ds}, \emptyset_{qs}, \emptyset_{dr}, \emptyset_{qr}$ = dynamic flux linkage of stator and rotor.

Voltage equations at synchronous reference frame:

$$V_{ds} = R_s i_{ds} + \frac{1}{\omega_b} p\emptyset_{ds} - \frac{\omega_s}{\omega_b}\emptyset_{qs}$$
$$V_{qs} = R_s i_{qs} + \frac{1}{\omega_b} p\emptyset_{qs} + \frac{\omega_s}{\omega_b}\emptyset_{ds} \quad \text{-------- (4)}$$
$$V_{dr} = R_r i_{dr} + \frac{1}{\omega_b} p\emptyset_{dr} - \frac{(\omega_s - \omega_r)}{\omega_b}\emptyset_{qr}$$
$$V_{qr} = R_r i_{qr} + \frac{1}{\omega_b} p\emptyset_{qr} + \frac{(\omega_s - \omega_r)}{\omega_b}\emptyset\lambda_{dr}$$

For squirrel cage rotor $V_{dr} = V_{qr} = 0$

The flux linkage equations can be written in term of currents as follows:

$$\lambda_{ds} = L_{ls} i_{ds} + L_m (i_{ds} + i_{dr})$$
$$\lambda_{dr} = L_{lr} i_{dr} + L_m (i_{ds} + i_{dr})$$
$$\lambda_{dm} = L_m (i_{ds} + i_{dr}) \quad \text{--------- (5)}$$
$$\lambda_{qs} = L_{ls} i_{qs} + L_m (i_{qs} + i_{qr})$$
$$\lambda_{qr} = L_{lr} i_{qr} + L_m (i_{qs} + i_{qr})$$
$$\lambda_{qm} = L_m (i_{qs} + i_{qr})$$

By multiplying equation (5) by the base angular frequency (ω_b) on both sides, the equation (5) can be written as:

$$\emptyset_{ds} = X_{ls} i_{ds} + X_m (i_{ds} + i_{dr})$$
$$\emptyset_{dr} = X_{lr} i_{dr} + X_m (i_{ds} + i_{dr})$$
$$\emptyset_{dm} = X_m (i_{ds} + i_{dr}) \quad \text{----------} \quad (6)$$
$$\emptyset_{qs} = X_{ls} i_{qs} + X_m (i_{qs} + i_{qr})$$
$$\emptyset_{qr} = X_{lr} i_{qr} + X_m (i_{qs} + i_{qr})$$
$$\emptyset_{qm} = X_m (i_{qs} + i_{qr})$$

Substituting the value of $\emptyset_{dm}$ and $\emptyset_{qm}$ in $\emptyset_{ds}$, $\emptyset_{dr}$ and $\emptyset_{qs}$,

$$\emptyset_{ds} = X_{ls} i_{ds} + \emptyset_{dm}$$
$$\emptyset_{dr} = X_{lr} i_{dr} + \emptyset_{dm} \quad \text{----------} \quad (7)$$
$$\emptyset_{qs} = X_{ls} i_{qs} + \emptyset_{qm}$$
$$\emptyset_{qr} = X_{lr} i_{qr} + \emptyset_{qm} \quad \text{----------} \quad (8)$$

From the equation (7} and (8), current equations can be obtained as:

$$i_{ds} = \frac{(\emptyset_{ds} - \emptyset_{dm})}{X_{ls}}; \quad i_{dr} = \frac{(\emptyset_{dr} - \emptyset_{dm})}{X_{lr}} \quad \text{---- (9)}$$
$$i_{qs} = \frac{(\emptyset_{qs} - \emptyset_{qm})}{X_{ls}}; \quad i_{qr} = \frac{(\emptyset_{qr} - \emptyset_{qm})}{X_{lr}}$$

Substituting the current equation (9) to find $\emptyset_{dm}$ and $\emptyset_{qm}$ equation as follows:

$$\emptyset_{dm} = \frac{X_{lm}}{X_{ls}}\emptyset_{ds} + \frac{X_{lm}}{X_{lr}}\emptyset_{dr} \quad \text{-------- (10)}$$
$$\emptyset_{qm} = \frac{X_{lm}}{X_{ls}}\emptyset_{qs} + \frac{X_{lm}}{X_{lr}}\emptyset_{qr}$$

By substituting the current equation (9) the voltage equations can be rewritten as follows:

$$V_{ds} = \frac{R_s}{X_{ls}}(\emptyset_{ds} - \emptyset_{dm}) + \frac{1}{\omega_b} p\emptyset_{ds} - \frac{\omega_s}{\omega_b}\emptyset_{qs}$$
$$V_{qs} = \frac{R_s}{X_{ls}}(\emptyset_{qs} - \emptyset_{qm}) + \frac{1}{\omega_b} p\emptyset_{qs} + \frac{\omega_s}{\omega_b}\emptyset_{ds}$$
$$V_{dr} = 0 = \frac{R_r}{X_{lr}}(\emptyset_{dr} - \emptyset_{dm}) + \frac{1}{\omega_b} p\emptyset_{dr} - \frac{(\omega_s - \omega_r)}{\omega_b}\emptyset_{qr}$$
$$V_{qr} = 0 = \frac{R_r}{X_{lr}}(\emptyset_{qr} - \emptyset_{qm}) + \frac{1}{\omega_b} p\emptyset_{qr} - \frac{(\omega_s - \omega_r)}{\omega_b}\emptyset_{dr} \quad \text{--- (11)}$$

The torque equation of SEIG is expressed as,

$$T_e = \frac{J}{P}\frac{d(\omega)}{dt} + \frac{B}{P}\omega + T_m \quad \text{----------} \quad (12)$$

Where,

T_e = Electromagnetic torque (N-m)
J = Rotor inertia (N-m^2)
P = Number of pole pairs
ω = Electrical angular speed (rad/sec)
B =Viscous frictional co-efficient
T_m = Mechanical Torque

Electromagnetic torque can express in term of reactances flux linkages and current as follow,

$$T_e = \frac{3}{2}\frac{P}{2}\frac{X_m}{(X_{lr}+X_m)\omega}\left(i_{qs}\emptyset_{dr} - i_{ds}\emptyset_{qs}\right) \quad \text{------} \quad (13)$$

And the electrical angular frequency by ignoring frictional Torque

$$\frac{d(\omega)}{dt} = \frac{P}{J}(T_e - T_m) \quad \text{----------} \quad (14)$$

Excitation capacitor model can be expressed as:

$$d\frac{V_{ds}}{dt} = -\frac{1}{C}i_{ds} + \frac{1}{C}i_{Ld}$$
$$d\frac{V_{qs}}{dt} = -\frac{1}{C}i_{qs} + \frac{1}{C}i_{Lq} \quad \text{----------} \quad (15)$$

Load impedance of SEIG expressed as:

$$\frac{d(i_{Ld})}{dt} = \frac{1}{L_l}(V_{ds} - R_l i_{Ld}) + \omega_s i_{Ld}$$
$$\frac{d(i_{Lq})}{dt} = \frac{1}{L_l}(V_{qs} - R_l i_{Lq}) + \omega_s i_{Lq} \quad \text{--------} \quad (16)$$

Where,

i_{Ld}; i_{Lq} = Load current of d and q- axis

R_l ; L_l *and* C = Load resistance, load inductance and excitation Capacitance

5. MATLAB/SIMULINK of SEIG

MATLAB/SIMULINK of IG is driven by hydro turbine. The hydro turbine model has been developed by using a potential and torque equation (17) and (18) respectively,

$$\boldsymbol{P = H * Q * \rho * g * \eta} \quad \text{----------} \quad \textbf{(17)}$$

$$T = P/\omega \quad \text{----------} \quad (18)$$

An induction motor block has been used from "SimpowerSystem" in MATLAB/ SIMULINK tool library as a self-excited induction generator. The specification of induction machine is as shown in table 2.

Table 2: Induction Machine Specification

Power (HP)	5.4 (4 KW)
Voltage	400 V
Current	8.24 A
Phase	3
Nominal Speed	1430 rpm
Synchronous Speed	1500 rpm
Frequency	50 Hz
No. of pole pair	2

The Induction machine (4KW) paramaters can be calculated by using MATLAB "power_AsynchronousMachineParams" and it is shown in fig. 3.

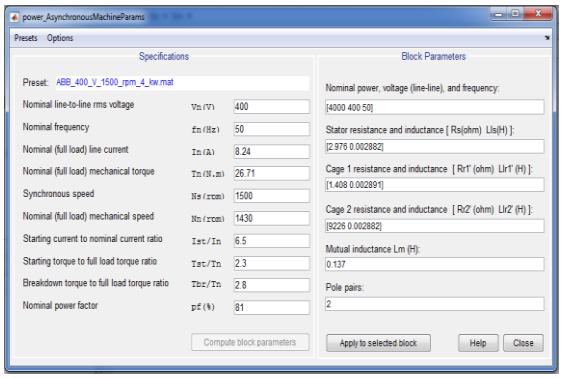

Fig. 3: Induction Machine Parameters

5.1 MATLAB SIMULATION model of SEIG

Figure 4 shows the whole model of self excited induction generator to be studied with simulink which consist of turbine model, capacitor bank model, load model, measurement tool and visulization blocks. Inbuilt blocks are used from "SimPowerSystem" tool of MATLAB/ SIMULINK.

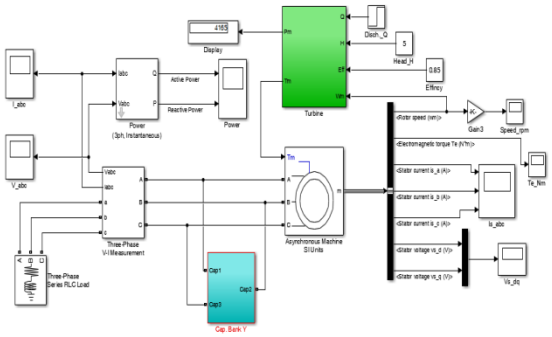

Fig. 4: The whole model of SEIG in simulink

6. Simulation results and discussion

6.1 Process of voltage build up in the SEIG at no load

A 850 µF excitation capacitors bank connected in star is choosen for a 4 KW induction motor described above, the SEIG voltage build up is shown in fig. 5. The excitation starts when motor speed exceed the synchronous speed. The voltage start to build up at 1.1 sec. and it reaches maximum value after 1.6 sec.

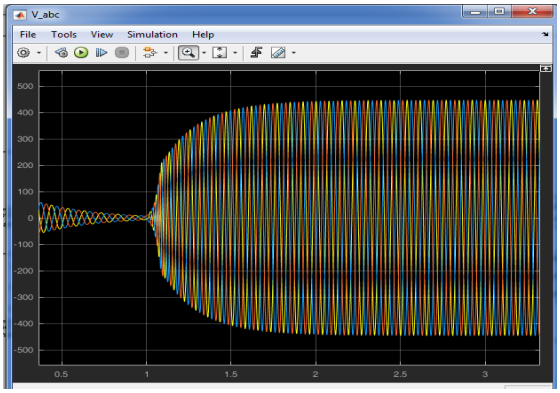

Fig. 5: SEIG voltage at no load

Figure 6 shows the electromagnetic torque at no load its stabilization lead for a terminal voltage to reach a stabilize peak value of -50 N-m.

Figure 7 shows that the current build up at stator terminal of SEIG at no load is 30 Amp. and the active power is depends on the load connected at SEIG terminal. As there is no any connected load, hence active power is zero, which is shown in fig. 8 below.

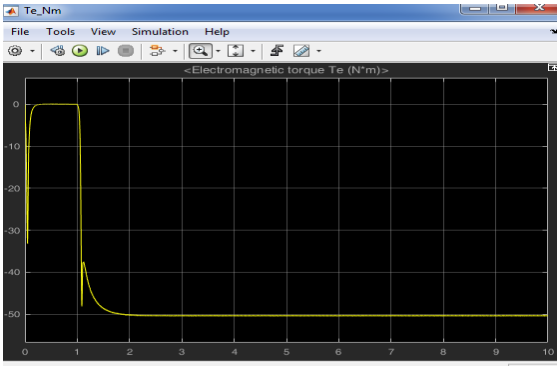

Fig. 6: Electromagnetic torque of SEIG at no load

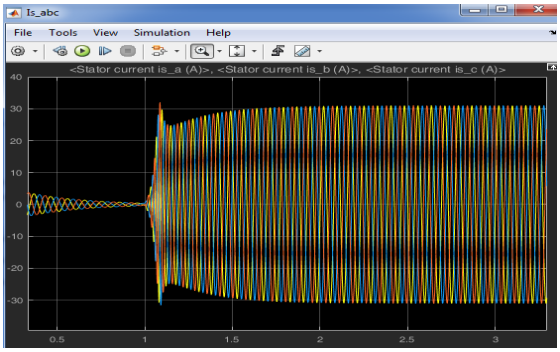

Fig. 7: Stator current of SEIG at no load

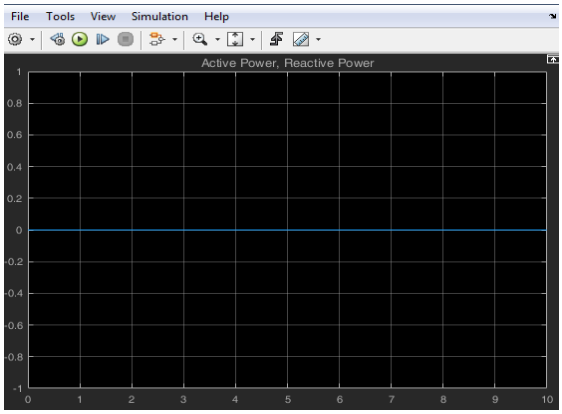

Fig. 8: Output power of SEIG at no load

6.2 Process of voltage build up in the SEIG at full load

A 4 KW pure resistive load is connected across the SEIG, with constant value of 65µF excitation capacitor. More than 300V but less ihan rated voltage is contineously obtained as shown in figure 9, the voltage can be adjusted by increasing the speed of rotation in the shaft.

Figure 10 shows the full load active power output of SEIG. The SEIG delivers full load output power after 1.6 sec.

The electromagnetic torque of SEIG reaches its constant value of -24 N-m after 1.6 sec which is shown in figure 11.

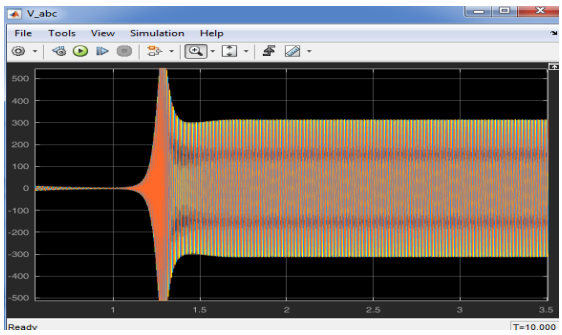

Fig. 9: SEIG voltage at full load

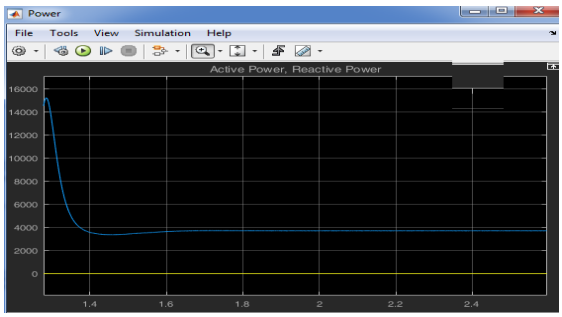

Fig. 10: Output power of SEIG at full load

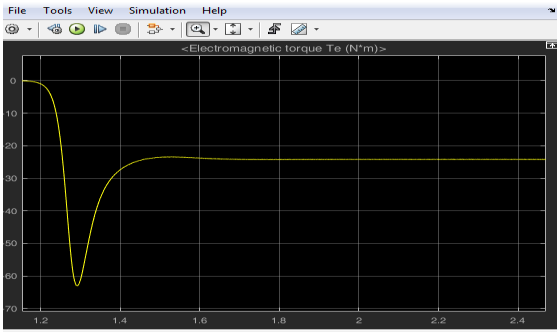

Fig. 11: Full load torque of SEIG

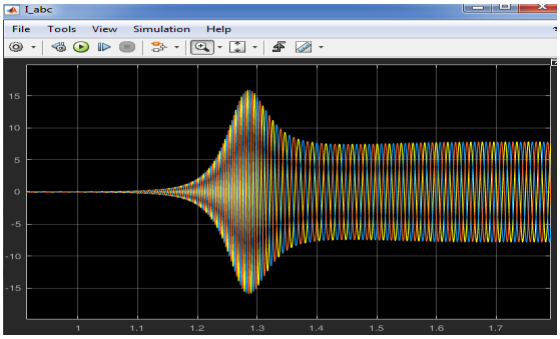

Fig. 12: Full load current of SEIG

6.3 Process of voltage build up when SEIG at over load

To observe the over loading condition of SEIG, constant value of 65µF excitation capacitor is connected across stator terminals and pure resistive load is gradually increased. It is observed that voltage build up continue till certain limits and then voltage collapse. Figure 13 shows that voltage build up is continue at 6.5 KW pure resistive load but when load changes to 6.6 KW voltage collapse as shown in figure 14.

From the figure 15 it observed that at over load condition when voltage collapse to zero the machine picks up dengerously high speed which cause machine itself and other connected equipment may damages.

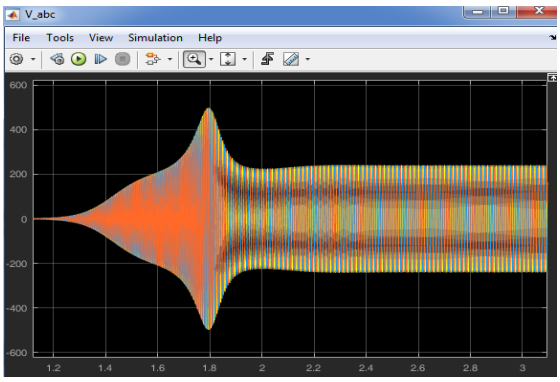

Fig. 13: Voltage build up of SEIG at 6.5 KW load

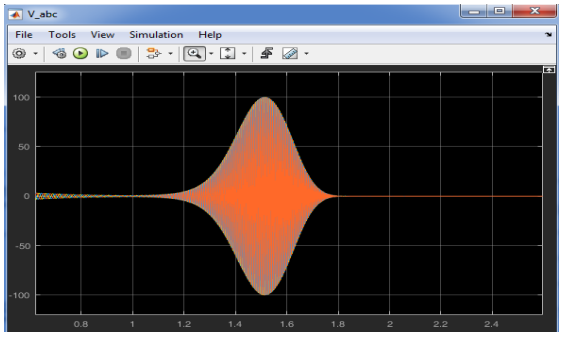

Fig. 14: Voltage build up of SEIG at 6.6 KW load

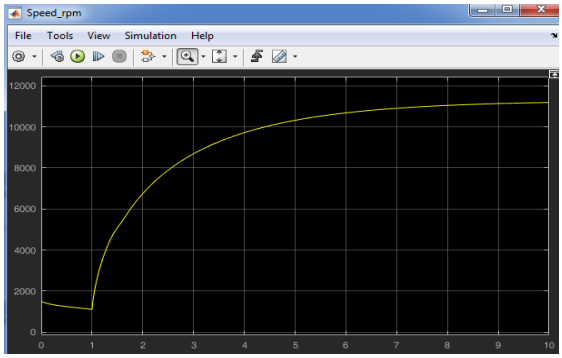

Fig. 15: Speed of SEIG at 6.6 KW load

6.4 Process of voltage build up when load is Inductive

When inductive (1 kvar) full load is connected, electro-magnetic torque of -23.78 N-m is stablize after 1.8 sec. as shown in fig. 18 and voltage build up arround 380 V after 1.7 sec. as shown in fig. 16. Fig.17 and 19 shows load current and power respectively.

When inductive load is increased (4 kvar), SEIG terminal voltage build up after 2.6 sec. aproximately 500 V as shown in fig. 20 and load current also increased to 12 Amp. which is more than the rated current of machine as shown in fig. 22. electeo-magnetic torque -17.89 N-m is stablize after 2.6 sec before that it shows more transient as shown in fig. 21. Active power output increases and reactive power increases as shown in fig. 23.

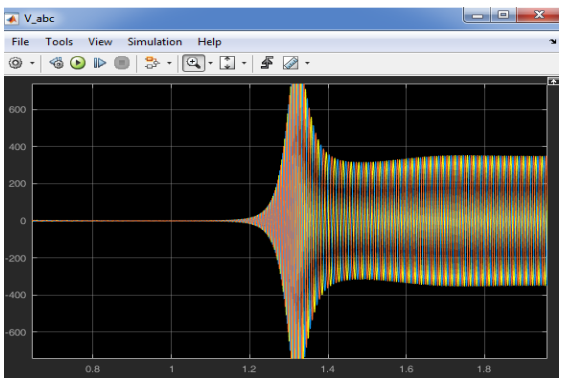

Fig. 16: SEIG voltage at Inductive load

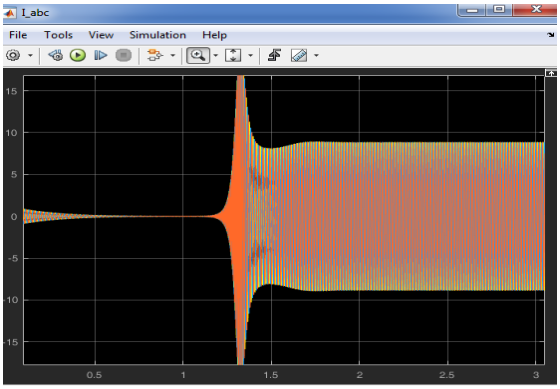

Fig. 17: SEIG load current at Inductive load

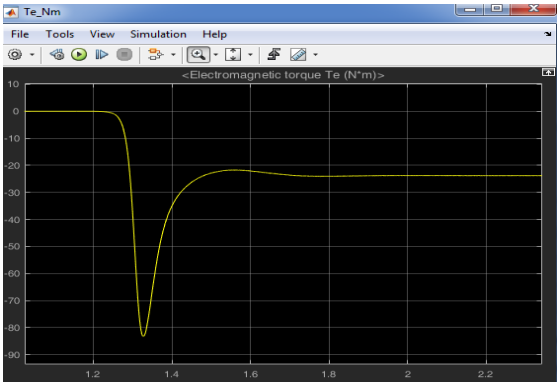

Fig. 18: SEIG Electomagnetic torque at Inductive load

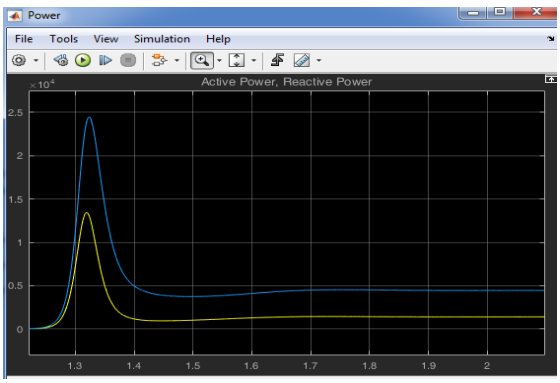

Fig. 19: SEIG active an reactive power of Inductive load

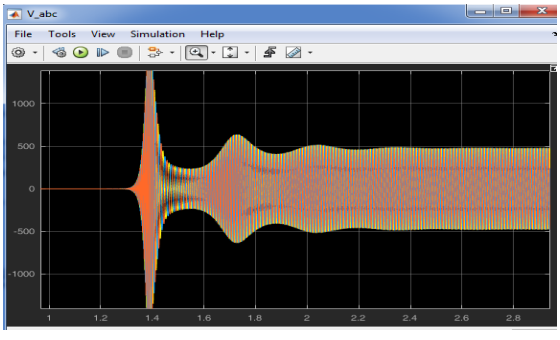

Fig. 20: SEIG voltage at Inductive (4 kvar) load

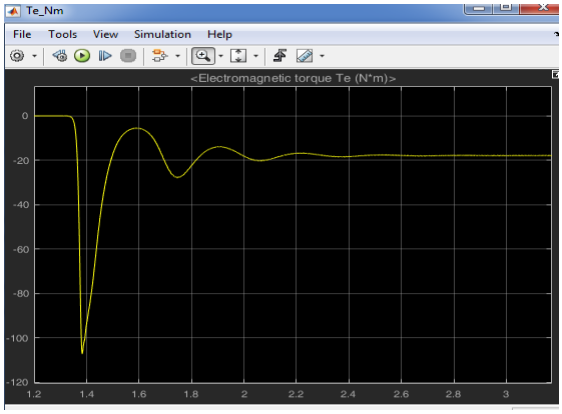

Fig. 21: Electro-magnetic torque at Inductive (4 kvar) load

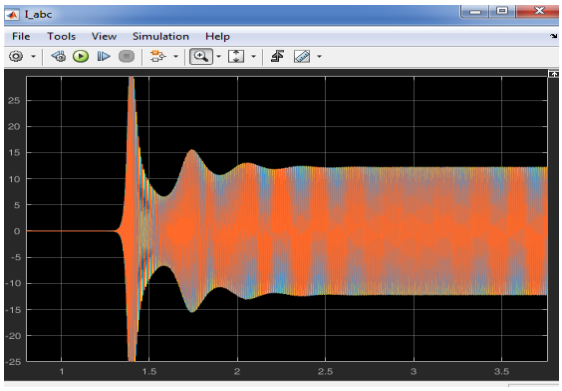

Fig. 22: Load current at Inductive (4 kvar) load

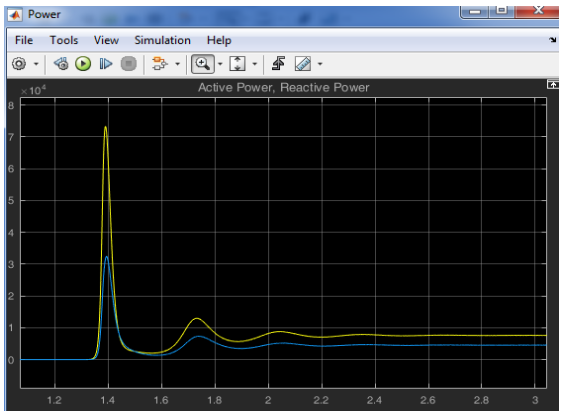

Fig. 23: Active and reactive Power of Inductive (4 kvar) load

6.5 Process of voltage build up when load is Inductive and capacitive

When R-L-C load of positive 4 kvar and negative 4 kvar is connected to the SEIG at full load, torque is stabilized -40.68 N-m after 1.27 sec. and voltage build up to 400 V as shown in fig 25 and fig. 24 respectively where as load current is 8.5 amp. and active power is 4.5 Kw as shown in fig. 26 and fig. 27 respectively.

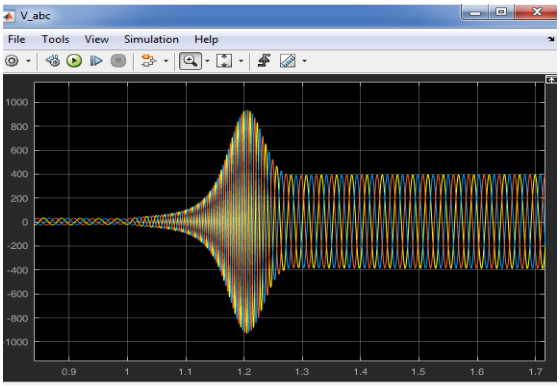

Fig. 24: SEIG voltage when *R-L-C* load is connected

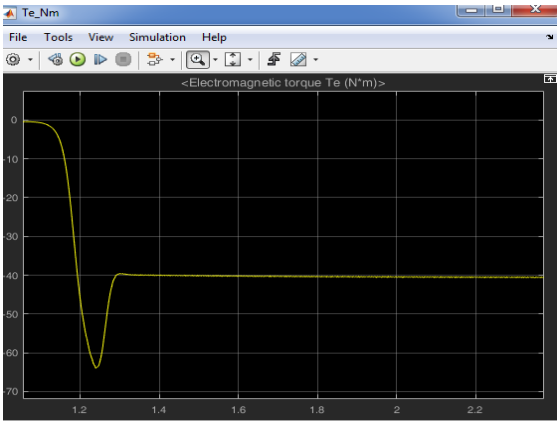

Fig. 25: Electro-magnetic torque of SEIG when *R-L-C* load is connected

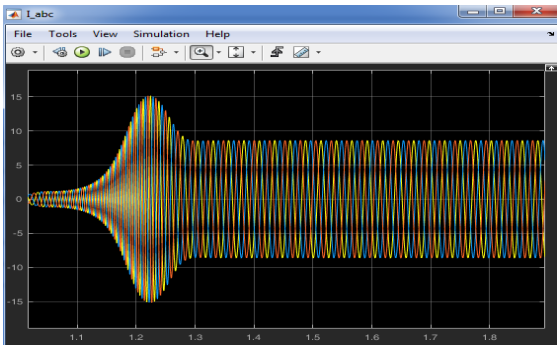

Fig. 26: Load current of SEIG when *R-L-C* load is connected

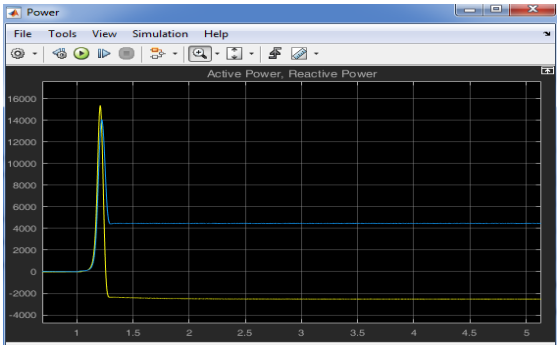

Fig. 27: Load current of SEIG when *R-L-C* load is connected

7. Conclusion and future work

7.1 Conclusion

This paper studies the dynamic behavior of self-excited induction generator (SEIG) which is driven by water turbine at constant torque based on d-q axes reference frame. At negative slip and negative torque an induction motor works as induction generator. The SEIG is studied under various loading conditions. While carrying out the simulation, core loss is ignored. From various results, it concludes that voltage build up process is mainly depends on connected load, speed of IG and value of excitation capacitors. From the MATLAB result it is seen that inductive load also very much affect voltage build up process of SEIG

MATLAB SIMULATION result shows that SEIG can sustain overload up to certain limit and then voltage collapse drastically to zero and speed of the generator picks up dangerously high. It is also seen that when inductive and capacitive load VAR are equal, we can obtain the desired voltage by adjusting the speed of turbine

7.2 Future Research

Under dynamic condition the self-excited induction generator model can be extended to the following:

(i) d-q reference frame model for 1-phase configuration to analyze the behavior of 3-Φ induction motor used as 1-Φ, self-excited induction generator.

(ii) d-q reference frame model of self-excited induction generator considering the speed limitation when SEIG voltage collapse to zero under overloading condition.

(iii) In actual practice ELC is used for voltage and frequency control of SEIG which is costly, so it is necessary to develop a cheapest switching mechanism to connect and disconnect external VAR required by the SEIG according to load and speed.

References

[1] R. C. Bansal, T. S. Bhatti and D. P. Kothari, "Bibliography on the application of induction generators in nonconventional energy systems", *IEEE Transactions on Energy Conversion*, Vol. 18, Issue No. 3, Sept. 2003, pp. 433-439. Doi: 10.1109/TEC.2003.815856

[2] G. K. Singh, "Self-excited induction generator research - A survey", *Electric Power Systems Research*, Vol. 69, Issues 2–3, May 2004, pp. 107-1144. Doi: https://doi.org/10.1016/j.epsr.2003.08.004

[3] S. S. Murthy, G. Bhuvaneswari, S. Gao and R. K. Ahuja, "Self excited induction

generator for renewable energy applications to supply single-phase loads in remote locations", *2010 IEEE International Conference on Sustainable Energy Technologies (ICSET)*, Kandy, 2010, pp. 1-8. Doi: 10.1109/ICSET.2010.5684947

[4] E. D. Bassett and F. M. Potter, "Capacitive Excitation for Induction Generators", *AIEE Trans. Electrical Engineering*, Vol. 54, Issue No. 5, pp. 540 – 545, 1935.

[5] J. M. Elder, J. T. Boys and J. L. Woodward, "The process of self excitation in induction generators", *IEE Proceedings B - Electric Power Applications*, Vol. 130, Issue No. 2, March 1983, pp. 103-108. Doi: 10.1049/ip-b.1983.0016

[6] C. F. Wagner, "Self-Excitation of Induction Motors With Series Capacitors", *Transactions of the American Institute of Electrical Engineers*, Vol. 60, Issue No. 12, Dec. 1941, pp. 1241-1247. Doi: 10.1109/T-AIEE.1941.5058259

[7] M. B. Brennen and A. Abbondanti, "Static Exciters for Induction Generators", *IEEE Transactions on Industry Applications*, Vol. IA-13, Issue No. 5, Sept. 1977, pp. 422-428. Doi: 10.1109/TIA.1977.4503433

[8] C. F. DeSieno and B. J. Beaudoin, "A Guide to the Application of Capacitors without Induction Motor Self-Excitation", *IEEE Transactions on Power Apparatus and Systems*, Vol. 84, Issue No. 1, 1965. Doi: 10.1109/TPAS.1965.4766102

[9] H. P. Tiwari and J. K. Diwedi, "Minimum Capacitance Requirement for Self-Excited Induction Generator", *Proc. of National Power System Conference (NPSC 2002)*, Indian Institute of Technology, Kharagpur, December 27-29, 2002, pp. 5-10. Retrieved from http://www.iitk.ac.in/npsc/Papers/NPSC2002/16.pdf

[10] N. H. Malik and A. A. Mazi, "Capacitance Requirements for Isolated Self Excited Induction Generators", *IEEE Transactions on Energy Conversion*, Vol. EC-2, Issue No. 1, March 1987, pp. 62-69. Doi: 10.1109/TEC.1987.4765805

[11] M. Senthilkumar, "Optimal Capacitor for Maximum Output Power Tracking of Self Excited Induction Generator using Fuzzy Logic Approach", *International Journal on Computer Science and Engineering*, Vol. 02, Issue No. 5, 2010, pp. 1758-1762. Retrieved from https://pdfs.semanticscholar.org/f231/bd153c5f102279384e1ff28737d960745c60.pdf

[12] T. F. Chan, "Capacitance requirements of self-excited induction generators", *IEEE Transactions on Energy Conversion*, Vol. 8, Issue No. 2, June 1993, pp. 304-311. Doi: 10.1109/60.222721

[13] A. Kumari, A. G. Thosar and S. S. Mopari, "Determination of Excitation Capacitance of a Three Phase Self Excited Induction Generator", *International Journal of Advanced Research in Electrical, Electronics and Instrumentation Engineering*, Vol. 4, Issue 5, May 2015, pp. 4069-4074. Retrieved from http://www.ijareeie.com/upload/2015/may/38_DETERMINATION.pdf

[14] A. K. Al Jabri and A. I. Alolah, "Capacitance requirement for insolated self-exicted induction generator", *IEE Proceedings B - Electric Power Applications*, Vol. 137, Issue No. 3, May 1990, pp. 154-159. Doi: 10.1049/ip-b.1990.0016

[15] V. P. Chandran and S. Vadhera, "Capacitance requirements of self excited induction generator for different operating conditions", *Proc. of 2011 International Conference on Energy, Automation and Signal*, Bhubaneswar, India. 28-31, Dec 2011, pp. 1-6. Doi: 10.1109/ICEAS.2011.6147177

[16] S. S. Murthy, R. Jose and B. Singh, "Experience in the Development of Microhydel Grid Independent Power Generation Scheme using Induction Generators for Indian Cconditions", *Proceedings of IEEE TENCON'98: IEEE Region 10 International Conference on Global Connectivity in Energy, Computer, Communication and Control (Cat. No. 98CH36229)*, New Delhi, India, 17-19 Dec. 1998, Vol. 2, pp. 461-465. Doi: https://doi.org/10.1109/TENCON.1998.798246

[17] B. Singh, S. S. Murthy, and S. Gupta, "STATCOM-Based Voltage Regulator for Self-Excited Induction Generator Feeding Nonlinear Loads", *IEEE Transactions on Industrial Electronics*, Vol. 53, Issue No. 5, 2006, pp. 1437–1452. Doi: 10.1109/TIE.2006.882008

[18] B. Nia Roodsari, E. P. Nowicki and P. Freere, "An experimental investigation of the Distributed Electronic Load Controller: A new concept for voltage regulation in microhydro systems with transfer of excess power to household water heaters", *Proc. of 2014 IEEE Canada International*

Humanitarian Technology Conference - (IHTC), Montreal, QC, 1-4 June 2014, pp. 1-4. Doi: 10.1109/IHTC.2014.7147548

[19] L. G. Scherer, C. B. Tischer, F. C. Posser, C. M. Franchi and R. F. de Camargo, "Hybrid topology for voltage regulation applied in three-phase four-wire micro hydro power station", *Proc. of IECON 2013 - 39th Annual Conference of the IEEE Industrial Electronics Society*, Vienna, 2013, pp. 7169-7174. Doi: 10.1109/IECON.2013.6700324

[20] "Induction Generator | Application of Induction Generator", *Electrical4u.com*. [Online]. Available: http://www.electrical4u.com/induction-generator/ (Accessed: Apr 24, 2018).

Authors' Profile

Dinesh Kumar Mallik is working as senior instructor in electrical department of "Council for Technical Education and Vocational Training" (CTEVT), Nepal. He has completed his M.Tech. Degree in Electrical and Electronics Engineering from Assam Don Bosco University in 2018.

Jesif Ahmed is working as an Assistant Professor in the Department of Electrical and Electronics Engineering, School Of Technology, Assam Don Bosco University, Guwahati, Assam, India. He is pursuing his Ph.D. from Gauhati University, Assam, India. His research interest includes study of electricity market, Power system optimization and transmission congestion management.

A High Voltage Gain Boost Converter: Concept of DC Power Transfer Using Mutual Inductors

Saurav Bharadwaj[1], Indrajit Barman[2], Midar Riba[3], Asish Arpan Dadhara[4], Biswajit Sengupta[5]

[1,2,3,4,5]Don Bosco College of Engineering and Technology, Assam Don Bosco University
Airport Road, Azara, Guwahati - 781017, Assam, INDIA.
[1]*sauravbharadwaj41@gmail.com**,[5]*biswajit.sengupta@dbuniversity.ac.in*

Abstract: ***A high voltage boost converter is being prototyped in an artificial software based environment of MATLAB/ SIMULINK and identifies the practical conditions of the converter. A direct current (DC) input voltage is being boosted to a higher magnitude by multiplying a gain factor in a dynamic process of DC power transfer by cascading three mutual inductors in a single core. Input voltage is being switched by primary IGBT switches creating simultaneous charging and discharging of primary inductor, hence induces identical voltage in two secondary inductors. Inductors are charged and power is transferred to a parallel capacitor and finally to the resistive load in accurate control of duty cycles.***

Keywords: Coupled inductors, Voltage spikes, Semi-conductor switches, Switching frequency, Voltage boosting, DC power transfer and Voltage ripples.

1. Introduction

Boost converters consist of an inductor switched by a semi-conductor switch in a periodic phenomenon of charge and discharge in transferring the power to a parallel resistance-capacitance pair, limiting the DC voltage transfer gain to 2-3 times of the input voltage. The applications of the boost converter are not only limited to power plants and grids but also in multi-disciplinary functional systems. In large applications of these converters, it is a challenge to design a modified converter providing all the necessary parameters. A number of designers and researchers use various techniques to boost the input voltage including parallel inductors to a capacitor, single inductor to parallel capacitors, concept of mutual inductors and transformers and some complex circuitry for efficient power transfer. An important parameter of any converter is its practical stability; designing in an artificial environment like Simulink limits its practical operational analysis. The disadvantage of the software is that it is unable to determine exact physical disturbances, noises and other factors effecting each modal operation. On the other hand, it is mandatory to design in such artificial environment initially considering the maximum possible practical cases. Finally, a general boost converter losses its boosted power in power switches, inductors and series circuits of resistors and capacitors.

In the paper, a high voltage boost converter is designed using the principle of DC power transfer using mutual inductors. Boost converter can produce a significant amount of voltage of higher magnitude. A number of simulation issues and conditions of software failure can be defined from this innovative design in the artificial environment.

2. High Voltage Gain Boost Converter

High voltage gain boost converter circuit is designed for an input voltage of 100V, applied to the primary of the three mutual inductors (fig. 1). Each of the identical inductor has an inductance and a resistance of 50mH and 5Ω respectively. Coefficient of coupling is considered depending on how the coils are winded in the core and these coupled coils have a mutual inductance and resistance of 1μH and 1Ω respectively. Four switches are being configured in the model and are switched in independent periodic duties depending on the directional flow of current and flux. Mutual coupled inductors play an important role in inducing voltage due to dynamic change in current of the inductors and charge transfer to a parallel capacitor and resistive load.

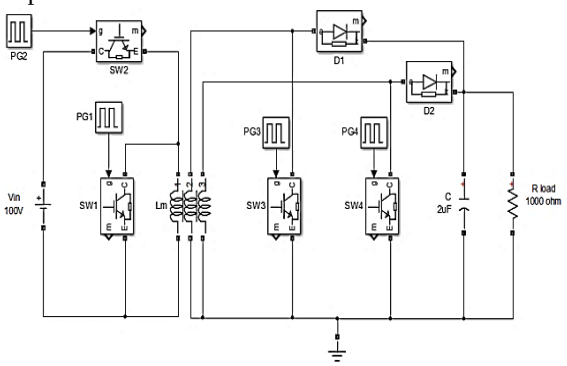

Figure1: High Voltage Gain Boost Converter

3. Operations and Modes

In modeling of the circuit (fig. 2, 3 and 4), four switches are switched in different time intervals. Comparing the three switching intervals in a single time axis, switching periods of SW_1 and SW_2 is periodically repeated in switching curve of SW_3 and SW_4 (fig.2).

Figure 2: Time Intervals of Different Modes

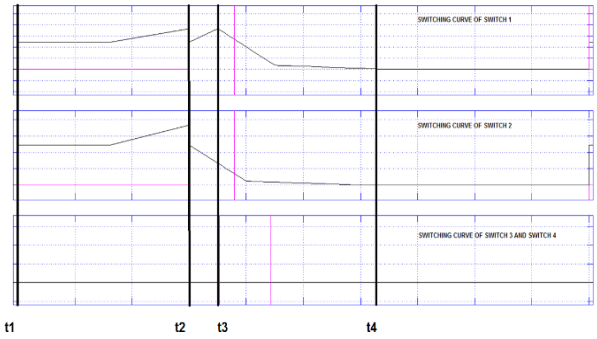

Figure3: Time Intervals of t_1 to t_4

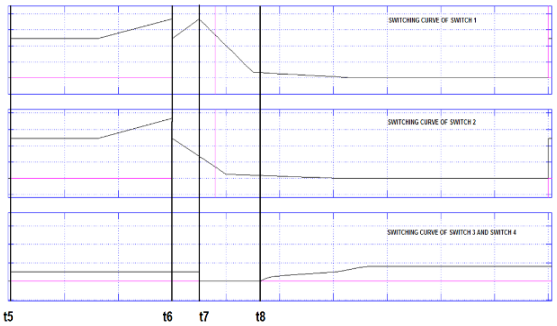

Figure4: Time Intervals of t_5 to t_8

Mode 1 (t_1-t_2):

In this time interval, switches SW_1 and SW_2 are switched in a periodic interval causing a phenomenon of charging and discharging, where SW_1 has an initial delay of 50us. A charging current of $i_1(t)$ and discharging current of $i_2(t)$ of the primary inductor changes fluxes in the secondary inductors. Currents $i_4(t)$ and $i_5(t)$ induced in the secondary inductors L_2 and L_3produces a voltage $V_2(t)$ which charge the capacitor C with a current of $i_6(t)$ and providing power to the load (fig.5).

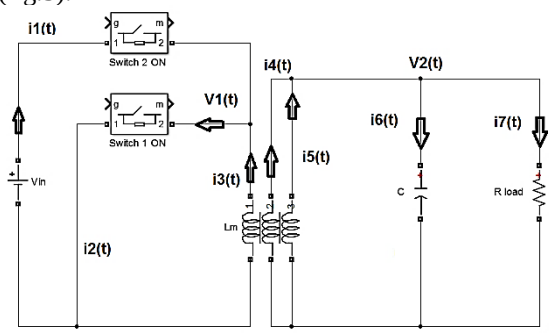

Figure 5: Mode 1 Operation

Mode 2 (t_2-t_3):

In this time interval, switches SW_1 is turned on and inductor L_1 finds a path to discharge. Secondary currents $i_2(t)$ and $i_3(t)$ induced in the inductors, L_2 and L_3 produce a nodal voltage V(t) and currents $i_4(t)$ and $i_5(t)$flows through the capacitor to charge and the resistive load (R_{load})respectively (fig. 6).

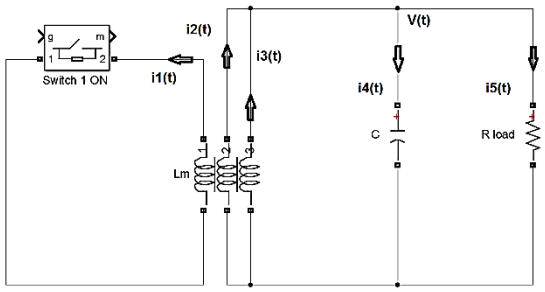

Figure 6: Mode 2 Operation

Mode 3 (t_3-t_4):

In this time interval, all the switches are turned off and the primary inductor is open circuited. Secondary currents,$i_1(t)$ and $i_2(t)$ passes through the

inductors, L_2 and L_3 results in charging of capacitor through current $i_3(t)$ and dissipates power in the load.

Since, time durations of all the switches are not identical, so time laps between duration of time t_4 and $t_5$is omitted as a number of repeated time periods of SW_1 and $SW_2$is present within a time period of SW_3 and SW_4(fig. 7).

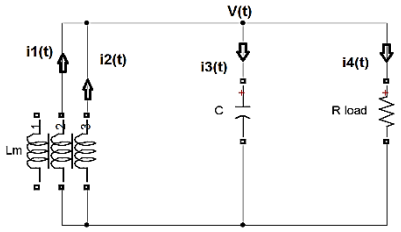

Figure 7: Mode 3 Operation

Mode 4 (t_5-t_6):

In this time interval, all the switches are turned on and secondary inductors L_2 and L_3 are being charged by the currents $i_4(t)$ and $i_5(t)$ as primary inductor current creates a flux due to the change in current $i_3(t)$. Simultaneously capacitor is responsible to maintain a constant output voltage and starts discharging in a condition as change in voltage drops across the load are negligible (fig. 8).

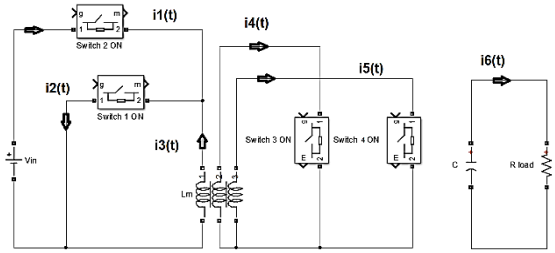

Figure 8: Mode 4 Operation

Mode 5 (t_6-t_7):

In this time interval, the primary inductor is responsible to charge the secondary inductors by induced current $i_2(t)$ and $i_3(t)$.Gradually, the current in the primary inductor and capacitor $i_1(t)$ and $i_4(t)$ respectively starts to decrease but before reaching a nominal lower value the circuit operates in the corresponding mode (fig. 9).

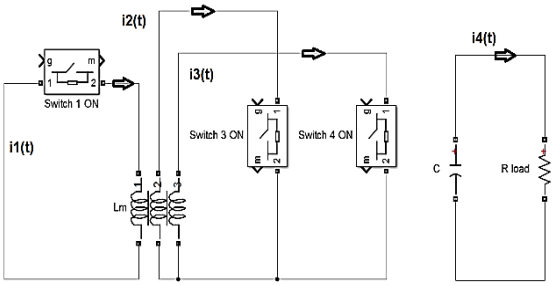

Figure 9: Mode 5 Operation

Mode 6 (t_7-t_8):

In this time interval, the primary inductor L_1 is kept open and mutual fluxes of the inductors, L_2 and L_3 are decreased and induce a mutual current on the coupled inductor pair. The cycle of mode 4-6 is repeated till the operation reaches a time instant of t_9 and modes 1-3 is repeated till it reaches a time instant of t_5(fig. 10).

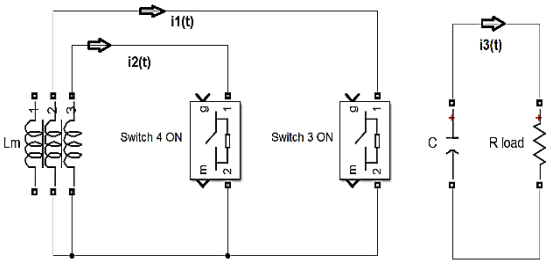

Figure 10: Mode 6 Operation

4. Mathematical Analysis of the Converter

The operation of the circuit can be illustrated in six modes and a number of equations of mutual inductance, current and voltage relation with respect to time is described. The equations are derived from the circuit operating in the six modes.

Mode 1:

$$V_2(t) + R_2 i_4(t) + L_2 \frac{di_4(t)}{dt} + M \frac{d}{dt}(i_3(t) + i_5(t)) = 0 \quad \text{---- (1)}$$

$$V_2(t) + R_3 . i_5(t) + L_3 \frac{di_5(t)}{dt} + M\left(\frac{di_3(t)}{dt} + \frac{di_4(t)}{dt}\right) = 0 \quad \text{---- (2)}$$

$$V_2(t) = \frac{1}{C}\int i_6(t).dt \quad \text{---- (3)}$$

$$V_2(t) = R_{load} . i_7(t) \quad \text{---- (4)}$$

$$i_3(t) = \frac{V_1(t)}{L_1} e^{\left(\frac{-R_1}{L_1}\right)t} - \frac{M}{L_1}\left[\delta(t) - \left(\frac{R_1}{L_1}\right) e^{\left(\frac{-R_1}{L_1}\right)t}\right][i_4(t) + i5(t) \quad \text{---- (5)}$$

$$i_1(t) = \frac{V_{in} - V_1(t)}{R_{SW\,2}} \quad \text{---- (6)}$$

$$i_2(t) = \frac{V_1(t)}{R_{SW\,1}} \quad \text{---- (7)}$$

Mode 2:

$$i_1(t) = \frac{M}{L_1}\left[\delta(t) - \frac{(R_1+R_{SW\,1})}{L_1} e^{-\left(\frac{R_1+R_{SW\,1}}{L_1}\right)t}\right][i_2(t) + i3(t)$$ ----- (8)

$$i_2(t) = -\frac{V(t)}{L_2} e^{\left(\frac{-R_2}{L_2}\right)t} - \frac{M}{L_2}\left[\delta(t) - \frac{R_2}{L_2} e^{\left(\frac{-R_2}{L_2}\right)t}\right][i_1(t) + i3(t)$$ ---- (9)

$$i_3(t) = -\frac{V(t)}{L_3} e^{\left(\frac{-R_3}{L_3}\right)t} - \frac{M}{L_3}\left[\delta(t) - \frac{R_3}{L_3} e^{\left(\frac{-R_3}{L_3}\right)t}\right][i_1(t) + i2(t)$$ ---- (10)

$$V(t) = \frac{1}{C}\int i_4(t).dt$$ ---- (11)

$$V(t) = R_{load}.i_5(t)$$ ---- (12)

Mode 3:

$$i_1(t) = -\frac{V(t)}{L_2} e^{\left(\frac{-R_2}{L_2}\right)t} - \frac{M}{L_2}\left[\delta(t) - \frac{R_2}{L_2} e^{\left(\frac{-R_2}{L_2}\right)t}\right]$$ -- (13)

$$V(t) = \frac{1}{C}\int i_3(t).dt$$ -- (14)

$$V(t) = R_{load}.i_4(t)$$ -- (15)

$$i_2(t) = -\frac{V(t)}{L_1} e^{\left(\frac{-R_1}{L_1}\right)t} - \frac{M}{L_1}\left[\delta(t) - \frac{R_1}{L_1} e^{\left(\frac{-R_1}{L_1}\right)t}\right] i_1(t)$$ -- (16)

Mode 4:

$$i_1(t) = \frac{V_{in} - V(t)}{R_{SW\,2}}$$ -- (17)

$$i_2(t) = \frac{V(t)}{R_{SW\,1}}$$ -- (18)

$$V(t) = R_1.i_3(t) + L_1\frac{di_3(t)}{dt} + M\left(\frac{di_4(t)}{dt} + \frac{di_5(t)}{dt}\right)$$ -- (19)

$$i_4(t) = -\frac{M}{L_2}\left[\delta(t) - \frac{(R_{SW\,3}+R_2)}{L_2} e^{-\left(\frac{R_{SW\,3}+R_2}{L_2}\right)t}\right][i_3(t) + i5t$$ --- (20)

$$i_5(t) = -\frac{M}{L_3}\left[\delta(t) - \frac{(R_{SW\,4}+R_3)}{L_3} e^{-\left(\frac{R_{SW\,4}+R_3}{L_3}\right)t}\right][i_3(t) + i4t$$ --- (21)

$$R_{load}.i_6(t) - \frac{1}{C}\int i_6(t).dt = 0$$ --- (22)

Mode 5:

$$i_1(t) = -\frac{M}{L_1}\left[\delta(t) - \frac{(R_{SW\,1}+R_1)}{L_1} e^{-\left(\frac{R_{SW\,1}+R_1}{L_1}\right)t}\right][i_2(t) + i3(t)$$ -- (23)

$$i_2(t) = -\frac{M}{L_2}\left[\delta(t) - \frac{(R_{SW\,3}+R_2)}{L_2} e^{-\left(\frac{R_{SW\,3}+R_2}{L_2}\right)t}\right][i_1(t) + i3(t)$$ -- (24)

$$i_3(t) = -\frac{M}{L_3}\left[\delta(t) - \frac{(R_{SW\,4}+R_3)}{L_3} e^{-\left(\frac{R_{SW\,4}+R_3}{L_3}\right)t}\right][i_1(t) + i2(t)$$ -- (25)

$$R_{load}.i_4(t) - \frac{1}{C}\int i_4(t).dt = 0$$ -- (26)

Mode 6:

$$(R_2 + R_{SW3})i_1(t) + L_2.\frac{di_1(t)}{dt} + M\frac{di_2(t)}{dt} = 0$$ -- (27)

$$(R_3 + R_{SW4})i_2(t) + L_3.\frac{di_2(t)}{dt} + M\frac{di_1(t)}{dt} = 0$$ -- (28)

$$R_{load}.i_3(t) - \frac{1}{C}\int i_3(t).dt = 0$$ -- (29)

4.1 Mutual inductance of the inductor coils

Induced voltage in coil 1

$$V_{L1} = N_1 \frac{d}{dt}(\Phi_{21} + \Phi_{31}) = M \frac{d}{dt}(i_2 + i_3) \quad \text{-- (30)}$$

Induced voltage in coil 2

$$V_{L2} = N_2 \frac{d}{dt}(\Phi_{12} + \Phi_{32}) = M \frac{d}{dt}(i_1 + i_3) \quad \text{-- (31)}$$

Induced voltage in coil 3

$$V_{L3} = N_3 \frac{d}{dt}(\Phi_{13} + \Phi_{23}) = M \frac{d}{dt}(i_1 + i_2) \quad \text{-- (32)}$$

Mutual inductance of inductor L_1:

$$M_1 = N_1 \frac{(\Phi_{21}+\Phi_{31})}{(i_2+i_3)} \quad \text{-- (33)}$$

Mutual inductance of inductor L_2:

$$M_2 = N_2 \frac{(\Phi_{12}+\Phi_{32})}{(i_1+i_3)} \quad \text{-- (34)}$$

Mutual inductance of inductor L_3:

$$M_3 = N_3 \frac{(\Phi_{13}+\Phi_{23})}{(i_1+i_3)} \quad \text{-- (35)}$$

4.2 Total mutual inductance

$$M^3 = M_1 . M_2 . M_3 \quad \text{-- (36)}$$

$$M^3 = N_1 \frac{(\Phi_{21} + \Phi_{31})}{(i_2 + i_3)} . N_2 \frac{(\Phi_{12} + \Phi_{32})}{(i_1 + i_3)} . N_3 \frac{(\Phi_{13} + \Phi_{23})}{(i_1 + i_3)} \quad \text{-- (37)}$$

$$M^3 = N_1 . N_2 . N_3 \frac{(2k\Phi_1)(2k\Phi_2)(2k\Phi_3)}{(i_1+i_2)(i_2+i_3)(i_1+i_3)} \quad \text{-- (38)}$$

$$M = 2kN \sqrt[3]{\frac{\Phi_1 . \Phi_2 . \Phi_3}{(i_1+i_2)(i_2+i_3)(i_1+i_3)}} \quad \text{-- (39)}$$

5. Simulation Results of the Model

The phenomenon of switching is accurately done inducing a sinusoidal current in the secondary inductors converting a direct current from the input voltage source to an alternating current of -6.3kA to 3kA throughthe secondary inductors L_2 and L_3.

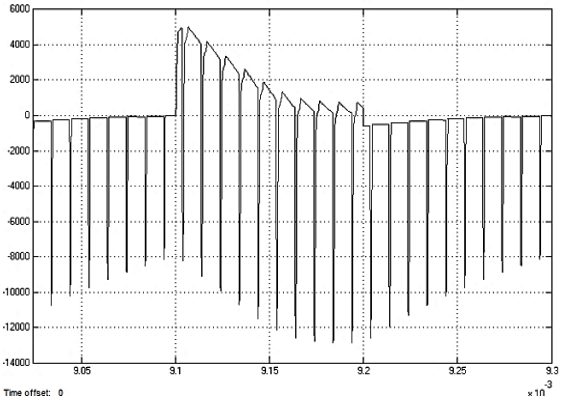

Figure 11: Capacitor Current Curve

Effect of $\frac{dv}{dt}$can be identified in the primary inductor producing a high voltage of 2250MV which is considered to be unrealistic in practical scenario and can be reduced by implementing an accurate RC snubber circuit. A change in fluctuating current in the secondary inductors creates a continuous change in flux resulting in an induced voltage in the coupled inductors.

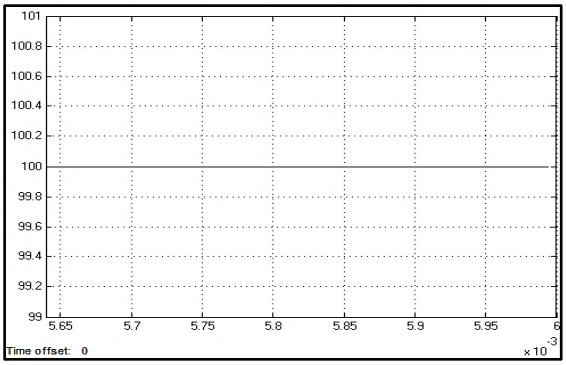

Figure 12: Input Voltage Curve

Capacitor and two identical mutual inductors L_2 and L_3 are acting to be charged and discharged at the same time. A complete time period of SW_3 and SW_4 consisting of two intervals, an interval where the inductors are charged and capacitor is discharged simultaneously and vice-versa. The maximum voltage across the capacitor is 432kV and discharges to a value of 376kV in a cycle. An output voltage of the converter consists of harmonics producing ripples in the output voltage.

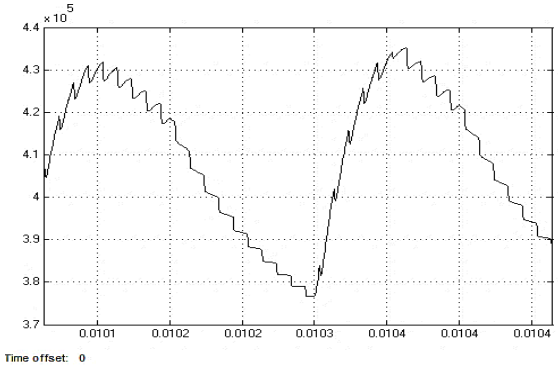

Figure 13: Capacitor Voltage Curve

Load considered in the circuit is resistive of a magnitude of 1kΩ and current flowing through it is 370A to 425A. An effect of harmonics shown in ripples in the output current, resembles to be a periodic signal; whereas the signal should remain constant.

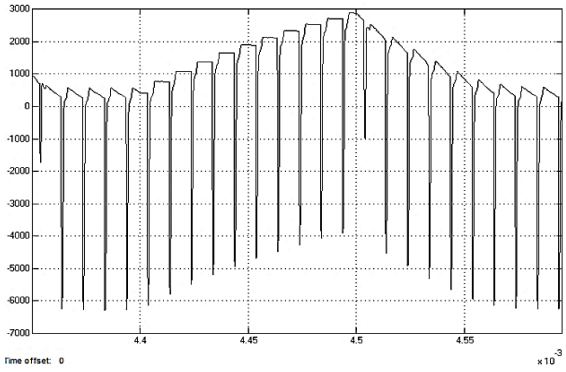

Figure 14: Secondary Inductors Current Curve

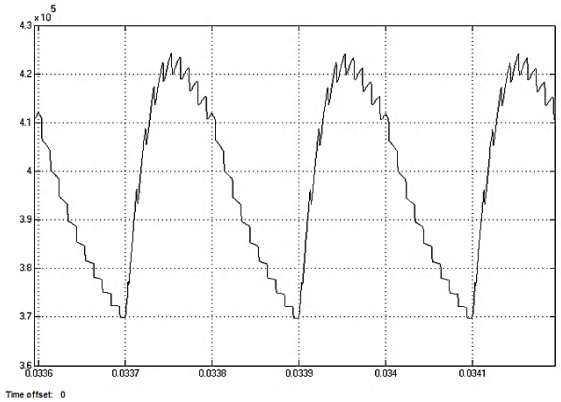

Figure 15: Output Load Voltage Curve

The fundamental component of the circuit is to implement a direct current harmonic filter to reduce the harmonics present in the output waveform which increases the losses in the circuit in the form of heat energy.

Diodes are a component allowing the power to flow unidirectional from inductors to the capacitor. Current from the capacitor reduces from 5kA to 0A as the capacitor is fully charged within a time period of 0.1ms.

6. Conclusion

In concluding the results of the boost converter, the secondary inductors current starts to increase when the switches SW_3 and SW_4 are turned on and decreases when they are turned off. The load current and voltage are linear for the resistive load, voltage across the load falls when inductors are charged and raised when they turns off as the inductor discharges through the capacitor finally end up charging it. Diodes D_1 and D_2 are forward biased when the switches SW_3 and SW_4 are turned off and reversed biased when they are turned on. Voltages across the secondary inductors are built when the switches are turned off and decreases they are being short circuited by a switching resistance during charging the inductor.

On the other hand, a number of issues are being found in simulating the design in artificial environment. Problem of $\frac{di}{dt}$ is seen in the primary inductors partially reflecting in the secondary inductors and can be reduced by implementing the high $\frac{di}{dt}$ snubber circuit where inductor are connected in specific configuration reducing the sudden increase in current in a short time. A problem of $\frac{dv}{dt}$is also been found across the inductors and the primary switches and need to be reduced by using the specific configurations of resistance- capacitor snubber circuit.

References

[1] Y. P. Hsieh, J. F. Chen, T. J. Liang and L. S. Yang, "Novel High Step-Up DC–DC Converter for Distributed Generation System", *IEEE Transactions on Industrial Electronics*, Vol. 60, Issue No. 4, April 2013, pp. 1473-1482. Doi: doi: 10.1109/TIE.2011.2107721

[2] O. Cornea, G. D. Andreescu, N. Muntean and D. Hulea, "Bidirectional Power Flow Control in a DC Microgrid Through a Switched-Capacitor Cell Hybrid DC–DC Converter", *IEEE Transactions on Industrial Electronics*, Vol. 64, Issue No. 4, April 2017, pp. 3012-3022. Doi: 10.1109/TIE.2016.2631527

[3] D. D. C. Lu, D. K. W. Cheng, and Y. S. Lee, "A Single-Switch Continuous-Conduction-Mode Boost Converter With Reduced Reverse-Recovery and Switching Losses",

IEEE Transactions on Industrial Electronics, Vol. 50, Issue No. 4, August 2003, pp. 767-776. Doi: 10.1109/TIE.2003.814989

[4] C. Álvarez-Mariño, F. de León, and X. M. López- Fernández, "Equivalent Circuit for the Leakage Inductance of Multiwinding Transformers: Unification of Terminal and Duality Models", *IEEE Transactions on Power Delivery*, Vol. 27, Issue No. 1, January 2012, pp. 353-361. Doi: 10.1109/TPWRD.2011.2173216

[5] F. de León and J. A. Martinez, "Dual Three-Winding Transformer Equivalent Circuit Matching Leakage Measurements", *IEEE Transactions on Power Delivery*, Vol. 24, Issue No. 1, January 2009, pp. 160-168. Doi: 10.1109/TPWRD.2008.2007012

[6] Y. C. Hsieh, T. C. Hsueh and H. C. Yen, "A dual-boost converter with zero voltage transition", *2008 IEEE Power Electronics Specialists Conference*, Rhodes, 2008, pp. 692-696. Doi: 10.1109/PESC.2008.4592010

[7] M. Veerachary and J. Prakash, "Zero-voltage switching of high-gain boost converter", *2016 IEEE 1st International Conference on Power Electronics, Intelligent Control and Energy Systems (ICPEICES)*, Delhi, 2016, pp. 1-6. Doi: 10.1109/ICPEICES.2016.7853674

[8] M. H. Rashid (Ed.), *Power Electronics Handbook: Devices, Circuits and Applications*, Third Edition, pp. 249, Elsevier, MA, USA, 2011.

[9] C. W. T. McLyman, *Transformer and Inductor Design Handbook, 4th Edition*, CRC Press, 2011.

[10] A. Chakraborty, *Circuit theory Analysis and Synthesis*, Sixth Revised Edition, pp. 455, Dhanpat Rai & Co. Pvt. Ltd, New Delhi, 2006.

[11] S. Chowdhury, S. P. Chowdhury and P. Crossley, *Microgrids and Active Distribution Networks*, The Institution of Engineering and Technology, 2009. Doi: http://dx.doi.org/10.1049/PBRN006E

[12] N. Jenkins, G. Strbac and J. Ekanayake, *Distributed Generation*, The Institution of Engineering and Technology, 2010. Doi: http://dx.doi.org/10.1049/PBRN001E

[13] S. Jain, *Modeling and Simulation Using MATLAB-Simulink*, 2nd Edition, pp. 429, Wiley India Publication, New Delhi, 2015, ISBN: 9788126551972.

Design of Horizontal Axis Micro Wind Turbine for Low Wind Speed Areas

Deibanehbok Nongdhar[1], Bikramjit Goswami[2], Pallav Gogoi[3], Sidharth Borkataky[4]

[1,2]Department of Electrical and Electronics Engineering, Assam Don Bosco University, School of Technology
Airport Road, Azara, Guwahati-781017, Assam, INDIA
[1]deibaneh001@gmail.com, [2]bikramjit.goswami@dbuniversity.ac.in*

[3,4]Department of Mechanical Engineering, Assam Don Bosco University, School of Technology
Airport Road, Azara, Guwahati-781017, Assam, INDIA
[3]pallav.gogoi@dbuniversity.ac.in, [4]sidharth.borkataky@dbuniversity.ac.in

Abstract: ***Micro wind turbines play an important role in becoming the alternative technology in the generation of electricity because of the increase in fossil fuel prices and the increase in demand for renewable energy sources. Similarly, Wind energy is becoming one of the best renewable sources of energy for generation of electricity because of the fact that wind is a clean and unbounded source of renewable energy. This paper presents the ideas of designing a horizontal axis small-sized wind turbine or horizontal axis micro wind turbine for low wind speed areas to produce electricity. A small-sized wind turbine or micro wind turbine is a type of turbine that converts the kinetic energy of wind into electrical energy and it is used to generate power for small power needs. It can also be used in many applications like homes, villages, and so on, requiring a very low cost for installation and maintenance.***

Keywords: Micro Wind Turbine, Renewable Energy, HAWT, VAWT.

1. Introduction

One of the major challenges in this new century is the production of energy as well as its efficient use from renewable sources. Researchers around the world have shown that global warming has been caused in part by the greenhouse effect which is largely due to the use of fossil fuels for transportation and electricity. So, the use of renewable energy sources such as geothermal, solar, wind and hydroelectric power needs to be increased to protect the environment. As a renewable energy, wind energy has taken an increasingly important place in energy policies at the national and international level as a response to climate change. Wind power usage in India is growing and research in the field of wind energy will further improve the current situation.

In recent years, the importance of renewable sources of energy in power generation has been growing day by day around the world. Also, due to the lack of fossil fuel resources, utilization of renewable sources of energy has become even more important. Large wind farms, either in the countryside, offshore, in the mountains or at the seaside have already been invested by many countries around the world. Since wind speed and direction are well known and there are only a few factors that will influence them, the energy gathered from these wind farms can easily be predicted and calculated. However, in cities, where there are a crowded population and the land being used to a maximum extent, the availability of such huge area for setting up a wind farm is difficult. Also in the urban environment, the wind speed required for harnessing higher power is less. For these reasons, small wind turbines which can be installed on rooftops are suitable for use in urban areas, as well as rural areas that are not connected to any electricity network. Apart from all the renewable energy resources, cleaner energy systems such as micro wind turbines played a key role in the renewable electricity generation. In wind turbines, some mechanical and electrical aspects of the turbines are necessary to study in details so that the turbine can achieve its electrical output efficiency [1, 2].

Wind turbines convert wind energy into electricity via mechanical energy. There are two primary types of wind turbines, namely horizontal axis (HAWT) and vertical axis (VAWT) wind turbines, and the efficiency of each wind turbine type varies by its design and fabrication.Similarly, these two main group of a wind turbine is classified depending on their axis in which the turbine rotates. Because the horizontal axis has the ability to collect the maximum amount of wind energy for the time of the day and can adjust their blades pitch angle to avoid high windstorms, they are considered more familiar and more common than the vertical axis. HAWTs are most commonly used in wind farms.

Fig. 1: Vertical and Horizontal Axis Wind Turbine [1, 5].

Micro wind turbines can be designed using PVC blades as it can give better power capacity and less costly. It can be used in areas where the velocity of wind is low, that is, as low as 2 m/s, like a plateau or hilly region or in places where large wind turbine does not give a good result. Because of low cost and being of economical, it can be installed in residential areas over the houses for power generation. Moreover, utilization of small wind turbines for the household would result in fewer burdens on the grid and also plays a vital role in reducing utilization of conventional energy and mobility to utilize the power. These micro wind turbines can be used where wind velocity is low like hilly regions or especially rooftops of building and they are less costly, easier to install and can power electrical devices like the LED sign, Cell phones, lighting a lamp, etc. [17, 20].

2. Design and Construction of Horizontal Axis Micro Wind Turbine

Some of the components of the wind turbine and electrical parts associated with it are DC Motors: 12 V, 3 Inch diameter PVC PIPE and 10 Inch in Length, Round base: 2.5 Inch Diameter, Hand Cutter, Drill and Cycle Screw.

A wind turbine blade converts wind energy into rotational mechanical energy. It is the most important part of a wind turbine. Before the design of turbine blade, two important points should be taken into consideration, i.e., (1) the weight of each blade should be equal. (2) Each blade should be positioned on the plate at equal distances. Following are the steps and the materials required for the construction of the turbine blades. In this case, the turbine blades are constructed of thermoplastic material (PVC PIPE) which is of 10 inches in length and 3 inches in diameter. Firstly, the pipe is cut into blades in three equal parts and every three parts are cut into two. Then, from six identical blades, three blades are taken into consideration and at one end of the pieces, holes have been made with the help of a drill. Moreover, a 2.5 inches diameter round base is cut to join these three pieces of turbine blades and then holes are drilled at equal distances from this round base. Lastly, the three blades are then joined to the round base at an equal distance using cycle screws tightly.

Fig. 2: Construction Stages of Wind Turbine Blades

3. Mechanical Aspects of the Horizontal Axis Micro Wind Turbine

The aerodynamics of flow around the wind turbine blades plays an important role in comparing all the factors responsible for efficient energy production. In order to better treat the wind turbine aerodynamics, one of the approaches is by application of computational fluid dynamics (CFD). It can be also be observed that CFD can be used as a potential tool to study the detailed flow field around wind turbine rotor. To better understand the aerodynamics of wind turbines one of the alternative methods is the use of dedicated experiments to increase knowledge and physical understanding of the phenomena and the validation of models. The simulations have been carried out in commercial CFD code FLUENT. The results from CFD simulations aid in better understanding of the flow structure around the turbine.

3.1 Mechanical Design of the Turbine Blade

Following are the dimensions of the wind turbine blade which are designed by a software known as AutoCAD Software. The blade of the wind turbine was designed accordingly to the given dimensions.

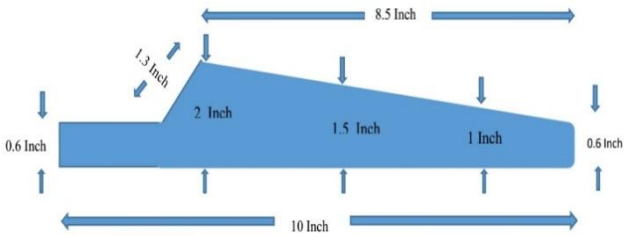

Fig. 3: Blade dimension of the Turbine blade

Fig. 4: Horizontal Axis Micro wind turbine blade under study

Following are the AutoCAD Designs of the wind turbine blade which have been designed according to the given dimension.

Fig. 5: Isometric view of the full blade model design

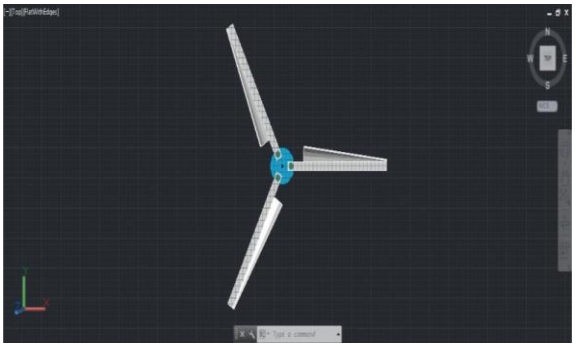

Fig. 6: Top view of the full blade design

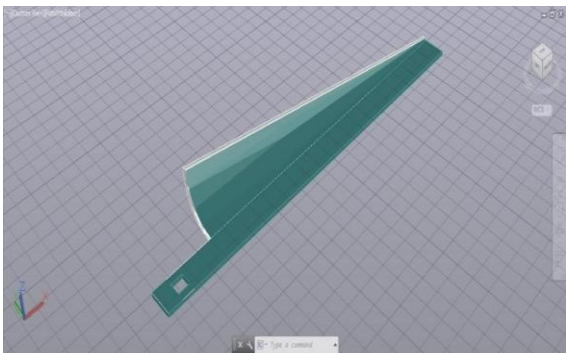

Fig. 7: Isometric view of the single blade design

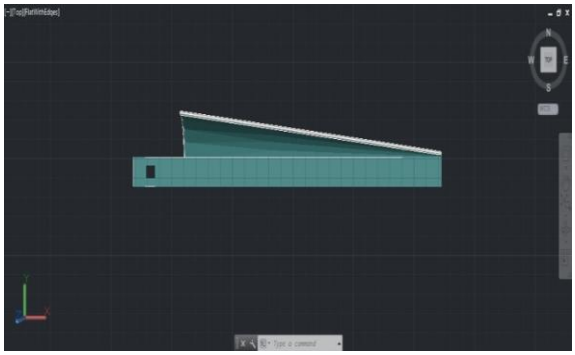

Fig. 8: Top view of the single blade design

3.1.1 Mechanical Simulation of the Turbine Blade

A 3-D computational model of the rotor system has been created and CFD simulations or mechanical simulation of the turbine blade have been carried out using commercial CFD code FLUENT or Ansys Fluent Software. The inputs given in this analysis includes Chord length =0.254m (10 inches), radius of the turbine blade=0.254m (10 Inches), blade RPM= 300, Wind Velocity= 2.5m/s, 3.1 m/s, and 3.5m/s and blade material=Thermoplastic material (PVC blade). In this Simulation, Pressure Distribution on the Turbine Blade has been determined.The analysis has been carried out for a constant blade RPM of 300 RPM at various Wind Speed, viz., 2.5 m/s, 3.1 m/s and 3.5 m/s. As a result, the pressure distribution on the turbine blade shows good results that it can withstand at any wind speed.

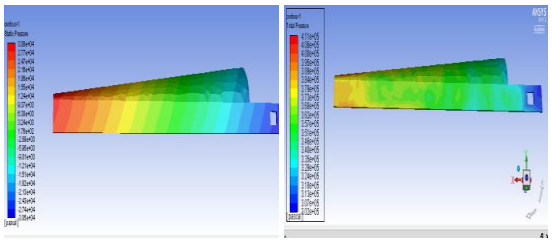

Fig. 9: Pressure for Wind velocity=2.5m/sec, RPM=300

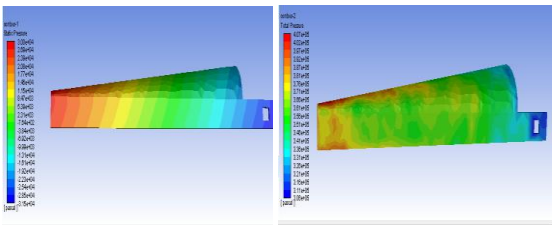

Fig. 10: Pressure for Wind velocity=3.1m/sec, RPM=300

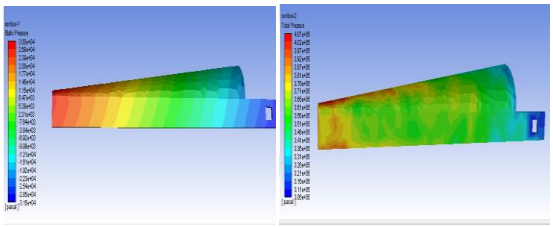

Fig. 11: Pressure for Wind velocity=3.5m/sec, RPM=300

The figures given above show the pressure distribution on all the parts of the turbine blade. It can be identified or determined by different colors such that the red color on the tip of the turbine blade indicates the maximum pressure whereas the blue color on the turbine blade indicates the minimum pressure.

4. Electrical Simulation of the Wind Turbine Generator using Matlab-Simulink

Since wind is a source of energy which is clean, easy access and sustainable source of energy. Therefore, Wind energy utilization for power generation purpose isbecoming high interest in electrical power production. However, understanding of wind properties is very importantfor wind energy exploitation. The speed of wind is highly variable depending on the season and in hourly means and both geometrically from place to place and temporally. Moreover, the output of micro wind turbine mostly depends on the wind. Therefore, the more is the wind speed, the greater is the amount of power the wind turbine generates. Different regions have different wind speeds. As a result, determination of the value of the wind speed for a particular region is necessary.In thepresent study, a mathematical model and its simulation technique has beenstudied that affect the electrical output power generated by the wind turbine. Therefore, these modeling and electrical simulation techniques will play a great role in thedesign and analysis of these wind turbines.

5.1 Electrical Simulation of Wind turbine

A wind power plant has been designed by using Matlab-Simulink as shown in figure 12. The designed system consists of a 1.5 MW (can be changed to any value) wind turbine connected to a load 400 KVA and electric power source 25 KV through a three-phase transformer, the active and reactive power is measured for different wind speed and a different pitch angle of the blade. The values or parameters of the designed system can be changed by changing the system blocks parameters very easily and this is the advantage of using Matlab-Simulink.The model in this study has been used for higher power output which is of 1.5 MW at a wind speed of 12 m/s. Therefore, with the changing of the different parameters of the designed model, it can be implemented in a micro or mini wind turbine as well. Therefore, Figure 13 shows an image of the Matlab-Simulink scope display which shows the output power curve of the designed wind turbine at a wind speed of 12 m/s.

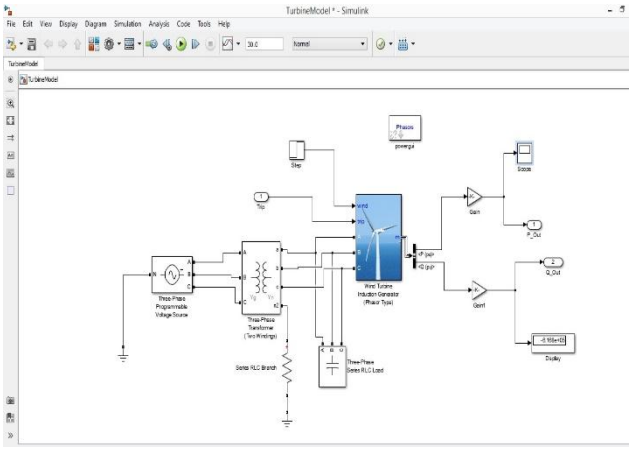

Fig. 12: 1.5 MW wind turbine power plant [32]

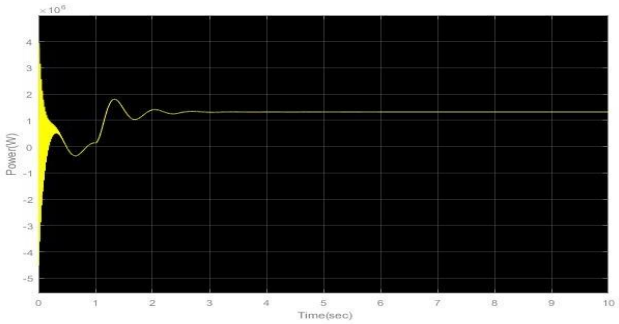

Fig. 13: Output Power curve at wind speed 12m/s [32]

4.1.1 Output Power for different Wind Speed

Following are the output power graph for different wind speed which is obtained by simulated the designed model with respect to the different wind speed. From the figures given below, it is shown that the output power curve increases with the increase of wind speed and decrease with the decrease of wind speed. Therefore, the output power of the wind turbine depends on wind speed, that is, the output power varies when the wind speed is also varying.

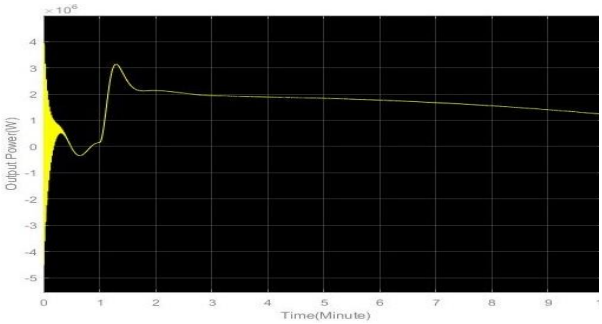

Fig. 14: Output Power curve at wind speed 16m/s

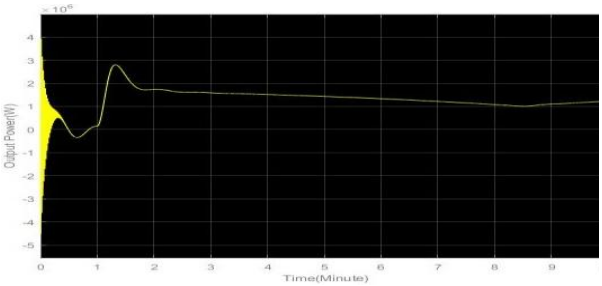

Fig. 15: Output Power curve at wind speed 14m/s

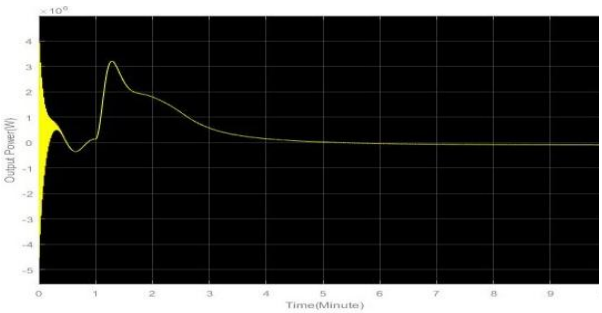

Fig. 16: Output Power curve at wind speed 8 m/s

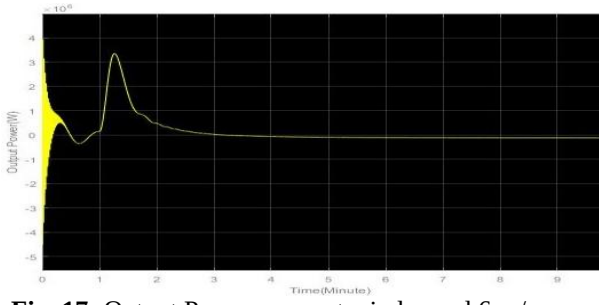

Fig. 17: Output Power curve at wind speed 6 m/s

5. Electrical Power Output Measurement with respect to Wind Speed

A designed micro horizontal axis wind turbine is taken to the rooftop for measuring the electrical power output of the Wind Turbine coupled with a DC Generator can generate, with respect to the available wind speed. This experiment was done in Azara (Guwahati) and Mawlynrei (Shillong) and the tools used are Anemometer, Multimeter, Resistors, LED strips and connecting wires.

Fig. 18: Snapshots of the Experimental Set-up

Therefore, the electrical power output that was obtained with respect to wind speed taken both in Azara (Guwahati) and Mawlynrei (Shillong) are represented in graphical form as follows:

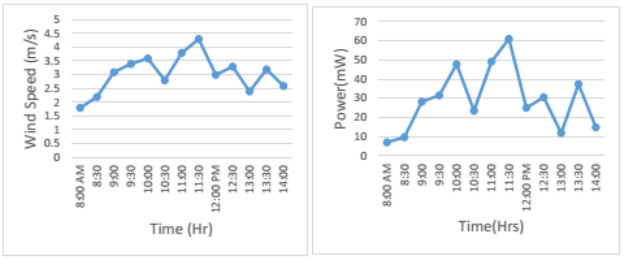

Fig. 19: Velocity duration curve and Power duration curve as on 28/09/2017

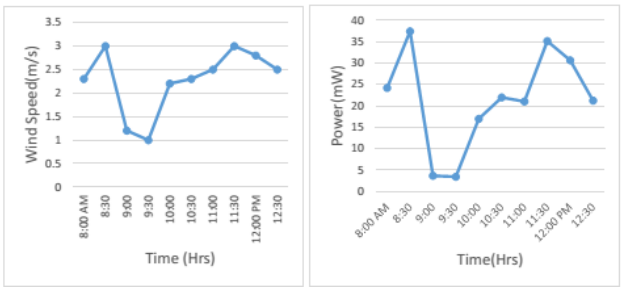

Fig. 20: Velocity duration curve and Power duration curve as on 03/10/2017

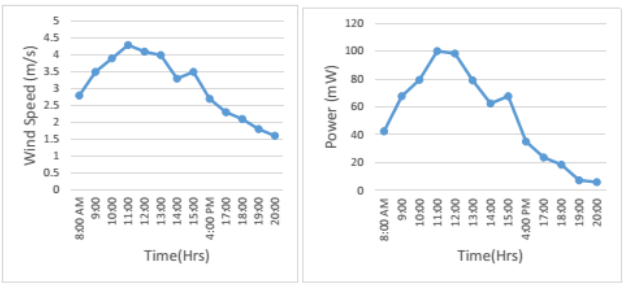

Fig. 21: Velocity duration curve and Power duration curve as on 17/10/2017

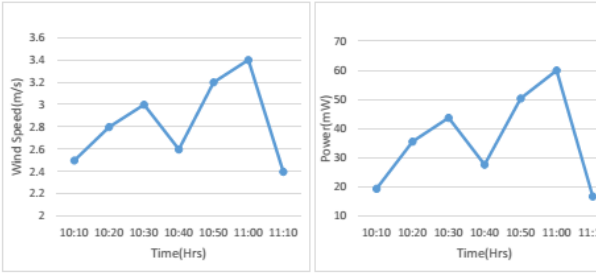

Fig. 22: Velocity duration curve and Power duration curve as on 10/05/2018

5.1 A Relationship between Wind Power (P) and maximum obtained Electrical Output

Wind Turbine Power is calculated as,

$$P = \frac{1}{2}.\ \rho.\ A.\ C_P.V^3 \ \ldots\ldots\ldots\ldots\ldots\ldots\ldots (1)$$

Where,

P = Wind Power in watts

ρ = air density in Kg/m^3 (Typically ρ = 1.225 kg/m^3 at sea level)

A = rotor swept area (m^2) ($A = \pi r^2$)

C_P = Power Coefficient (Typically C_P = 0.35 - 0.45, 0.35 for a good design)

V = wind speed in m/s (Wind speed = 3 - 4 m/s)

Therefore Wind Turbine Power is calculated as follows,

$$P = 0.5 * 1.225 * 0.\ 2026 * (3)^3 * 0.35$$
$$= 1.1726 \text{ Watts}$$

Where,

ρ = 1.225 kg/m^3,

$A = \pi r^2 = \pi * (0.254)^2$ = 0.2026 m^2, $C_P = 0.35$,

V = 3 m/s

Similarly, Efficiency is obtained as follows,

$$\eta = \frac{Electrical\ Power}{Wind\ Power} \times 100\% \ \ldots\ldots\ldots\ldots (2)$$

$$\eta = \frac{60.02 * 10^{-3}}{1.1726} \times 100\%$$

Where,

Electrical Power = 60.02 mW

Wind Power = 1.1726 W

Therefore, Efficiency,

$$\eta = 5.11\ \%$$

6. Conclusion

This paper presents the design of Horizontal axis micro wind turbine for low wind speed areas. The Micro Horizontal Axis Wind Turbine has been designed and has also been tested under variable wind speed conditions, in Shillong and Azara (Guwhati). Then, incorporation of DC generator with the Turbine has been done to obtain electrical power output and electrical power output measurement has been done successfully. Similarly, MechanicalDesign of the Turbine Blade has been done by using AutoCAD Software and Mechanical Simulation of the Turbine Blade i.e., Pressure Distribution on the Turbine Blade has been done by using Ansys Fluent Software. Moreover, Electrical Simulation and modelling of the wind turbine has been done for higher power output and Relationship between Wind Power (P) and Electrical Output has been calculated for Efficiency Improvement.

The further directions to the work include Electrical Simulation of the Horizontal Axis Micro Wind turbine can be done by changing the parameters of the designed model and further design modifications of the turbine for efficiency improvement.

References

[1] D. M. Bui and W. J. C. Melis, "Micro wind Turbine for Energy Gathering in built-up areas", *International Journal of Sustainable Energy Development (IJSED)*, Vol. 2, Issue No. 2, 2013. Doi: 20533/ijsed 2046.3707.2013.0016

[2] Z. Li, F. Boyle and A. Reynolds, "Domestic Application of Micro wind Turbines in Ireland: Investigation of their economic viability", *Renewable Energy*, Vol. 41, 2011, pp. 64-74. Doi: https://doi.org/10.1016/j.renene.2011.10.001

[3] J. K. Sahu and M. Sahu, "Micro Wind Turbine Technology: To Enhance Self Generative System in Passenger Train", *International Research Journal of Engineering and Technology (IRJET)*, Vol. 3, Issue No. 11, November 2016. Retrieved from https://irjet.net/archives/V3/i11/IRJET-V3I11110.pdf

[4] A.R. Sengupta, A. Biswas and R.Gupta, "Vertical Axis Wind Turbines in the Built Environment: A Review", *ISESCO Journal of Science and Technology*, Vol. 12, Issue No. 22, pp. 11-16. Retrieved from https://www.isesco.org.ma/ISESCO_Technology_Vision/NUM22/doc/2.pdf

[5] A. Deo, J. N. Goundar, S. Narayan, and N. Chettiar, "Design and Performance Analysis of Micro Wind Turbines for Fiji", *International Journal of Information and Electronics Engineering*, Vol. 6, Issue No. 1,

January 2016. Retrieved from http://www.ijiee.org/vol6/590-SE307.pdf

[6] N. N. Sorte and S. M. Shiekh, "Design and Development of Micro Vertical Axis wind turbine for Rural Application", *International Journal of Engineering and Computer Science*, Vol. 03, Issue No. 07, July 2014, pp. 7035-7040. Retrieved from https://dokumen.tips/documents/design-and-development-of-micro-vertical-axis-wind-turbine-ijecspdf1pg-student.html

[7] J. Zhang, Z. Zhou and Y. Lei, "Design and research of high- performance low-speed wind turbines blades", *2009 World Non-Grid-Connected Wind Power and Energy Conference*, Nanjing, 2009, pp. 1-5. Doi: 10.1109/WNWEC.2009.5335818

[8] M. Mohammadi, A. Mohammadi, M. Mohammadi and H. N. Minaei, "Optimization of small-scale wind turbine blades for low-speed conditions", *Journal of Clean Energy Technologies*, Vol. 4, Issue No. 2, March 2016, pp. 140-143. Retrieved from http://www.jocet.org/vol4/268-H1007.pdf

[9] N. Prasad E., Janakiram S., Prabu T. and Sivasubramaniam S., "Design and development of Horizontal small turbine blade for low wind speed", *International Journal of Engineering Science & Advanced Technology (IJESAT)*, Vol. 4, Issue No.1, 2014. Retrieved from http://ijesat.org/Volumes/2014_Vol_04_Iss_01/IJESAT_2014_01_01_14.pdf

[10] N. Korprasertsak and T. Leephakpreeda, "Analysis and optimal design of wind boosters for Vertical Axis Wind Turbines (VAWTs) at low wind speed", *Journal of Wind Engineering and Industrial Aerodynamics*, Vol. 159, 2016, pp. 9-18. Doi: https://doi.org/10.1016/j.jweia.2016.10.007

[11] Y. Vidal, L. Acho, N. Luo, M. Zapateiro and F. Pozo, "Power control design for variable speed wind turbines," *Energies*, Vol. 5, Issue No. 8, 2012, pp. 3033-3050; https://doi.org/10.3390/en5083033

[12] S. Rajendran and D. Jena, "Control of variable speed variable pitch wind turbine at above and below rated wind speed", *Journal of Wind Energy*, Vol. 2014, Article ID 709128.
Doi: http://dx.doi.org/10.1155/2014/709128

[13] A. Mclever, D. G. Holmes, P. Freeze, "Optimal control of a variable speed wind turbine under dynamic wind conditions", *IAS'96: Conference Record of the 1996 IEEE Industry Applications Conference, Thirty-First IAS Annual Meeting*, San Diego, CA, USA, 1996, Vol. 3, pp. 1692-1698. Doi: 10.1109/IAS.1996.559297

[14] M. Izadbakhsh, A. Rezvani, M. Gandomkar and S. Mirsaeidi, "Dynamic analysis of PMSG wind turbine under variable wind speeds and load conditions in the grid connected mode", *Indian Journal of Science and Technology*, Volume 8, Issue No. 14, July 2015. Doi: 10.17485/ijst/2015/v8i14/51864

[15] L. Wu and D. Enfield, "Investigation on the interaction between inertial response and droop control from variable speed wind turbines under changing wind conditions", *2012 47th International Universities Power Engineering Conference (UPEC)*, London, 2012, pp. 1-6. Doi: 10.1109/UPEC.2012.6398429

[16] Abubakkar A, T. Ravisankar and M. Makeshkumar, "Design and fabrication of micro wind turbine", *International Journal of Science, Engineering and Technology Research (IJSETR)*, Vol. 5, Issue No. 5, May 2016, pp. 1785-1787. Retrieved from http://ijsetr.org/wp-content/uploads/2016/05/IJSETR-VOL-5-ISSUE-5-1785-1787.pdf

[17] V. K. Rathod and S. Y. Kamdi, "Design and Fabrication of PVC bladed inexpensive wind turbine", *IOSR Journal of Mechanical and Civil Engineering (IOSR-JMCE)*, Vol. 11, Issue No. 4, Ver. II, Jul- Aug. 2014, pp. 114-119. Retrieved from http://iosrjournals.org/iosr-jmce/papers/vol11-issue4/Version-2/O01142114119.pdf

[18] A. Dhote and V. Bankar, "Design, analysis and fabrication of Savanius Vertical axis wind turbine", *International Research Journal of Engineering and Technology (IRJET)*, Vol. 02, Issue No. 03, June 2015. Retrieved from https://www.irjet.net/archives/V2/i3/Irjet-v2i3331.pdf

[19] M. Kumari, H. K. Singh, "Small Scale Wind Turbines: As alternative Energy system", *International Journal of Science and Research (IJSR)*, Vol. 3, Issue No. 6, 2014, pp. 1607-1609. Retrieved from https://www.ijsr.net/archive/v3i6/MDIwMTQ1MTc=.pdf

[20] D. P. Drumheller, G. C. D'Antonio, B. A. Chapman, C. P. Allison and O. Pierrakos, "Design of a micro wind turbine for implementation in low wind speed environment", *2015 Systems and Information Engineering Design Symposium*, Charlottesville, VA, 2015, pp. 125-130. Doi: 10.1109/SIEDS.2015.7116959

[21] A. Suresh and S. Rajakumar, "Design and experimental investigation of a micro wind turbine", *International Journal of Advances in Engineering Research (IJAER)*, 2015, Vol. No. 10, Issue No. VI, December. Retrieved from http://www.ijaer.com/images/short_pdf/1451677792_A_Suresh_22.pdf

[22] M. M. M. Saad and N. Asmuin, "Comparison of Horizontal Axis Wind Turbines and Vertical Axis Wind Turbines", *IOSR Journal of Engineering (IOSRJEN)*, Vol. 04, Issue No. 08, August 2014, pp. 27-30. Retrieved from http://www.iosrjen.org/Papers/vol4_issue8%20(part-2)/E04822730.pdf

[23] A. Sarkar and D. K. Behera, "Wind Turbine Blade Efficiency and Power Calculationwith Electrical Analogy", *International Journal of Scientific and Research Publications*, Vol. 2, Issue No. 2, February 2012. Retrieved from http://www.ijsrp.org/research_paper_feb2012/ijsrp-feb-2012-06.pdf

[24] M. Keerthana, M. Sriramkrishnan, T. Velayutham, A. Abraham, S. S. Rajan and K. M. Parammasivam, "Aerodynamic Analysis of a small horizontal axis wind turbine using CFD", *Journal of Wind and Engineering*, Vol. 9, Issue No. 2, July 2012, pp 14-28. Retrieved from https://www.researchgate.net/publication/263567112

[25] T. Miloş, A. Bej, E. Dobândă, A. Manea, R. Bădăräu and D. Stroiţă, "Blade design using CAD technique for small power wind turbine", *2010 International Joint Conference on Computational Cybernetics and Technical Informatics*, Timisoara, 2010, pp. 571-575. Doi: 10.1109/ICCCYB.2010.5491209

[26] R. Lanzafame, S. Mauro and M. Messina, "Numerical and experimental analysis of micro HAWTs designed for wind tunnel applications", *International Journal of Energy and Environmental* Engineering, Vol. 7, Issue No. 2, 2016, pp. 199-210. Doi: https://doi.org/10.1007/s40095-016-0202-8

[27] M. A. Abrar, A. M. I. Mahbub and M. Mamun, "Design Optimization of a Horizontal Axis Micro Wind Turbine through Development of CFD Model and Experimentation", *10th International Conference on Mechanical Engineering, ICME-2013*, *Procedia Engineering*, Vol. 90, 2014, pp. 333-338. Doi: https://doi.org/10.1016/j.proeng.2014.11.858.

[28] U. E. Y. Gomez, Z. J. A. Lopez., R. A. Jimenez, Victor Lopez G., J. Jesus Villalon L., "Design and Manufacturing of Wind Turbine Blades of Low Capacity using CAD/CAM Techniques and Composite Materials", *2013 ISES Solar Congress*, *Energy Procedia*, Vol. 57, 2014, pp. 682-690, doi: 10.1016/j.egypro.2014.10.223

[29] P. Pathike, T. Katpradit, P. Terdtoon and P. Sakulchangsatjatai, "Small Horizontal-Axis Wind Turbine Blade for Low Wind Speed Operation", *Journal of Applied Science and Engineering*, Vol. 16, Issue No. 4, 2013, pp. 345-351. Retrieved from http://www2.tku.edu.tw/~tkjse/16-4/02-ME10121_875.pdf

[30] H. Mamur , "Design, application, and power performance analyses of a micro wind turbine", *Turkish Journal of Electrical Engineering & Computer Sciences*, Vol. 23 Issue No. 6, 2015, pp. 1619-1637. Doi: 10.3906/elk-1401-174

[31] P. K. Nigam, N. Tenguria and M. K. Pradhan, "Analysis of horizontal axis wind turbine blade using CFD", *International Journal of Engineering, Science and Technology*, Vol. 9, Issue No. 2, 2017, pp. 46-60. Doi: http://dx.doi.org/10.4314/ijest.v9i2.5

[32] R. T. Ahmad and M. A. Abdul-Hussein, "Modelling and Simulation of Wind Turbine Generator Using Matlab-Simulink", *Journal of Al Rafidain University College*, Issue No. 40, 2017, pp. 282-300. Retrieved from https://www.researchgate.net/publication/319136680

[33] P. Pathike, T. Katpradit, P. Terdtoon and P. Sakulchangsatjatai, "A New Design of Blade for Small Horizontal-Axis Wind Turbine with Low Wind Speed Operation", *Energy Research Journal*, Vol. 4, Issue No. 1, 2013, pp. 1-7. Doi: 10.3844/erjsp.2013.1.7

Authors' Profile

Deibanehbok Nongdhar is a student of M.Tech. 4th semester in the Department of Electrical and Electronics Engineering, School of Technology, Assam Don Bosco University, India.

Bikramjit Goswami is working as an Assistant Professor in the Department of Electrical and Electronics Engineering, School of Technology, Assam Don Bosco University, India. He is also a Ph.D. Research Scholar in Assam Don Bosco University currently. His research interests are Reconfigurable Antenna, Microwave Remote Sensing, Artificial Neural Networks, renewable Energy, Disaster Forecasting.

Pallav Gogoi is working as an Assistant Professor in the Department of Mechanical Engineering, School of Technology, Assam Don Bosco University, India.

Sidharth Borkataky is working as an Assistant Professor in the Department of Mechanical Engineering, School of Technology, Assam Don Bosco University, India.

Comparative Analysis of Different Control Schemes for DC-DC Converter

Ferrarison B. Lynser[1], Morningstar Sun[2], Maiarta Sungoh[3], Nuki Taggu[4], Pushpanjalee Konwar[5]

[1,2,3,4,5]Don Bosco College of Engineering and Technology, Assam Don Bosco University
Airport Road, Azara, Guwahati - 781017, Assam, INDIA.

*[1]ferlynser123@gmail.com, [2]msun413@gmail.com, [3]maiaz1302@gmail.com, [4]nukitaggu.aru@gmail.com, [5]pushpanjalee.konwar@dbuniversity.ac.in**

Abstract: ***DC-DC converters are some power electronic circuits that convert the DC voltage from one level to another. They have a very large area of applications ranging from computing to communication. They are widely used in appliance control transportations, and high-power transmission. Its increasing demand is based on its capability of electrical energy conversion. The basic topology of DC-DC converter are Buck converter and Boost converter, other topologies are derived from this two-basic topology. In this paper, mathematical modelling of both Buck and Boost converters has been done. Some of the control schemes are summarized in this paper. Current mode control (CMC), PID, control including their advantages and disadvantages are highlighted in this paper.***

Keywords: DC-DC converter, PID, IMC and Buck converter.

1. Introduction

The switch mode DC-DC converters are the simplest power electronic circuit that efficiently converts an unregulated DC voltage into a regulated DC voltage. Solid-state device such as transistors and diodes are used as switching power supplies. They operate as switch either in completely ON or completely OFF state. The energy storing elements such as inductor and capacitor are used for energy transfer and works as a low pass filter. The buck and boost converters are the two fundamental topologies of switch mode DC-DC converter. DC-DC converters have a wide area of applications. The drastic use of these converters in appliances control, telecommunication equipment's, DC-motor drives, automotive, aircrafts, etc. increases its interests in many fields.

The analysis along with the control of switching converters is the main factor to be considered. Various control schemes are used to control the switch mode DC-DC converter. There are many advantages and disadvantages related to every control methods. Preference is always given to the methods under which best performance is obtainable.

The most commonly used control technique is PWM voltage mode control, PWM current mode control, PID controller. The disadvantage of these controllers is that satisfied results are not achievable under large parameter or variation of load.

DC-DC converter usually operates in two modes of operation: continuous mode and discontinuous mode. In case of continuous mode, the current through the inductor never falls to zero whereas in case of discontinuous mode the current through the inductor falls to zero as the switch is turned off.

1.1 Advantages of Buck Converter

(i) Step down of voltage is possible with minimum component count.
(ii) Less costly compared to most of the other converters if compromised performance is desired for a low cost.

1.2 Disadvantages of Buck Converter

(i) Input current and charging current of the output capacitor is discontinuous resulting in larger filter size.
(ii) This converter is difficult to control. The transfer function of this converter contains a right half plane zero which introduces the control complexity.

1.3 Applications of Buck Converter

(i) **Battery Chargers:** In order to reduce the heat in the portable devices a buck converter is used.
(ii) **Solar chargers:** A solar charger is often a buck converter with a microcontroller control, converting a high voltage to low voltage efficiently

(iii) **Quadcopters:** Quadcopters often are powered from a multi cell lithium battery pack. These battery packs produce a voltage where buck converter drops the battery voltage down.

(iv) **POL converter for PC and Laptops:** a point-of-load converter is a non-isolated buck converter that is capable of efficiently driving power to high current load. This is especially helpful in PC and laptop motherboards.

The converter such as buck converters gives high power efficiency as DC-to-DC converter compare to linear regulators which are simpler circuits and lower voltages by dissipating power as heat, but do not step up output current. We have designed the mathematical model of both single input and dual input buck converter and have implemented with different control schemes for the converters and to compare the responses of different control schemes implemented in the converter.

2. Buck Converter

The buck converter is shown in figure 1. It is the step-down converter in which a fixed high voltage is step down to a desired low voltage level. It consists of non-dissipative switch, inductor, and capacitor. The switches will operate at the rate of PWM switching frequency. The ratio of ON time when the switch is closed to the entire switching period is known as the duty cycle and is represented as:

$$d = \frac{t_{ON}}{T}$$

and the output voltage is controlled by varying the duty cycle. During steady state, the ratio of output voltage over input voltage is d, which is given by:

$$d = \frac{V_{out}}{V_{in}}$$

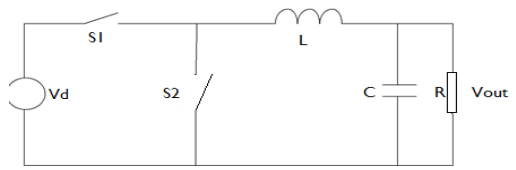

Figure 1: Basic Buck Converter

In the first sub circuit state when the switch S_1 is closed, the diode is reversed biased and the energy is transferred from the source to the inductor and the current through the inductor gradually increases during this time interval as shown in figure 2(a). In the next sub-circuit state when the switch S_2 is closed, the source is disconnected from the network. The diode will be forward biased and the current will flow through the freewheeling diode. During the second-time interval, the current through the circuit decreases linearly as the energy in the inductor discharges as shown in the figure 2(b).

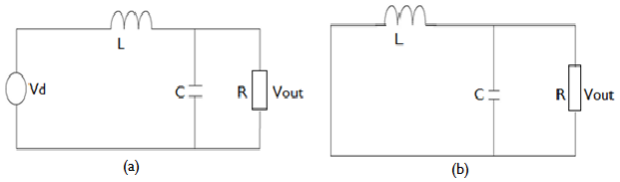

Figure 2: Buck Converter when (a)Switch is ON (b) Switch is OFF

3. PID Controller design for Buck Converters

To design a controller using the frequency response method, phase-lead, phase-lag or lead-lag compensation is usually used. A proportional-derivative (PD) controller is phase-lead compensation. The advantage of using PD controllers is that it leads to the increase of phase margin and improvement of cross-over frequency. The transfer function of a PD controller is:

$$G_C(s) = K_P + K_D(s)$$

A proportional-integral (PI) controller is a phase-lag controller. A PI controller is used to increase the low frequency loop gain, therefore reducing steady-state error. The transfer function of a PI controller is:

$$G_C(s) = K_p + \frac{K_I}{s} = \frac{K_p s + K_I}{s}$$

The PI controller has a pole at the origin. Both PD and PI controllers are first-order controllers.

By using a lead-lag compensator, the advantages of lead compensation and lag compensation can be combined to obtain sufficient phase margin, high loop gain and wide control bandwidth. A proportional-integral-derivative (PID) controller is a lead-lag compensator. It is the most widely used compensator in feedback control systems. The PID controller is defined as:

$$u(t) = K_P e(t) + K_I \int_0^{\tau} e(t)dt + K_D \frac{de(t)}{dt}$$

Where, e(t) is the compensator input and u(t) is the compensator output.

The Laplace transform of above equation yields the transfer function:

$$G_C(s) = \frac{U(s)}{E(s)} = K_P + \frac{K_I}{s} + K_D(s)$$

The integral term is phase-lag and the derivative term is phase-lead. The low frequency gain is improved by the integral term, and the low-frequency components of the output voltage are accurately regulated. At high frequency, the phase margin and cross-over frequency are improved by the derivative term, which improves the system's stability and the speed of the transient response. An increase in the proportional term will increase the speed of system response; however, too much proportional gain will make the system unstable.

For operation during a startup transient and steady state, a PID and a PI controller were designed for the buck converter respectively. The derivative term in a PID controller is susceptible to noise and measurement error of the system, which could result in oscillation of the duty cycle during steady state. However, the derivative term is needed during a transient period to reduce the settling time by predicting the changes in error. Therefore, to obtain the desired response, the system switches between PID and PI controllers during transient and steady state period. The PID controller is applied during start up to obtain a fast-transient response. The PI controller is applied during steady state to reduce oscillation of the duty cycle and improve the system's stability.

4. Internal Model Control

In process control applications, model-based control systems are used to track set points and remove low disturbances. The internal model control (IMC) idea relies on the internal model principle which states that if any control system comprises within it, indirectly or openly, to easily achieve a perfect control, some representation of the process is to be controlled. In particular, if the control scheme has been developed based on the exact model of the process then perfect control is theoretically possible.

4.1 Internal Model Control Strategy

If we assume there exists model of the plant with transfer function modeled as $\tilde{g}_p(s)$ such that $\tilde{g}_p(s)$ is an exact representation of the process (plant), i.e. $\tilde{g}_p(s) = g_p(s)$ then set point tracking can be achieved by designing a controller such that:

$$g_c(s) = \tilde{g}_p(s)^{-1}$$

This control performance characteristic is achieved without feedback and highlights two important characteristic features of this control modeling. These features are:

- Feedback control can be theoretically achieved if complete characteristic features of the process are known or easily identifiable.
- Feedback control is only necessary of knowledge about the process is inaccurate or incomplete.

This control performance as already said has been achieved without feedback and assumed that the process model represents the process exactly i.e. process model has all features of parent model. In real life applications, however, process models have capabilities of mismatch with the parent process; hence feedback control schemes are designed to counteract the effects of this mismatching. A control scheme that has gained popularity in process control has been formulated and known as the Internal Model Control (IMC) scheme. This design is a simple build up from the ideas implemented in the open loop model strategy and has general structure as depicted by figure below.

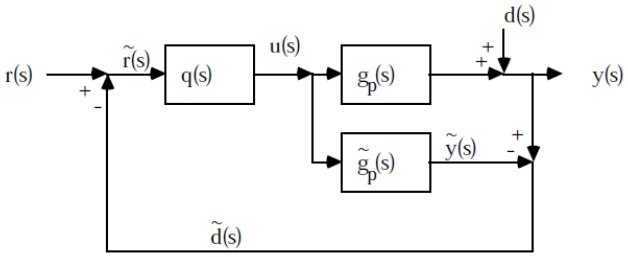

Figure 3: Block Diagram of IMC.

From the above figure, description of blocks is given as follows:

Controller = $g_c(s)$
Process = $g_p(s)$
Internal model = $g_p(s)$
Disturbance = d(s)

4.2 Equivalent Feedback To IMC

The feedback equivalence to IMC by using block diagram manipulation begins with the IMC structure shown in Figure 4.

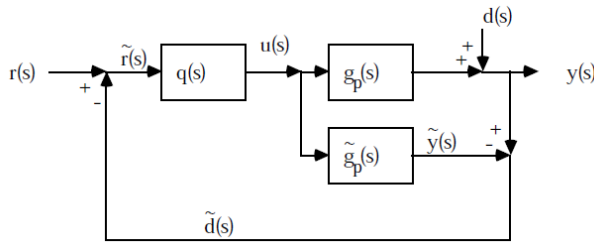

Figure 4: IMC Structure

Figure 4 can be rearranged to the form of Figure 5.

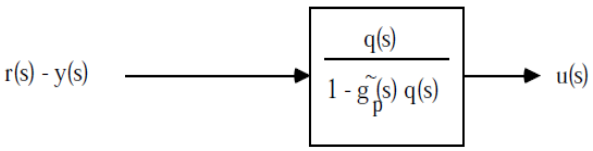

Figure 5: Equivalent Block

The r(s)-y(s) is simply the error term used by a standard feedback controller. Therefore, we have found that the IMC structure can be rearranged to the feedback control (FBC) structure. This reformulation is advantageous because we will find that a PID controller often results when the IMC design procedure is used. Also, the standard IMC block diagram cannot be used for unstable systems, so this feedback form must be used for those cases.

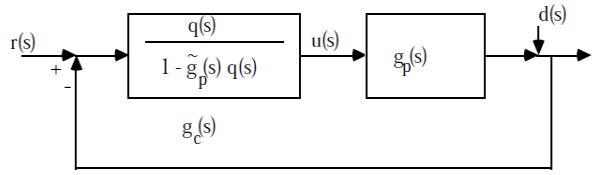

Figure 6: Standard Feedback Diagram Illustrating the Equivalence with IMC.

Where, the feedback controller, $g_c(s)$, contains both the internal model: $\tilde{g}_P(s)$ and $q(s)$.

The standard feedback controller which is equivalent to IMC is:

$$g_c(s) = \frac{q(s)}{1 - g_p(s).q(s)}$$

4.3 Internal Model Control Based PID Controller

The IMC configuration is designed for setting up a comparison between the process and model output to form a standard feedback structure. Figure 5 shows the basic IMC implementation in the process transfer function.

The transfer function for our Buck converter is:

$$\tilde{g}_p(s) = \frac{k_p(\beta s+1)}{\tau^2 s^2 + 2\varepsilon\tau s + 1}$$

$$\tilde{g}_p(s) = \tilde{g}_{p+}(s)\,\tilde{g}_{p-}(s)$$

$$\tilde{g}_{p+}(s) = \frac{k_p(\beta s+1)}{\tau^2 s^2 + 2\varepsilon\tau s + 1}$$

$$q(s) = \tilde{g}_{p+}(s)^{-1} f(s) = \frac{\tau^2 s^2 + 2\varepsilon\tau s + 1}{k_p(\beta s+1)}$$

$$g_c(s) = \frac{q(s)}{1 - q(s)\,\tilde{g}_p(s)}$$

$$g_c(s) = \frac{\tau^2 s^2 + 2\varepsilon\tau s + 1}{\lambda s(\beta s+1)}$$

The transfer function for the PID controller is:

$$g_c(s) = k_c\left[\frac{\tau_i\tau_d s^2 + \tau_i s + 1}{\tau_i s}\right]$$

Then the PID parameters based on IMC will be derived as shown in Table 1.

Table 1: IMC based PID parameters for Buck Converter

$\tilde{g}_p(s)$	$f(s)$	k_c	τ_i	τ_d
$\frac{k_p(\beta s+1)}{\tau^2 s^2 + 2\varepsilon\tau s + 1}$	$\frac{1}{(\lambda s+1)}$	$\frac{2\varepsilon\tau}{k_p(\beta s+1)}$	$2\varepsilon\tau$	$\frac{\tau}{2\varepsilon}$

5. Results

In this work, more emphasis is given for improving the dynamic response of the DC-DC buck converter by identifying proper controller parameter. The following dynamic parameters are considered in this work: i) Rise Time ii) Settling Time iii) Peak Overshoot.

In order to examine the effectiveness of the proposed algorithm, extensive simulation and experimental studies have been carried out on the closed loop system of Buck converter.

5.1 Response Based on IMC based PID controller

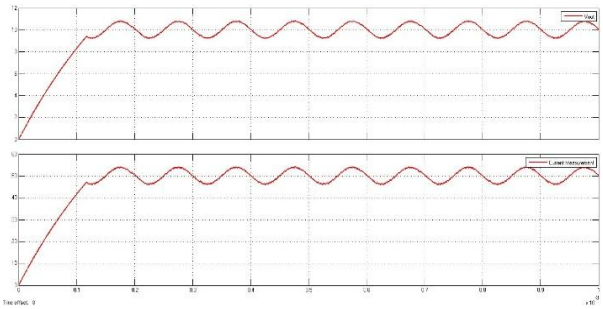

Figure 7: Response of Buck Converter based on IMC-PID Control

Table 2: Transient Response of the Buck Converter based on two control schemes

Sl. No.	Transient Parameters	IMC-PID Control
1	Settling Time	1.63 X 10^{-3} sec
2	Peak Time	665 sec
3	Rise Time	101.19 sec
4	Overshoot	7.56 volt

6. Conclusion

The design of controller for the buck converter is perceived as an optimization task and the controller constants are estimated through different control algorithms. Initially the designs of PID controller parameters for the buck converter were designed based on Internal Model Control (IMC)) and later the results are compared with Genetic Algorithm (GA). By observing the rise time, settling time, peak overshoot from the response curves which are obtained by using the controller parameters of two different control schemes it can be concluded that GA based parameter gives good and robust response compared to IMC.

Acknowledgement

Authors Ferrarison B. Lynser, Morningstar Sun, Maiarta Sungoh and Nuki Taggu express their deep sense of gratitude to their guide Ms. Pushpanjalee Konwar, Assistant Professor, Department of Electrical and Electronics Engineering, School of Technology, Assam Don Bosco University, Guwahati, for her valuable suggestions, continuous motivation & cooperation throughout this project work apart from providing useful material. Authors would like to sincerely thank her for her patience and guidance in providing them a clear understanding about the intricate detail of the topics and strengthening our foundation throughout the work. Only by the grace of God, have they come this far. God's never-ending grace and mercy and his ultimate plan for the lives of the authors had moulded them for his desired purpose. At last, authors would like to thank their parents for rendering their full support and continuous love and care during the course of this work, also to their friends for helping them out to carry out their work directly or indirectly.

References

[1] R. Priewasser, M. Agostinelli, S. Marsili, D. Straeussnigg and M. H. Ove, "Comparative study of linear and non-linear integrated control schemes applied to a Buck converter for mobile applications", *e & I Elektrotechnik & Informationstechnik*, Vol. 127, Issue No. 4, April 2010, pp. 103–108. Doi: https://doi.org/10.1007/s00502-010-0705-6

[2] K. Bhattacharyya and P. Mandal, "Design and implementation of a switched capacitor-based embedded hybrid DC–DC converter", *International Journal of Electronics*, Vol. 99, Issue No. 6, 2012, pp. 823-849. Doi: http://dx.doi.org/10.1080/00207217.2011.647290.

[3] B. P. Divakar IV and D. Sutanto "Novel topologies for DC-DC converter with PWM control", *International Journal of Electronics*, Vol. 87, Issue No. 6, 2000, pp. 741-756. Doi: http://dx.doi.org/10.1080/002072100131931

[4] Y. V. Hote, "A new approach to time domain analysis of perturbed PWM push-pull DC-DC converter", *Journal of Control Theory and Applications*, Vol. 10, Issue No. 4, November 2012, pp. 465-469. Retrieved from https://link.springer.com/article/10.1007/s11768-012-0064-4

[5] T. B. Petrovic and A. T. Juloski, "Robust H_∞ controller design for current mode-controlled dc/dc converters", *Electrical Engineering*, Vol. 82, Issue No. 2, November 1999, pp. 83–88. Retrieved from https://link.springer.com/article/10.1007/s002020050079

[6] X. Wei, K. M. Tsang and W. L Chan, "DC/DC Buck Converter Using Internal Model Control", *Electric Power Components and Systems*, Vol. 37, Issue No. 3, 2009, pp.

320-330. Doi: https://doi.org/10.1080/15325000802454500

[7] C. Olalla, C. Carrejo, R. Leyva, C. Alonso and B. Estibals, "Digital QFT robust control of DC–DC current-mode converters", *Electrical Engineering*, Vol. 95, Issue No. 1, 2012, pp. 21-31. Doi: https://link.springer.com/article/10.1007/s00202-012-0236-8

[8] A. B. Ponniran, A *study on optimization of circuit components in high boost dc-dc converter with hybrid-based configuration*, Ph.D. Thesis, Nagaoka University of Technology, June 2016. Retrieved from http://hdl.handle.net/10649/814

[9] H. Sira-Ramirez and R. Silva-Ortigoza, *Control Design Techniques in Power Electronics Devices*, 1st Edition, Springer-Verlag, London, 2006.

[10] K. Kayisli, S. Tunner and M. Poyrax, "A Novel Power Factor Correction System Based on Sliding Mode Fuzzy Control", *Electric Power Components and Systems*, Vol. 45, Issue No. 4, February 2017, pp. 430-441. Doi: http://dx.doi.org/10.1080/15325008.2016.1266418

[11] W. Feng-yan, X. Jian-ping, "Modeling and Analysis of V^2C Controlled Buck Converter", *Proceedings of the Chinese Society of Electrical Engineering: CSEE 2006-02*, Vol. 26, Issue No. 2, 2006, pp. 121-126. Retrieved from http://en.cnki.com.cn/Article_en/CJFDTOTAL-ZGDC200602021.htm

[12] M. Wens and M. Steyaert, *Design and Implementation of Fully-Integrated Inductive DC-DC Converters in Standard CMOS*, 1st Edition, Springer, Dordrecht, Netherlands, 2011.

Authors' Profile

Ferrarison B. Lynser

Morningstar Sun

Maiarta Sungoh

Nuki Taggu

B.Tech. 8th Semester, Dept. of Electrical and Electronics Engineering, School of Technology, Assam Don Bosco University

Ms. Pushpanjalee Konwar is an Assistant Professor in the department of Electrical and Electronics Engineering,School of Technology, Assam Don Bosco University, Guwahati. She received her M. Tech. degree from Assam Don Bosco University in 2014 and pursuing Ph.D. from NIT Nagaland. Till now, she has authored one book chapter published by IGI Global Journals and published four research papers in journals and conferences. Her area of research is biomedical instrumentation and power systems.

Design of DC Microgrid Based on Photovoltaic Power Supply System

[1]Risalin Lyngdoh Mairang, [2]Bikramjit Goswami

[1,2]Department of Electrical and Electronics Engineering, School of Technology, Assam Don Bosco University
Airport Road, Azara, Guwahati - 781017, Assam, INDIA
*[1]risavecca@gmail.com**

Abstract: ***This paper describes the possibilities of the application of DC Microgrids to solve the energy problem in the country. DC Microgrids open a gateway for the integration of solar energy, which is an efficient and cleaner way of renewable energy generation, which can be integrated into the power distribution network. DC microgrid is an intelligent mix of smart grid and renewable source with an increase in the efficiency of energy. Therefore, very little energy is wasted during distribution and transmission. It has several other advantages, which include - reduction in transmission losses, improvement in power quality & reliability, reduction in emissions and even it is cost-effective. The circuit for solar power availability sensing and switching to battery supply is done on hardware. Design of DC microgrid from solar energy is done in MATLAB/SIMULINK. The most important characteristic is that it provides a possibility for electrification of remote villages which are far from the reach of the conventional grid.***

Keywords: DC Microgrid, Solar, MATLAB, Arduino.

1. Introduction

Renewable energy plays an important role in the global energy sector. Renewable energy sources which are also known as non-conventional type of energy, are the sources which are continuously replenished by natural processes. The primary concerns on the use of energy sources are the day-to-day increasing power demand [1]. However, the problem with the non-renewable energy sources such as coal, natural gases and oil is that they are decreasing day by day and not getting replenished, therefore after a few years, their reserve will be empty. Hence renewable energy sources become important. Additional advantages that they are pollution-free and it is environmentally friendly, which reduces the harmful gas emission to the surroundings. Once renewable energy technologies become more dominant, then energy would be produced anywhere without adversely affecting the environment [2].

DC microgrid comprises dc power generation, dc electrical storage, dc power distribution, etc. Converting that dc into synchronised ac for grid remains a challenge. Multiple rooftop micro generations can be connected together to form the microgrid. A microgrid is one of the new conceptual power systems for the smooth installation of many distributed generations (DGs) [3].

2. PV Modules Performance

The solar panel is kept exposed to direct sunlight to measure the solar panel voltage output with the help of a multi-meter, as shown in Figure 1.

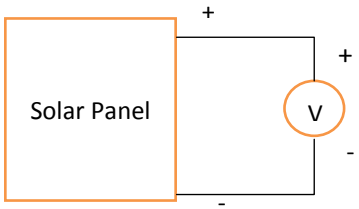

Figure 1: Circuit diagram used for measurement of voltage

Figure 2 shows the circuit diagram of power measurement with variable load resistance with the help of a multi-meter, which gives different values of output power.

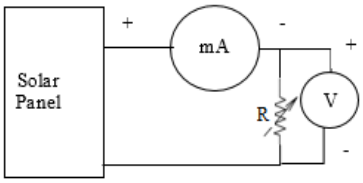

Figure 2: Power measurement circuit

2.1 Modelling of PV Array

When a solar cell is exposed to sunlight, then a current which is proportional to solar irradiation is generated. A simple ideal solar cell can be modelled in a circuit as a current source connected

to a diode in parallel. As no cell is ideal so for accurate modelling, there are shunt and series resistance connected [4]. The equivalent circuit is shown in figure 3.

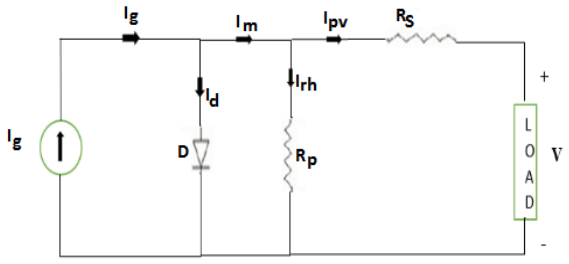

Figure 3: Equivalent model of PV cell

The current source I_g represents the current generated by the irradiation of sunlight, Id is the Shockley diode current, R_s and R_p are used to represent the intrinsic series and shunt resistance of the cell respectively. Usually, the value of R_p is very large, and that of Rs is very small, hence they may be neglected to simplify the analysis.

The mathematical equations for this model [5-6] can be given as:

$$I_{pv} = I_m - I_{sh} \quad (1)$$

Current through shunt resistor,

$$I_{sh} = \frac{V + I_{pv} R_s}{R_p} \quad (2)$$

$$I_m = I_g - I_d \quad (3)$$

$$I_g = \left(I_{gn} + K_i \ T\right)\frac{G}{G_n} \quad (4)$$

Where,

I_g – PV generated current.

I_{gn} – Nominal generated current

K_i – Current coefficient

G – Solar insolation

G_n - Nominal solar insolation

$$\Delta T = T_{amb} - T_{nom} \quad (5)$$

T_{amb} – Ambient temperature

T_{nom} – Nominal temperature

$$I_0 = \frac{I_{scn} + K_i \ T}{\exp\left(\frac{V_{ocn} + K_v \ T}{aV_t}\right) - 1} \quad (6)$$

I_0 – reverse saturation current of diode.

I_{scn} – Nominal short circuit current

K_v – Voltage coefficient

V_{ocn} – Nominal short circuit voltage

$$I_d = I_0 \exp\left(\frac{V + I_{pv} R_s}{V_t n}\right) - 1 \quad (7)$$

I_d – Shockley diode current

n – Diode ideality constant

The value of the diode constant n may be arbitrarily chosen. Usually, $1 \leq n \leq 1.5$ and the choice depend on other parameters of the I-V model.

R_s – Series resistance

$$V_t = \frac{N_S K T_{amb}}{q} \quad (8)$$

V_t – Thermal voltage of the array

N_s – No. of cell in series

K – Boltzman's constant

q – Electron charge

$$V_d = V_{pv} + I_{pv} \times R_s \quad (9)$$

V_{pv} – Photovoltaic voltage

I_{pv} – Photovoltaic current

Pyranometer is used for measuring solar irradiance, but it is very costly; therefore, another way to measure the solar irradiance can be used by the following formula:

$$I_{sc} G_{cal} = I_{cal} G_{STC} \quad (10)$$

Where,

I_{sc} – Rated short circuit current

I_{cal} – Short circuit current measured by the Ammeter

G_{STC} – Irradiance at Standard Test Condition (STC)

G_{cal} – irradiance to be calculated

2.2 Simulation Model of PV Array

The PV array has been designed in MATLAB/Simulation software taken into consideration its dependence upon the irradiance, temperature, number of PV cells connected in series and parallel. The PV array has been modelled using the equations (1) – (9). The detailed internal circuit of the PV array is given below:

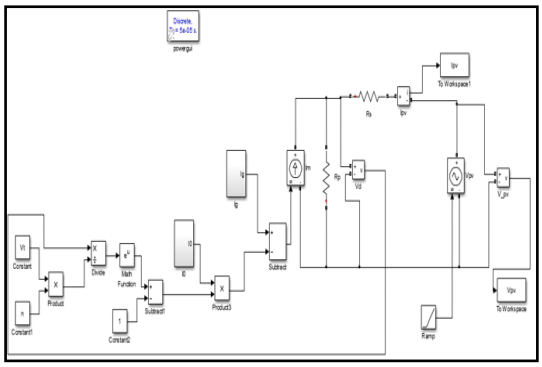

Figure 4: Complete simulation model of PV cell

The M-file for I_g function has been developed using the equation (4) and that for the I0 function using equation (6).

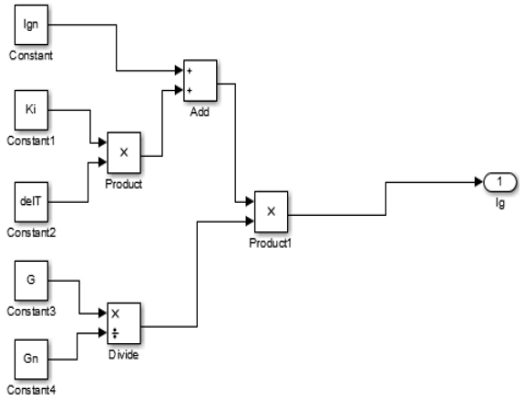

Figure 5: Simulation model of I_g

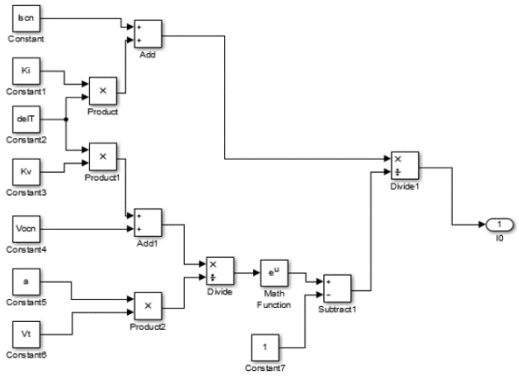

Figure 6: Simulation model of I_0

The current to voltage characteristic of a solar array is non-linear, which makes it difficult to determine the MPP. Figure 7 and figure 8 give the characteristic of I-V and P-V curve for a fixed level of solar irradiation and temperature.

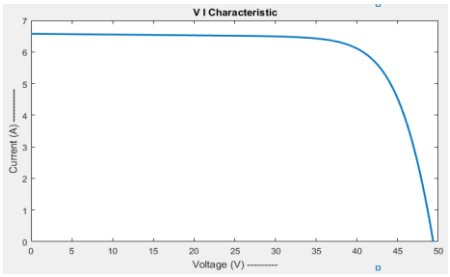

Figure 7: I-V curve

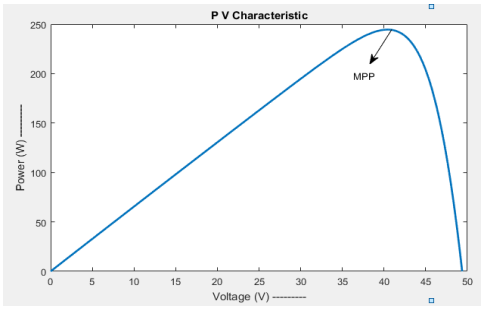

Figure 8: P-V curve

3. Proposed Solar Power Component of the Microgrid

The block diagram of the proposed solar power component of the microgrid consists of solar cells, Arduino microcontroller, relays, battery, battery charger and load.

According to the block diagram given in Figure 9, the algorithm can be described as when the solar panel voltage is greater than the threshold voltage; then relay 1 is switched on. As long as the load current is less than the maximum current that can be obtained from the solar cell, then relay 2 is switched on, which gives power supply to the load. However, if load current increases gradually and becomes greater than the maximum current, then relay 2 is switched off.

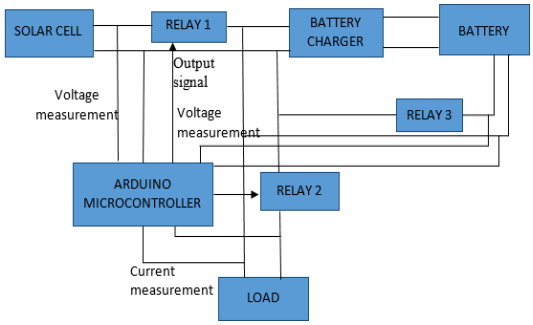

Figure 9: Block diagram of the individual units in the proposed microgrid

In case the load requires less amount of power supply or does not require power, then the relay 2 is kept off, and the battery continues to get charging current from the solar panel. By this way, the solar charging current is stored in the battery, as

long as the solar voltage is present. When the solar panel supply voltage is too low, i.e., less than the threshold voltage, the relay 1 is switched off, so that the load and the battery charger do not get power from the solar panel.

At dawn or night time, the battery can supply the power to the load. Similarly, if the battery voltage is greater than the threshold voltage, relay 3 is switched on. As long as the load current is less than the maximum current, then relay 2 is kept on, which gives power to the load. Otherwise, switch relay 2 is switched off if the load current is greater than the maximum current. Again, when the battery voltage is less than the threshold voltage, then relay 3 is switched off.

4. Voltage Divider Circuit Used

Arduino analog inputs can be used to measure DC voltage between 0 and 5V. A voltage divider circuit consisting of two resistors in series will divide the input voltage to bring it within the range of the Arduino analog inputs. The circuit with the particular values shown has an input impedance of 1MΩ + 300kΩ = 1.3MΩ and is suitable for measuring DC voltages up to about 20V, for applying to the analog input of Arduino.

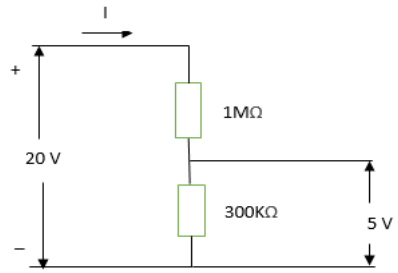

Figure 10: Voltage Divider

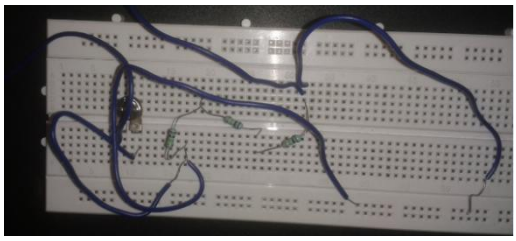

Figure 11: Circuit of Voltage Divider

Any voltage higher than about 20V could damage the Arduino. Providing this basic over-voltage protection is at the expense of not using the full 10-bit range of the analog input ADC if only lower voltages are to be measured. No other protection for voltage spikes, reverse voltage or voltages higher than 20V is shown in the circuit.

5. Circuit Used for the Load to get Supply from Solar or Battery

In order to switch a motor or a light bulb, the first step is to determine the voltage and current of the load. In general, we can use both PNP or NPN transistors as switches. However, PNP transistors can only control the same voltage as is supplied to the Arduino chip. In this case, since the voltage, we are controlling (18.22V) is different from the Arduino voltage (5V); therefore, NPN transistor has to be used.

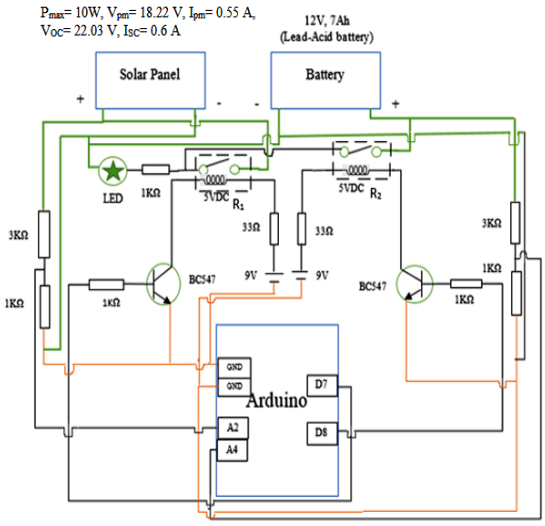

Figure 12: Circuit diagram of a design system

An LED (Light Emitting Diode) is connected to the collector of NPN transistor. It glows according to the base current. The base resistor (Rb) is connected to limit the base current.

When the source from solar panel can supply enough energy to the load then the first relay (R1) is switched on as long as the load current is less than the maximum current that can be obtained from the solar cell, so the second relay (R2) is switched on. In that case, the battery gives power supply to the load. Similarly, at dawn or night time, the battery can supply the power to the load. The flowchart of the process is shown in figure 13.

The maximum power of the solar panel used is 10W, the voltage and current are 18.22V and 0.55A respectively. The open-circuit voltage is 22.03V and the short circuit current is 0.6A. The rating of the lead-acid battery is 12V, 7Ah capacity.

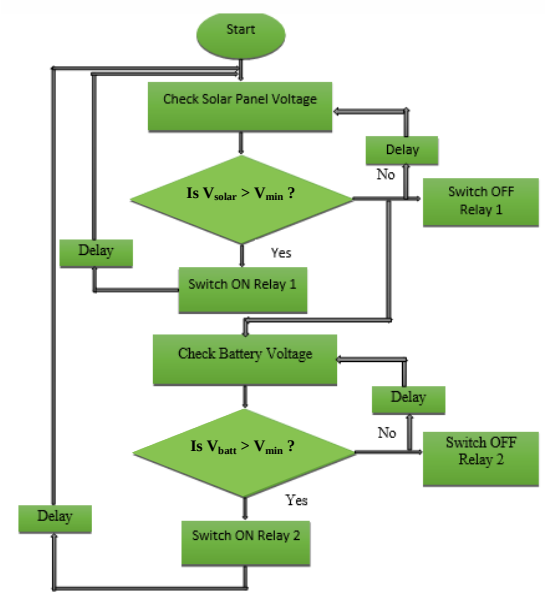

Figure 13: Flowchart of the Solar-Battery supply circuit

5.1 Analysis of Results

The Solar-Battery dual system can switch over the supply to the load (LEDs) from Solar to Battery when the solar voltage reaches below threshold set and vice-versa. The circuit is now ready to be connected to any load by using a suitable relay.

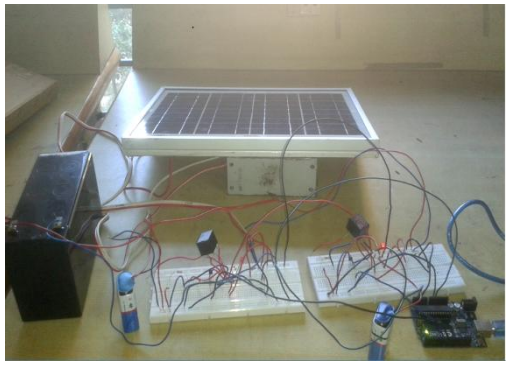

Figure 14: Load powered by solar source

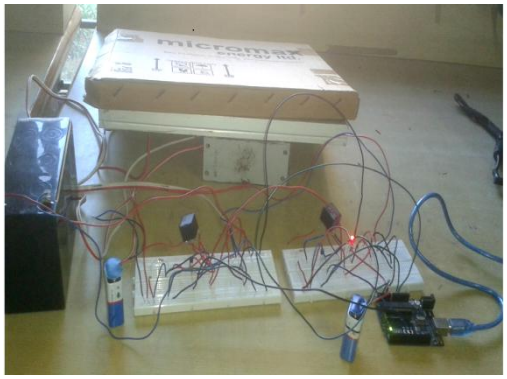

Figure 15: Load powered by Battery as a source (automatic switching in the absence of solar output).

6. Measurement of Voltage using Arduino

A voltage divider circuit consisting of two resistors in series will divide the input voltage to bring it within the range of the Arduino analog inputs. The circuit with the particular values shown has an input impedance of 1MΩ + 300kΩ = 1.3MΩ and is suitable for measuring DC voltages up to about 20V. Figure 16 shows the serial monitor output voltage from the power supply.

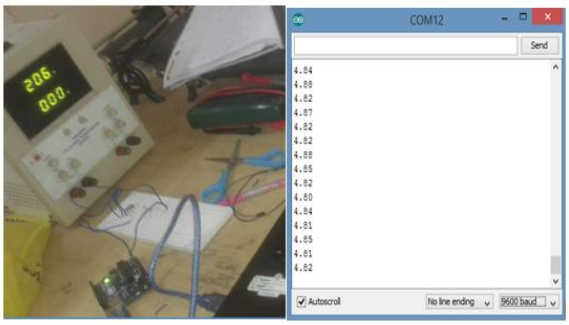

Figure 16: Testing of Voltage measurement using Arduino and Serial Monitor Output Voltage with 20V supply

7. DC-DC Converter

A DC-DC converter is an electronic circuit device that converts a source of direct current (DC) from one voltage level to another.

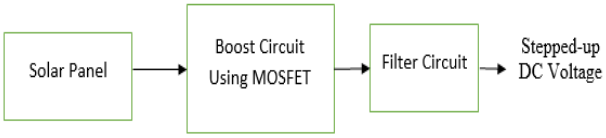

Figure 17: System block

This load is supposed to get only a DC voltage. The DC voltage can be given by a DC source. However, the DC source that we have used and the load may not be compatible. In such a case, it cannot be directly connected to the load, which may require higher volt. Therefore, a DC-DC converter is needed.

Semiconductors such as diodes, switches and passive devices such as resistors, inductors and capacitors are the basic components to construct a converter [7-8]. Not only converting energy, but converters with proper controllers also keep the power quality of microgrid within acceptable levels. So, all these major components are put together in specific topologies to achieve specific outputs.

7.1 Boost Converter

As the output power given by the solar panel is very low, so the use of a boost converter is one of the methods used to increase the output power. The boost converter is used to step up the voltage from a lower level to higher level. The step-up level is determined by the duty cycle of the converter. The converter consists of a switch, inductor, diode and capacitor.

The boost converter that we have designed in MATLAB/Simulink is 50 V and boosted to 100 V, which can be used to connect to DC bus of different loads.

Table 1: Specification of Boost converter

Sl. No.	Parameters	Specifications	Values
1	Input voltage	V_s	50 V
2	Output voltage	V_o	100 V
3	Output Power	P	67.16 W
4	Output voltage ripple	ΔV_{out}	1%
5	Input current peak ripple	ΔI_L	53%
6	Switching frequency	Fs	20 KHz

Necessary calculations for each circuit element are given below.

The first step in the design procedure is to verify whether the maximum possible output current of the boost converter supports the specific application requirements.

Maximum Duty Cycle: $$D = 1 - \frac{V_i \times \eta}{V_{out}} \quad (11)$$

The value of the inductor (L), decides the peak input current, which corresponds to the withstanding capacity of the converter switches.
Inductor Ripple Current:

$$I_L = \frac{V_{(min)} \times D}{f_s \times L} \quad (12)$$

The capacitor serves as an energy storage device. Energy is stored in the capacitor near the peak values of input voltage and current, and it gets discharged in order to maintain the load current constant irrespective of the circuit conditions. The factor that plays a vital role in capacitor selection is the ripple in the output voltage.

Average Forward Current of Rectifier Diode:

$$I_F = I_{out(max)} \quad (13)$$

Power Dissipation in Rectifier Diode:

$$P_D = I_F \times V_F \quad (14)$$

Minimum Output Capacitance:

$$C_{out(min)} = \frac{I_{out(max)} \times D}{f_s \times V_{out}} \quad (15)$$

7.2 Simulation of DC-DC Boost Converter

Modelling of a boost converter is done in MATLAB/Simulink software.

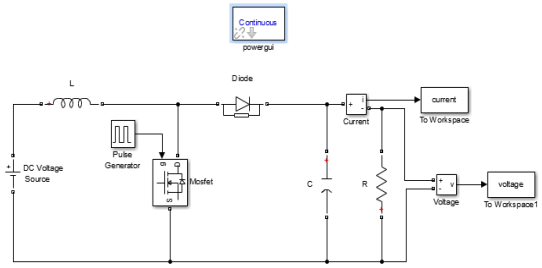

Figure 18: Simulation model of Boost Converter

8. Interfacing of the PV Array with Boost Converter

The model below shows the interfacing of the PV array with a boost converter.

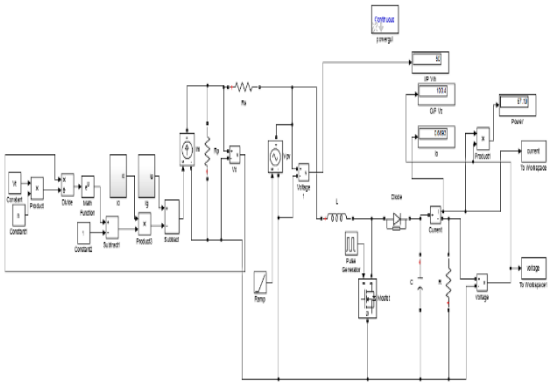

Figure 19: The complete Simulink circuit model showing the coupling of PV array with the boost converter

The interfacing of the PV array with the boost converter has been achieved using a voltage-controlled source.

9. Testing of DC Microgrid

DC microgrid is an emerging technology due to the increment of modern DC loads such as electric vehicle (EV), light-emitting diode (LED) lighting and that the majority of electronic devices are DC, as well as DC storage elements. DC microgrid is considered to be more reliable, and topology is simpler [9-10].

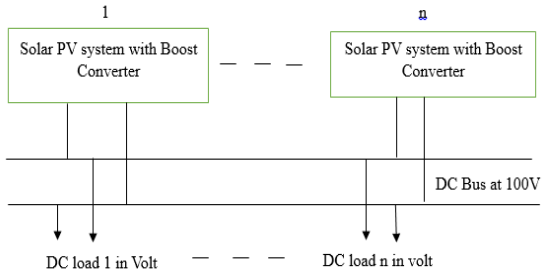

Figure 20: System block diagram

9.1 Connection of One PV Module to DC Bus

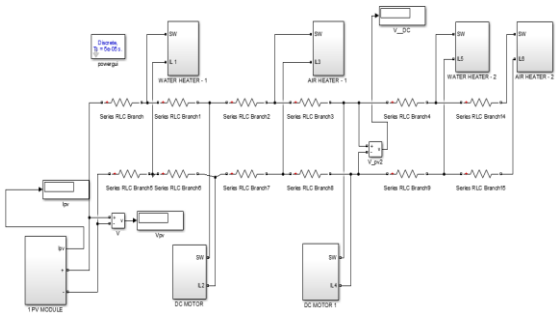

Figure 21: One PV module connected to DC bus with six loads

From the above model shown in Figure 21, we have considered a water heater, air heater and a DC motor of load resistance, R=1Ω. A one PV module is connected to a DC bus which provides the power supply to all the loads connected through a DC bus. When the switch is switched ON the current drawn by the loads are noted as shown in Table 2.

Table 2: One PV module with six loads are connected to DC bus

Parameters	Values
V_{PV}	50 V
V_{DCBus}	39.88 V
I_{L1}	45.79 A
I_{L2}	27.55 A
I_{L3}	39.84 A
I_{L4}	22.95 A
I_{L5}	36.49 A
I_{L6}	35.78 A

From the above table, the load currents are obtained for one PV module supplying the power. Let us look in the next testing with more PV modules with respect to the loads.

9.2 Connection of Ten PV Modules plus Twelve PV Modules to DC Bus

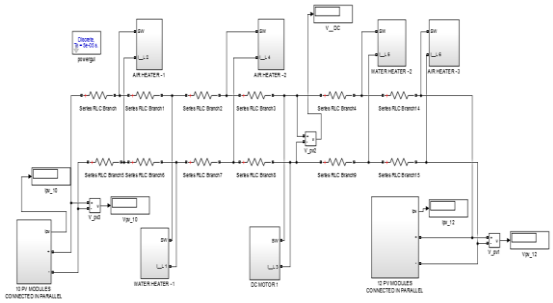

Figure 22: Ten plus twelve PV modules connected to DC bus with six loads

From the above model shown in Figure 22, we have considered with six loads connected to the DC bus of load resistance, R=1Ω. In this test, ten PV modules are connected in series to increase the current which are connected to the left side of a DC bus, and twelve PV modules are also connected in series which are connected to the right side of a DC bus as shown in the above figure. When the switch is made ON, the current drawn by the loads are noted as shown in Table 3.

Table 3: When six loads are connected to DC bus

Parameters	Values
V_{PV}	50 V
V_{DCBus}	27.46 V
$I_{PV(10)}$	65.03 A
$I_{PV(12)}$	78.06 A
I_{L1}	25.92 A
I_{L2}	26.69 A
I_{L3}	10.93 A
I_{L4}	25.67 A
I_{L5}	26.42 A
I_{L6}	27.43 A

9.3 Interfacing of Boost Converter with PV Module connected to a DC Bus

The boost converter controls the PV panel to operate at the Maximum Power Point.

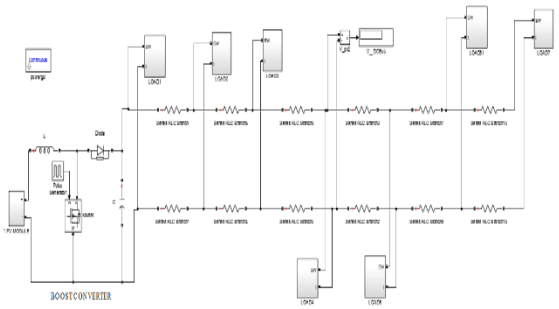

Figure 23: A boost converter interfaced with PV module connected to a DC bus

From the above model shown in Figure 23, one PV module is interfaced with the boost converter and connected to a DC bus. In this test, seven loads are connected to a DC bus and the load resistance, R=1 Ω. When the switch is made ON, the current drawn by the loads are noted as shown in Table 4.

Table 4: One PV module interfacing with a boost converter connected to DC bus

Parameters	Values
V_{PV}	50 V
V_{Boost}	100 V
V_{DCBus}	60.73 V
I_{L1}	76.84 A
I_{L2}	70.18 A
I_{L3}	49.94 A
I_{L4}	60.67 A
I_{L5}	42.64 A
I_{L6}	55.43 A
I_{L7}	54.34 A

In this case, the voltage between the buses is higher compared to the above cases, i.e., without boost. Similarly, the load currents also increased.

9.4 Two PV Modules connected to a DC Bus with a Boost Converter

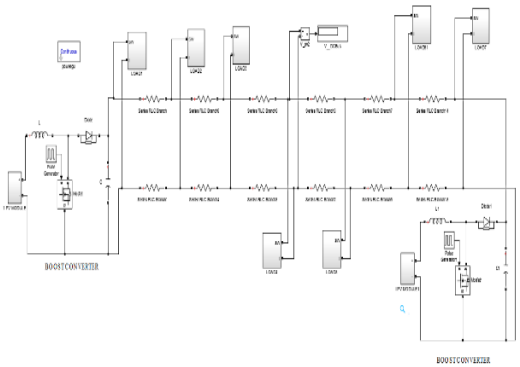

Figure 24: A boost converter interfaced with PV module connected to a DC bus

From the above model shown in figure 24 two PV modules are connected to a DC bus and each PV module are interfaced with a boost converter. In this test, seven loads are connected to a DC bus and the load resistance, R=1 Ω. When the switch is made ON, the currents draw by the loads are noted as shown in table 5.

Table 5: Two PV modules with a boost converter connected to DC bus

Parameters	Values
V_{PV}	50 V
V_{Boost}	100 V
V_{DCBus}	83.73 V
I_{L1}	90.66 A
I_{L2}	86.7 A
I_{L3}	69.5 A
I_{L4}	83.65 A
I_{L5}	69.5 A
I_{L6}	86.7 A
I_{L7}	90.66 A

In this case, the voltage between the buses is higher compared to the above cases for one PV module with the boost. Similarly, the load currents are increased higher compared to the previous case. From the same model shown in Figure 24 when the load resistance, R=10 Ω the currents drawn by the loads are noted as shown in Table 6.

Table 6: Two PV modules with a boost converter connected to DC bus

Parameters	Values
V_{PV}	50 V
V_{Boost}	100 V
V_{DCBus}	107.5 V
I_{L1}	10.84 A
I_{L2}	10.79 A
I_{L3}	9.26 A
I_{L4}	10.75 A
I_{L5}	9.26 A
I_{L6}	10.79 A
I_{L7}	10.84 A

In this case, the voltage between the buses is high, and the load currents are decreased.

Again, from the same model shown in Figure 24, when the load resistance, R=12 Ω the currents drawn by the loads are noted, as shown in Table 7.

Table 7: Two PV modules with a boost converter connected to DC bus

Parameters	Values
V_{PV}	50 V
V_{Boost}	100 V
V_{DCBus}	106.5 V
I_{L1}	8.94 A

I_{L2}	8.9 A
I_{L3}	7.6 A
I_{L4}	8.88 A
I_{L5}	7.63 A
I_{L6}	8.9 A
I_{L7}	8.94 A

In this case, the voltage between the buses is high, and the load currents are decreased. Therefore when loads resistance increases the load currents decreases.

9.5 One PV Module interfacing with a Boost Converter plus 100V Battery are to be connected

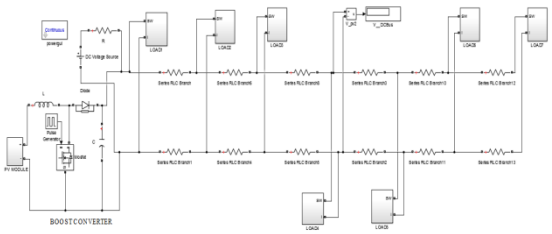

Figure 25: A boost converter interfaced with PV module connected to a DC bus

From the above model shown in Figure 25, one PV module is interfaced with a boost converter and connected to a DC bus, and also a 100V battery is connected. A small value of resistance is connected in series with a battery. In this test, seven loads are connected to a DC bus and the load resistance, R=1 Ω. When the switch is made ON, the current drawn by the loads are noted as shown in table 8.

Table 8: One PV module interfacing with boost plus 100V battery are connected to DC bus

Parameters	Values
V_{PV}	50 V
V_{Boost}	100 V
b_{attery}	100 V
V_{DCBus}	78.18 V
I_{L1}	99.34 A
I_{L2}	90.6 A
I_{L3}	68.68 A
I_{L4}	78.1 A
I_{L5}	59.12 A
I_{L6}	71.28 A
I_{L7}	69.89 A

In this case the voltage between the buses is higher compared to the other model shown in the previous case. The loads currents are also higher.

To conclude from all the observations discussed above, to improve the output power to the load side and to stabilize the voltage, a battery must be connected to the DC bus as it helps to reduce the losses. Therefore, together the PV modules interfaced with a boost converter and a battery, are expected to give better results.

10. Conclusions

The circuit for solar power supply and automatic switch-over to battery supply is completed. Microcontroller based circuit operation provides the flexibility of setting the threshold voltages for solar as well as battery supply to the load. The circuit designed so far is ready for integrating into the microgrid, where there would also be other sources, such as wind power supply. Interfacing of a boost converter with PV array has been done, to step up the voltage up to grid level. A designing of DC microgrid having solar energy as the source has been done. Overall, the DC microgrid is a viable option for distributing power in both rural and urban households, utilizing solar power which is available freely.

References

[1] N. Pratap, P. Singh, S. Sharma and R. Rani, "Solar energy: Trends and enabling technologies", *International Journal of Education and Science Research Review*, Vol.1, Issue No. N3, June 2014, pp. 21-30. Retrieved from http://www.ijesrr.org/publication/8/IJESRR%20V-1-3-4E.pdf

[2] "Solar energy", *Edugreen*. [Online]. Available: http://edugreen.teri.res.in/explore/renew/solar.htm (Accessed March 12, 2018).

[3] H. Kakigano, Y. Miura, and T. Ise, "Low-Voltage Bipolar-Type DC Microgrid for Super High Quality Distribution", *IEEE Transactions on Power Electronics*, Vol. 25, Issue No. 12, Dec. 2010, pp. 3066- 3075. Doi: 10.1109/TPEL.2010.2077682

[4] M. G. Villalva, J. R. Gazoli and E. R. Filho, "Modeling and circuit-based simulation of photovoltaic arrays", *Brazilian Journal of Electronics*, Vol. 14, Issue No. 1, 2009, pp. 35-45. Doi: 10.1109/COBEP.2009.5347680.

[5] A. Saleh, "Simulation of pv model using matlab simulink 2012", *YouTube Video Tutorial*, Dec. 11, 2015. [Online]. Available: https://www.youtube.com/watch?v=x0Kjg_zVHuQ (Accessed: April 12, 2018).

[6] Krismadinataa, N. A. Rahim, H. W. Ping and J. Selvaraj, "Photovoltaic module modeling using simulink/matlab", *Procedia Environmental Sciences*, Vol. 17, 2013, pp.

537-546. Doi: https://doi.org/10.1016/j.proenv.2013.02.069

[7] S. Sholapur, K. R. Mohan and T. R. Narsimhegowda, "Boost Converter Topology for PV System with Perturb And Observe MPPT Algorithm", *IOSR Journal of Electrical and Electronics Engineering (IOSR-JEEE)*, Vol. 9, Issue No. 4, Ver. II, Jul – Aug. 2014, pp. 50-56. Retrieved from http://www.iosrjournals.org/iosr-jeee/Papers/Vol9-issue4/Version-2/I09425056.pdf

[8] S. D. Stallon, K.V. Kumar, S. S. Kumar and J. Baby, "Simulation of High Step-Up DC–DC Converter for Photovoltaic Module Application using MATLAB/SIMULINK", *International Journal of Intelligent Systems and Applications(IJISA)*, Vol. 5, Issue No. 7, 2013. pp. 72-82. Doi: 10.5815/ijisa.2013.07.10

[9] A. T. Ghareeb, A. A. Mohamed and O. A. Mohammed, "DC microgrids and distribution systems: An overview", *Proc. of 2013 IEEE Power & Energy Society General Meeting*, Vancouver, BC, 2013, pp. 1-5. Doi: 10.1109/PESMG.2013.6672624

[10] D. Salomonsson, L. Soder and A. Sannino, "Protection of Low-Voltage DC Microgrids", *IEEE Transactions on Power Delivery*, Vol. 24, Issue No. 3, July 2009, pp. 1045-1053. Doi: 10.1109/TPWRD.2009.2016622

Authors' Profiles

Risalin Lyngdoh Mairang is a student of M.Tech. 4th semester in the department of Electrical and Electronics Engineering, School of Technology, Assam Don Bosco University.

Bikramjit Goswami is working as an Assistant Professor in the department of Electrical and Electronics Engineering, School of Technology, Assam Don Bosco University, India. He is also a Ph.D. Research Scholar in Assam Don Bosco University currently. His research interests are Reconfigurable Antenna, Microwave Remote Sensing, Artificial Neural Networks, renewable Energy, Disaster Forecasting.

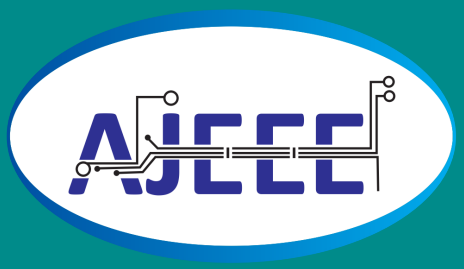

ADBU Journal of Electrical and Electronics Engineering

ISSN: 2582-0257

www.tinyurl.com/ajeee-adbu

ASSAM DON BOSCO UNIVERSITY

Azara Campus, Airport Road, Guwahati - 781017
+91-9435545754, 0361-2139291/92
www.dbuniversity.ac.in